Investigation of Post-Oxidation by Means of 3D-CFD Virtual Engine Development

Von der Fakultät Konstruktions-, Produktions- und Fahrzeugtechnik der Universität Stuttgart zur Erlangung der Würde eines Doktor-Ingenieurs (Dr.-Ing.) genehmigte Abhandlung

Vorgelegt von

Rodolfo Tromellini
aus Torino

Hauptberichter:	Prof. Dr.-Ing. M. Bargende
Mitberichter:	Prof. Dr. Eng. Y. Moriyoshi
Tag der mündlichen Prüfung:	14.07.2022

Institut für Fahrzeugtechnik Stuttgart
der Universität Stuttgart

2022

"Every foreign land
is like their homeland to them,
and every land of their birth
is like a land of strangers."

Letter to Diognetus

Preface

This work has been carried out during the time I spent as a research associate at the Institute of Automotive Engineering at the University (IFS) of Stuttgart.

My gratitude goes first of all to the Prof. Dr.-Ing. M. Bargende for the possibility he gave me, for the supervision of the work and for the interesting conversations about the project.

I want to thank also Dr. Marco Chiodi for the time he dedicated to my work, for his patience, the interesting discussions and the many inputs he gave me.

My thank goes to all the collegues who took part to this project: Dr. Jan Przewlocki in Stuttgart, Dr. Madan Kumar and M.Sc. Salaar Moeeni in Japan. A special thank goes to M.Sc. Viktoria Kelich for the great work of coordination and the help she was always ready to provide.

My gratitude goes to my collegues Edoardo, Antonino, Francesco, Andreas, Peter, Thomas, Robin, Mario, Oli, Hubert and all the other collegues of the IFS and FKFS I met during my years in Stuttgart.

Special thanks to my parents, my brothers, my family and friends in so many different parts of the world and to the Sängerknaben. I always feel very lucky and honored to have the chance to call you my friends and to spend time with you. To all of you I would like to dedicate this work.

Stuttgart, April 2022 Rodolfo Tromellini

Contents

Figures

Tables

Abbreviations

°CA	Degrees crank angle
1D-CFD	One dimensional computational fluid dynamic
3D-CFD	Three dimensional computational fluid dynamic
ADAS	Advanced driver-assistance systems
BDC	Bottom dead centre
BEV	Battery electric vehicles
BPA	By-pass adaptor
CAD	Computer aided design
CO	Carbon monoxide
CO_2	Carbon dioxide
DISI	Direct injection spark-ignition
DNS	Direct numerical simulation
EGR	Exhaust gas recirculation
EVC	Exhaust valve closing
EVO	Exhaust valve opening
EU	European Union
FBDC	Firing bottom dead centre
FKFS	Forschungsinstitut für Kraftfahrwesen und Fahrzeugmotoren Stuttgart
FTDC	Firing top dead centre
GHG	Greenhouse gases
H_2	Molecular hydrogen
H_2O	Water
HC	Unburned hydrocarbon
HEV	Hybrid electric vehicles
HPC	High performance computer

HR	Heat release
ICE	Internal combustion engines
ICEV	Internal combustion engines vehicles
IFS	Institut für Fahrzeugtechnik Stuttgart
IP	Ignition point
IVC	Intake valve closing
IVO	Intake valve opening
LCA	Life cycle assessment
LES	Large eddies simulation
LHV	Lower heating value
mol%	Percentage of the molar fraction
NDC	Nationally determined contributions
NO_X	Nitrogen oxides
NEDC	New European driving test
NS	Navier-Stokes
O_2	Molecular oxygen
OEM	Original equipment manufacturers
PM	Particulate matter
PO-rate	Post-oxidation rate
PRF	Primary reference fuels
r^2	Coefficient of determination of the linear regression
RDE	Real driving emissions
SBDC	Scavenging bottom dead centre
SI	Spark-ignition
STDC	Scavenging top dead centre
T_3	Temperature before the turbine
TDC	Top dead centre
THC	Tail hydrocarbons
TKE	Turbulent kinetic energy

TRF	Ternary reference fuels
TWC	Three-way-catalyst
VGT	Variable geometry turbocharger
WSG	Wastegate valve

Symbols

§	Paragraph
ν_i	Stoichiometric coefficient of the i-species
k_f	Reaction rate forward
k_r	Reaction rate reverse
A,B,C,D	General reaction products/reactants
[A]	Molar concentration of the generic species A
d[A]/dt	Time derivative of the molar concentration of the generic species A
T	Temperature
p	Pressure
V	Volume
m	Mass
ρ	Density
p_A	Partial pressure of the species A
E_A	Activation energy
R_u	Universal gas constant
K_C	Equilibrium constant of a chemical reaction
c_p	Specific heat
H	Enthalpy
S	Entropy
d/dφ	Partial derivative with respect to the °CA
div()	Divergence
grad()	Gradient
M_i	Molar fraction
w_i	Mass fraction
ω_i	Molar fraction rate
$\vec{v}$	Velocity vector
$\bar{\bar{P}}$	Pressure tensor
$\vec{j}$	Flux
μ	Fluid viscosity
λ	Air excess

Abstract

The introduction of real driving emissions cycles (RDE) and increasingly restrictive emissions regulations force the automotive industry to develop new and more efficient solutions for emission reductions. The introduction of limits of fleet CO_2 emissions poses even more challenging problems to the development, production and homologation of internal combustion engines. Therefore, there is a great interest in developing and applying new strategies to meet these goals, while at the same time reducing cost and time of the development process.

Post-oxidation is an interesting strategy that consists in performing a rich in-cylinder combustion that produces CO and H_2 as exhaust products. The rich combustion products are then completely oxidized in the exhaust manifold by means of fresh air. The oxidation reaction transforms the CO and H_2 into CO_2 and H_2O respectively, therefore reducing the emissions, and at the same time raises temperature and enthalpy of the exhaust gases thanks to the heat release rate of the reaction. The temperature increase can reduce the time needed for catalyst heating while keeping the overall engine operation close to stoichiometry.

Many different types of post-oxidation are possible. The most common solution is the so-called secondary air injection, which consists in injecting fresh air in the exhaust close to the exhaust valves so that the oxidation starts immediately. This strategy offers some advantages such as the possibility to precisely control the amount of air that is injected in order to match the stoichiometric conditions usually required at the three-way-catalyst. However, its implementation requires the use of an air-pump and complicated engine control logics. This increases the cost of the engine and represents the reason why the applications to production engines are limited.

A simpler solution that has been analysed in the following investigation is post-oxidation by means of scavenging. This strategy has been tested on a four-cylinder, turbocharged, direct injection, spark-ignition engine and it consists of a rich in-cylinder combustion followed by a great amount of scavenging air brought in the exhaust by means of a very long valve overlap and high boost pressure. Fresh air and rich-combustion products mix in the

exhaust manifold and start post-oxidation. This strategy has the advantage to be easy to implement in many engines with similar layout; moreover, scavenging can be used to increase the amount of air flowing to the turbine therefore reducing the turbo-lag and improving the transient behaviour of the engine. Another interesting effect of post-oxidation by means of scavenging is that the oxidation reaction that takes place in the exhaust manifold releases an important amount of heat that increases the enthalpy and temperature of the gases before the three-way-catalyst (TWC), which can be useful during cold starts and catalyst-heating engine operating points. Therefore, the project focused on exploring the potential of this strategy. In doing so, it was necessary to couple the investigations at test-bench with 3D-CFD simulations.

Indeed, it is practically impossible to directly measure and very difficult to visualize post-oxidation at the test-bench. Therefore, the description of the phenomena taking place inside the exhaust manifold and the relative influence of the factors require the simulation of the flow field and the chemical interaction of gases inside the volumes where post-oxidation occurs. The 3D-CFD simulation enables a precise description of both the flow field and the chemical reactions inside the volume; moreover, it permits to visualise and to quantify the mixing and the chemical heat release rate.

For the investigation of post-oxidation, a 3D-CFD methodology has been developed to work together with investigations at the test-bench. The methodology consisted of two different kinds of simulations: at first a simulation of the full engine has been carried out using the 3D-CFD Tool QuickSim developed at the FKFS/IFS-University of Stuttgart. This kind of simulation has the advantage to be able to simulate the whole engine from the air-box up to the turbine inlet including the four cylinders and the exhaust runners. By simulating the whole engine, a reduction of the boundary conditions complexity is possible, therefore reducing the influence of the boundary conditions assumptions on the final results.

The second kind of simulation has been performed using the commercial 3D-CFD tool Star-CCM+ and it focused on the exhaust manifold from the exhaust valves up to the turbine volute. This model used information from the 3D-CFD-full engine simulation as boundary conditions and is characterized by a finer mesh and the implementation of a chemical reaction mechanism to simulate the oxidation process of rich combustion gases inside the exhaust manifold.

The chemical reaction mechanism has been chosen after testing on a simplified 3D-CFD model a sample of selected chemical reaction mechanisms available in the literature, both some that are designed for general types of simulations and specifically for CO and H_2 oxidation. An important aspect of the simulation is the trade-off between accuracy and simulation time. The first investigations demonstrated that the simulation time is directly proportional to the number of species. The higher amount of species, however, does not ensure that the simulation increases in accuracy. Therefore, the choice fell for a reduced chemical reaction mechanism with a limited amount of species optimized for the oxidation of CO and H_2. This choice completed the preliminary work so that the simulations could start.

The methodology has been then validated against detailed experimental data that tested the quality of the simulation in reproducing many different parameters that are fundamental for post-oxidation, such as temperature, composition of the exhaust gases, pressure signals, air consumption etc. The validation demonstrated the capability of the simulation to reproduce the measurements and to give a deep insight in the phenomenon that has been analysed. In particular, it has been necessary to numerically mimic the specific behavior of the measurement methodologies. The attention focused on the comparison of mesurements and simulations for temperature profiles before the turbine and composition of the exhaust gases in various positions of the exhaust manifold.

The temperature measurements are based on thermocouples, which are characterized by a specific volume, material and thermal inertia. The simulation, on the other hand, evaluates the fluid temperature in a specific position of the computational domain without accounting for these effects. Therefore, a numerical model has been implemented that reproduces the effects of the real thermocouple and increases the accuracy of the comparison.

The composition of exhaust gases has been meausured at the test bench using a MEXA equipment. Also in this case, a numerical model reproduces the sampling methodology in order to have a realistic comparison.

These validation processes enabled a detailed tuning of the simulations and gave a better insight in the chemical and physical behavior of post-oxidation. Therefore, it has been possible to give a detailed description of post-oxidation as a chemical reaction taking place on a thin layer, where there are the best conditions in terms of temperature, mixing and pressure. Since the reactants

of post-oxidation are separate, it can be chemically modelled as a non-premixed, turbulent reaction.

The reaction is triggered by the exhaust event of each cylinder. The hot exhaust gases are pushed into the exhaust manifold at high speed through the clouds of fresh air from the previous cycle that gathered close to the exhaust valve. In these conditions, the temperature and the mixing happening at the interface between hot gases and fresh-air start the post-oxidation reactions that release heat, increasing also the temperature in the exhaust manifold. The higher temperature assures that a self-sustaining effect takes place that allows the chemical reactions to continue for the whole exhaust stroke.

At the end of the exhaust stroke, thanks the long valve overlap and the high boost pressure, cold air from the intake manifold flows directly to the exhaust at low speed and gathers close to the exhaust valves. During the remaining part of the cycle, although there is air-availability and some mixing goes on at the interface between fresh air and exhaust gases, there is usually very little heat release because the temperature is too low. Therefore, the fresh air remains available for the following exhaust event.

The last step of the validation consisted in testing if the assumption of a simplified chemical reaction mechanism applies not only to the simplified model used in the preliminary work but also to the detailed 3D-CFD model of the exhaust manifold. For this kind of simulations, a detailed chemical reaction mechanism has been implemented in the model. This increased greatly the computational times in comparison to the reduced chemical reaction mechanism. Only the adoption of a high performance computer cluster at the FKFS/IFS University of Stuttgart enabled to test the effect of different assumptions for the boundary conditions.

The simulation with the detailed chemical reaction mechanism have demonstrated that the amount of long-chain hydrocarbons present in the exhaust gases has a strong effect on post-oxidation by changing the reaction path. Moreover, the post-oxidation reaction becomes slower because the cracking of the long-chains of hydrocarbons consumes the radicals needed for the final oxidation of CO and H_2.

However, the accuracy of the model does not increase, which means that the assumption of long-chain hydrocarbons taking part to post-oxidation is not realistic. Indeed, the cracking of the hydrocarbon chains is more probable to

start in the combustion chamber because of the steep pressure and temperature gradients. Therefore, even though the molecules did not take part directly to the combustion, they are already broken into smaller molecules, when post-oxidation starts. Therefore, the assumption that most of the heat release from post-oxidation originates from CO and H_2 can be assumed to be appropriate. It is also demonstrated, that the application of a reduced chemical reaction mechanism is in this case correct.

The validated simulation methodology has been then applied to many different engine operating points in order to provide information about how post-oxidation behaves in different operating conditions.

Particular attention has been payed to keep the overall engine operation very close to stoichiometry. This is required for a safe operation of the TWC and it requires also a very narrow error limit in order to keep the efficiency high. In order to achieve an overall stoichiometric operation there are two factors that require some tuning.

The first factor is that the scavenging air must compensate as precisely as possible for the lack of oxygen in the combustion chamber. For this strategy, the tuning relies on the choice of the valve overlap and the regulation of the boost pressure. The simulations demonstrated that a too long valve overlap causes often a very high air consumption and an overall lean engine operation. Moreover, the engine operation becomes instable and very sensitive to pressure waves propagating from the exhaust. Also the boost pressure requires a precise tuning, which can be achieved by means of the throttle valve.

The second factor that is required in order to have a safe operation at the TWC is a good mixture of gases flowing to the turbine and then to the catalyst. At the beginning of post-oxidation, the reactants are separated in shape of clouds inside the exhaust manifold. The mixing should achieve that the air fuel ratio of the gases flowing to the turbine remains constantly very close stoichiometry. An incomplete mixing would cause the clouds of fresh air and rich combustion products to flow separate to the turbine and a probable loss of efficiency at the TWC.

A mapping of the heat release rate of post-oxidation has been performed in order to prove that the post-oxidation strategy can be applied also to different conditions than those used for the validation. For all the investigated engine

operating points, the overall engine operation has been kept very close to stoichiometry.

The mapping pointed out that post-oxidation by means of scavenging can be achieved in many different conditions but that the conversion of the CO and H_2 to CO_2 and H_2O is rearly complete before the turbine. The main reason is that the geometry of the investigated engine does not allow for a greater mixing of combustion products and fresh air in the right temperature conditions.

Moreover, the mapping of the heat release rate of post-oxidation pointed out the need of a trade-off between post-oxidation and the gas temperature before the turbine. Post-oxidation needs a high temperature in the exhaust in order to better complete the chemical reactions. However, the temperature of gases before the turbine is usually limited because of structural constraints of the turbine itself. Scavenging air has the effect of reducing the temperature in the exhaust, which might be useful to mitigate the temperature increase of post-oxidation. Nevertheless, the mapping showed clearly that there is a limit to the maximum amount of post-oxidation and that it depends mostly on temperature and geometrical factors.

Therefore, geometry changes and modifications of the temperature at the boundary conditions has been performed to gain sensitivity about the influence of these parameters on post-oxidation. The investigation confirmed that post-oxidation is particularly sensitive to the temperature of the exhaust gases for the start and self-sustain effect of the chemical reactions. The geometry can improve post-oxidation only if it increases the mixing of reactants by, e.g., creating a greater contact surface between exhaust gases and fresh air.

The information gained during the project has been applied to validate a simplified post-oxidation model in the 3D-CFD-Tool QuickSim, which proved to be simple and reliable because it exploits the better simulation of mixing due to the inclusion of the whole engine in the simulation.

The results of the 3D-CFD simulations have been used also for the development and validation of a post-oxidation model for a 1D-CFD engine simulation and for the tuning of the engine operation at the test-bench.

The investigation demonstrated that post-oxidation by means of scavenging is a flexible strategy that can be applied to many different conditions. This strategy has positive effects on reducing the turbo lag and increasing

substantially the temperature of the exhaust gases, which can be useful for catalyst heating. Post-oxidation is especially sensitive to temperature of the exhaust gases and mixing in the exhaust manifold. In order to have an overall stoichiometric engine operation, these two local parameters must match with full engine parameters such as scavenging and in-cylinder mixture formation.

Finally, the 3D-CFD simulation is a fundamental tool for the investigation of post-oxidation. The coupling of full engine simulations with detailed simulations of the exhaust manifold proved to be reliable and accurate and it enabled for the needed insight into the physics and chemistry of post-oxidation. The implementation of a reduced chemical reaction mechanism provided the chemical description of post-oxidation.

Post-oxidation by means of scavenging has the potential to meet the some of the upcoming challenges of the engine development.

Kurzfassung

Die Einführung von RDE Testzyklen und zunehmend restriktiverer Emissionsrechtlinien zwingen die Automobilindustrie, neue und effizientere Lösungen zur Emissionsreduzierung zu entwickeln. Die Einführung von Grenzwerten für CO_2-Flottenemissionen stellt die Entwicklung, Produktion und Zulassung von Verbrennungsmotoren vor noch größere Herausforderungen. Daher besteht ein großes Interesse an der Entwicklung und Anwendung neuer Strategien, um diese Ziele zu erreichen und gleichzeitig Kosten und Zeit des Entwicklungsprozesses zu reduzieren.

Die Nachoxidation ist eine interessante Strategie, die darin besteht, eine fette Verbrennung im Zylinder durchzuführen, bei der CO und H_2 als Abgasprodukte entstehen. Die fetten Verbrennungsprodukte werden dann im Abgaskrümmer mit Hilfe von Frischluft vollständig oxidiert. Die Oxidationsreaktion wandelt CO und H_2 in CO_2 und H_2O um, wodurch die Emissionen reduziert werden, und erhöht gleichzeitig die Temperatur und Enthalpie der Abgase dank der Wärmefreisetzung der Reaktion. Durch die Temperaturerhöhung kann die Zeit, die für die Aufheizung des Drei-Wege-Katalysators notwendig ist, reduziert werden, und der Gesamtbetrieb des Motors kann nahe der Stöchiometrie bleiben.

Es sind viele verschiedene Arten der Nachoxidation möglich. Die häufigste Lösung ist die so genannte Sekundärlufteinblasung, bei der Frischluft in den Auspuff nahe den Auslassventilen eingeblasen wird, so dass die Nachoxidation sofort beginnt. Diese Strategie bietet einige Vorteile, wie z. B. die Möglichkeit, die eingespritzte Luftmenge genau zu steuern, um die stöchiometrischen Bedingungen zu erreichen, die normalerweise am Drei-Wege-Katalysator erforderlich sind. Ihre Umsetzung erfordert jedoch den Einsatz einer Luftpumpe und eine kompliziertere Motorsteuerungslogik. Dies erhöht die Kosten des Motors und ist der Grund, warum die Anwendung auf Serienmotoren begrenzt ist.

Eine einfachere Lösung, die in der folgenden Untersuchung analysiert wird, ist die Nachoxidation mittels Scavenging. Die Strategie wurde an einem Vierzylindermotor mit Turboaufladung, Direkteinspritzung und Fremdzündung getestet und besteht aus einer fetten Verbrennung im Zylinder,

gefolgt von einer großen Menge Spülluft. Frischluft und fette Verbrennungsprodukte vermischen sich im Abgaskrümmer und beginnen die Nachoxidation. Diese Strategie hat den Vorteil, dass sie in vielen Motoren mit ähnlichem Layout einfach zu implementieren ist; außerdem kann die Spülung genutzt werden, um die Luftmenge, die durch die Turbine strömt, zu erhöhen, wodurch das Turboloch verringert und das Transientverhalten des Motors verbessert wird. Ein weiterer interessanter Effekt der Nachoxidation ist, dass die Oxidationsreaktion, die im Abgaskrümmer stattfindet, eine bedeutende Wärmemenge freisetzt, die die Enthalpie und Temperatur der Gase vor dem Drei-Wege-Katalysator erhöht, was bei Kaltstarts und beim Aufheizen des Katalysators nützlich sein kann. Daher konzentrierte sich das Projekt auf die Erforschung des Potenzials dieser Strategie. Dabei war es notwendig, die Untersuchungen am Prüfstand mit 3D-CFD-Simulationen zu koppeln.

Der Einsatz von 3D-CFD-Simulationen war notwendig, weil Nachoxidation am Prüfstand praktisch nicht direkt gemessen werden kann und sehr schwer zu visualisieren ist. Daher erfordert die Beschreibung der im Abgaskrümmer stattfindenden Phänomene und des relativen Einflusses der Faktoren die Simulation des Strömungsfeldes und der chemischen Reaktionen innerhalb der Volumina, in denen die Nachoxidation stattfindet. Die 3D-CFD-Simulation ermöglicht eine genaue Beschreibung sowohl des Strömungsfeldes als auch der chemischen Reaktionen innerhalb des Volumens und erlaubt darüber hinaus die Visualisierung und Quantifizierung der Durchmischung und der chemischen Wärmefreisetzungsrate.

Für die Untersuchung der Nachoxidation wurde eine 3D-CFD-Methodik entwickelt, die mit Untersuchungen am Prüfstand zusammenarbeitet. Die Methodik bestand aus zwei verschiedenen Arten von Simulationen: zunächst wurde eine Simulation des gesamten Motors mit dem am FKFS/IFS-Universität Stuttgart entwickelten 3D-CFD-Tool QuickSim durchgeführt. Diese Art der Simulation hat den Vorteil, dass der gesamte Motor von der Airbox bis zum Turbineneinlass einschließlich der vier Zylinder und der Abgaskanäle simuliert werden kann. Durch die Simulation des gesamten Motors ist eine Reduktion der Komplexität der Randbedingungen möglich, wodurch der Einfluss der Annahmen über die Randbedingungen auf die Endergebnisse verringert wird.

Die zweite Simulationsstufe der Methodik wurde mit dem kommerziellen Tool Star-CCM+ durchgeführt und konzentrierte sich auf den Abgaskrümmer

von den Auslassventilen bis zum Turbinengehäuse. Dieses Modell verwendet als Randbedingungen Informationen aus der Vollmotorsimulation und zeichnet sich durch ein feineres Netz und die Implementierung eines chemischen Reaktionsmechanismus aus, um den Oxidationsprozess der fetten Verbrennungsgase im Abgaskrümmer zu simulieren.

Der chemische Reaktionsmechanismus wurde nach einem Test von in der Literatur verfügbaren chemischen Reaktionsmechanismen ausgewählt, die sowohl für allgemeine Arten von Simulationen als auch speziell für CO- und H_2- Oxidationen ausgelegt sind. Ein wichtiger Aspekt der Simulation ist der Kompromiss zwischen der Genauigkeit und der Simulationszeit. Die ersten Untersuchungen wurden mit einem vereinfachten Modell durchgeführt und haben gezeigt, dass die Simulationszeit direkt proportional zur Anzahl der Spezies steigt. Die höhere Anzahl von Spezies gewährleistet jedoch nicht, dass die Simulation an Genauigkeit gewinnt. Daher fiel die endgültige Wahl auf einen reduzierten chemischen Reaktionsmechanismus mit einer begrenzten Anzahl von Spezies, der für die Oxidation von CO und H_2 optimiert wurde. Mit dieser Entscheidung war die Vorbereitungsarbeit abgeschlossen, so dass die Simulationen gestartet werden konnten.

Die Methodik wurde anhand detaillierter experimenteller Daten validiert, die die Qualität der Simulation bei der Reproduktion vieler verschiedener Parameter kontrolliert, die für die Nachoxidation von grundlegender Bedeutung sind, wie z. B. Temperatur, Zusammensetzung der Abgase, Drucksignale, Luftverbrauch etc. Die Validierung demonstriert die Fähigkeit der Simulation, die Messungen zu reproduzieren und ihre Fähigkeit, einen tiefen Einblick in das analysierte Phänomen zu geben. Insbesondere war es notwendig, das spezifische Verhalten der Messverfahren numerisch nachzubilden, damit die Ergebnisse aus Prüfstand und Simulation vergleicht werden konnten. Das Interesse konzentrierte sich auf den Vergleich von Messungen und Simulationen für das Temperaturprofil vor der Turbine und die Zusammensetzung der Abgase im Auspuff.

Die Temperaturmessungen basieren auf Thermoelementen, die durch ein bestimmtes Volumen, Material und thermische Trägheit definiert sind. Bei der Simulation hingegen wird die Temperatur des Fluids an einer bestimmten Stelle des Berechnungsmodells ausgewertet, ohne diese Effekte zu berücksichtigen. Daher wurde ein numerisches Modell implementiert, das die

Effekten des realen Thermoelementes reproduziert und einen besseren Vergleicht ermöglicht.

Die Zusammensetzung der Abgase wurde am Prüfstand unter Verwendung einer MEXA-Anlage gemessen. Auch in diesem Fall imitiert ein numerisches Modell die Methodik des Messverfahrens und erhöht die Genauigkeit des Vergleichs.

Diese Validierungsprozesse ermöglichten eine detaillierte Abstimmung der Simulationen und gaben einen besseren Einblick in das chemische und physikalische Verhalten der Nachoxidation. Daher war es möglich, die Nachoxidation als eine chemische Reaktion zu beschreiben, die in einer dünnen Schicht abläuft, in der die besten Bedingungen in Bezug auf Temperatur, Durchmischung und Druck herrschen. Da die Reaktanten der Nachoxidation getrennt sind, kann sie chemisch als eine nicht vorgemischte, turbulente Reaktion modelliert werden.

Die Reaktion wird durch das Ausstoßen des Zylinders ausgelöst. Die heißen Abgase werden mit hoher Geschwindigkeit durch die Frischluftwolken des vorherigen Zyklus, die sich in der Nähe des Auslassventils angesammelt haben, in den Auspuffkrümmer gedrückt. Unter diesen Bedingungen starten die Temperatur und die Vermischung an der Grenzfläche zwischen heißen Gasen und Frischluft die Nachoxidationsreaktionen, die Wärme freisetzen und somit die Temperatur im Auspuffkrümmer erhöhen. Die höhere Temperatur stellt sicher, dass ein selbsterhaltender Effekt eintritt, der die Fortsetzung der chemischen Reaktionen ermöglicht.

Am Ende des Auspufftakts strömt die kalte Luft dank der langen Ventilüberschneidung und des hohen Ladedrucks aus dem Ansaugkrümmer bei niedriger Geschwindigkeit direkt zum Auspuff und sammelt sich in der Nähe der Auslassventile. Während des verbleibenden Teils des Zyklus steht zwar Luft zur Verfügung und es findet eine gewisse Vermischung an der Grenzfläche zwischen Frischluft und Abgasen statt, doch wird in der Regel nur sehr wenig Wärme freigesetzt, da die Temperatur zu niedrig ist. Daher bleibt die Frischluft für den folgenden Abgasvorgang verfügbar.

Der letzte Schritt der Validierung wollte überprüfen, ob die Annahme eines vereinfachten chemischen Reaktionsmechanismus nicht nur für das vereinfachte Modell, das in der Vorbereitungsarbeit angewendet wurde, sondern auch für das detaillierte 3D-CFD-Modell des Abgaskrümmers gilt.

Für diese Art von Simulationen wurde der detaillierte chemische Reaktionsmechanismus in das 3D-CFD-Modell implementiert. Dies hat die Rechenzeiten im Vergleich zum reduzierten chemischen Reaktionsmechanismus stark erhöht. Nur der Einsatz eines Hochleistungs-Computerclusters am FKFS/IFS Universität Stuttgart ermöglichte es, die Auswirkungen verschiedener Annahmen für die Randbedingungen zu testen.

Es wurde nachgewiesen, dass die Menge an langkettigen Kohlenwasserstoffen in den Abgasen einen starken Einfluss auf die Nachoxidation hat, indem sie den Reaktionsweg verändert. Darüber hinaus wird die Nachoxidationsreaktion langsamer, weil das Aufbrechen der langen Kohlenwasserstoffketten die für die endgültige Oxidation von CO und H_2 benötigten Radikale absorbiert.

Es hat sich jedoch gezeigt, dass die Genauigkeit des Modells nicht verbessert wird. Insbesondere ist es im Fall dieser Anwendung nicht realistisch, anzunehmen, dass langkettige Kohlenwasserstoffe an der Nachoxidation beteiligt sind. Es ist wahrscheinlicher, dass die Aufbrechung der Kohlenwasserstoffketten aufgrund der steilen Druck- und Temperaturgradienten in der Brennkammer beginnt. Daher kann die Annahme, dass der größte Teil der Wärmefreisetzung bei der Nachoxidation aus CO und H_2 stammt, als realistisch angesehen werden. Es wird auch demonstriert, dass die Anwendung eines reduzierten chemischen Reaktionsmechanismus in diesem Fall korrekt ist.

Nach der Validierung der Methodik wurde diese auf viele verschiedene Betriebspunkte angewendet, um Informationen darüber zu erhalten, wie sich die Nachoxidation unter verschiedenen Betriebsbedingungen verhält.

Besonderes Gewicht wurde darauf gelegt, dass der gesamte Motorbetrieb sehr nahe an der Stöchiometrie bleibt. Dies ist für einen sicheren Betrieb des Drei-Wege-Katalysator erforderlich und erfordert auch eine sehr enge Fehlergrenze, um den Wirkungsgrad hoch zu halten. Um einen insgesamt stöchiometrischen Betrieb zu erreichen, müssen zwei Faktoren eingestellt werden.

Der erste Faktor ist, dass die Spülluft den Sauerstoffmangel im Brennraum so genau wie möglich ausgleichen muss. Bei dieser Strategie hängt die Abstimmung von der Wahl der Ventilüberschneidung und der Regelung des Ladedrucks ab. Die Simulationen haben gezeigt, dass eine zu große Ventilüberschneidung häufig einen sehr hohen Luftverbrauch und einen

insgesamt mageren Motorbetrieb verursacht. Außerdem wird der Motorbetrieb instabil und reagiert sehr empfindlich auf Druckwellen, die vom Auspuff ausgehen. Auch der Ladedruck erfordert eine präzise Abstimmung, die mit Hilfe der Drosselklappe erreicht werden kann.

Der zweite Faktor, der für einen sicheren Betrieb des Drei-Wege-Katalysators erforderlich ist, ist eine gute Mischung der Gase, die zur Turbine und dann zum Katalysator strömen. Zu Beginn der Nachoxidation werden die Reaktanten in Form von Wolken im Abgaskrümmer getrennt. Durch die Vermischung soll erreicht werden, dass das Luft-Kraftstoff-Verhältnis der zur Turbine strömenden Gase konstant und sehr nahe an der Stöchiometrie bleibt. Eine unvollständige Durchmischung würde dazu führen, dass die Wolken aus frischer Luft und fetten Verbrennungsprodukten getrennt zur Turbine strömen, was einen wahrscheinlichen Verlust des Wirkungsgrads am Drei-Wege-Katalysator zur Folge hätte.

Ein Mapping der Wärmefreisetzung der Nachoxidation wurde durchgeführt, um zu beweisen, dass die Nachoxidationsstrategie auch unter anderen Bedingungen als denen, die für die Validierung verwendet wurden, funktioniert. Für alle untersuchten Betriebspunkte wurde der Gesamtmotorbetrieb sehr nahe an der Stöchiometrie gehalten.

Bei dem Mapping wurde festgestellt, dass die Nachoxidation durch Spülung unter vielen verschiedenen Bedingungen erfolgen kann, dass aber die Umwandlung von CO und H_2 in CO_2 und H_2O vor der Turbine fast nie abgeschlossen ist. Der Hauptgrund dafür ist, dass die Geometrie des untersuchten Motors keine bessere Vermischung von Verbrennungsprodukten und Frischluft bei den richtigen Temperaturbedingungen zulässt.

Darüber hinaus zeigte das Mapping der Wärmefreisetzungsrate der Nachoxidation, dass ein Kompromiss zwischen der Nachoxidation und der Temperatur vor der Turbine erforderlich ist. Die Nachoxidation benötigt eine höhere Temperatur am Auspuff, um die chemischen Reaktionen besser abschließen zu können. Die Temperatur vor der Turbine ist jedoch in der Regel durch die konstruktiven Grenzen der Turbine selbst begrenzt. Durch die Luftspülung wird die Temperatur im Abgas gesenkt, was nützlich sein könnte, um den Temperaturanstieg bei der Nachoxidation abzuschwächen. Das Mapping hat jedoch deutlich gezeigt, dass Nachoxidation eine maximale Grenze hat und vor allem von der Temperatur und geometrischen Faktoren abhängt.

Daher wurden Geometrieänderungen und Modifikationen der Randbedingungen durchgeführt, um die Sensitivität zu erhöhen. Die Untersuchung hat gezeigt, dass die Nachoxidation besonders empfindlich auf die Temperatur der Abgase reagiert, wenn es um den Beginn und den Selbsterhaltungseffekt der chemischen Reaktionen geht. Die Geometrie kann die Nachoxidation nur verbessern, wenn sie die Durchmischung der Reaktanten erhöht, indem sie z. B. eine größere Kontaktfläche zwischen Abgasen und Frischluft schafft.

Die gewonnenen Informationen wurden verwendet, um ein vereinfachtes Nachoxidationsmodell in QuickSim zu testen, das sich als einfach und zuverlässig erwiesen hat, weil es die bessere Simulation der Vermischung durch die Einbeziehung des gesamten Motors in die Simulation ausnutzt.

Die Ergebnisse der 3D-CFD-Simulationen wurden auch für die Entwicklung und Validierung eines Nachoxidationsmodells für eine 1D-CFD-Motorsimulation und für die Abstimmung des Motorbetriebs am Prüfstand verwendet.

Die Nachoxidation ist besonders empfindlich gegenüber der Temperatur der Abgase und der Vermischung im Abgaskrümmer. Um einen insgesamt stöchiometrischen Motorbetrieb zu erreichen, müssen diese beiden lokalen Parameter mit den Gesamtmotorparametern wie Spülung und Gemischbildung im Zylinder übereinstimmen.

Schließlich ist die 3D-CFD-Simulation ein grundlegendes Werkzeug für die Untersuchung der Nachoxidation. Die Kopplung von vollständigen Motorsimulationen mit detaillierten Simulationen des Abgaskrümmers zeigte sich als zuverlässig und genau. Die Implementierung eines reduzierten chemischen Reaktionsmechanismus lieferte die chemische Beschreibung der Nachoxidation.

Die Nachoxidation mittels Scavenging hat das Potenzial, einige der kommenden Herausforderungen der Motorenentwicklung zu meistern.

1 Introduction

1.1 Global scenario

The discussion about the role of internal combustion engines and transportation in the future must be framed in the more general landscape of the turning point that world and humankind is living. The pandemic that is sweeping the world causing so many casualties and grief is partially the unwanted result of the not sustainable development of our society, which is exhausting the natural resources of our planet and undermining the quality of life of future generations [1]. New studies and reports are continuously raising the attention towards a more sustainable development and a reduction of the human footprint [2] [3] [4]. Therefore, also the future of transportation must allow for human development, i.e. people must have the possibility to access personal transportation, while at the same time diminishing the pressure on the planet, i.e. reducing greenhouse gases (GHG) and pollutants emissions.

The access to energy is fundamentally connected to the development of the society [1] and the demand for energy is expected to grow in the future mostly fuelled by emerging countries [5]. In this scenario, global transportation-related demand of energy is expected to grow by 25% by 2040 [6]. In particular, personal light-duty vehicles will represent an important part of the energy demand in the future. Gasoline engines will still represent a great share of the market, also because many hybrid vehicles will rely on gasoline ICE [6]. It is therefore of maximum interest to develop strategies that increase the efficiency of spark-ignition (SI) engines.

This scenario represents an alternative to the idea of a regulated decrease [7], which makes it more realistic but also poses the problem of how to reconcile the material growth with the reduced human footprint on the planet. In December 2015 the fundamental milestone of the Paris agreement has been signed by 196 parties [8]. Such agreement has the goal to limit the global warming “well below 2°C above pre-industrial levels” [8] that has to be achieved by means of nationally determined contributions (NDC), in which the countries declare their goals for the reduction of GHG emissions and mitigations of the effects of the global warming.

1.2 Automotive industry

Also the automotive industry will have to operate and possibly thrive in this scenario, meaning that all the possibilities must be considered that allow for a reduction of CO_2 and pollutants emissions. At the moment, the most common propulsions systems are the internal combustion engine (ICE), based on liquid fossil fuels, and the battery electric vehicles (BEV), which rely on electric motors and which in the last few years are experiencing an important growth. The third relevant configuration present on the market is the hybrid electric vehicle, which exploits the advantages of the two previous propulsion systems and for which many different configurations exist [9].

A new approach that has been intensively studied in recent years is the use of renewable fuels, i.e. liquid fuels that are produced starting from environmental CO_2 and renewable energy. These fuels offer the advantage to be used in ICE while remaining carbon neutral. Due to the scalabilty of their production it is possible that they will play an important role in the future of the automotive industry.

The definition of the best solution for the de-carbonisation of personal transportation among the many possible shall be pointed out by means of a life-cycle assessment (LCA). Any other kind of analysis, e.g. a well-to-wheel analysis, is a simplification, which might have the unpleasant effect of shifting the problem of GHG emissions to other sectors of the production chain without solving it. Since GHG emissions are a global problem, moving those to different countries or production sectors, e.g. vehicle production or end-of-life, that are not taken into account does not solve the problem.

The LCA is a methodology that identifies and quantifies the environmental impact of a product during its whole life. In the case of the automotive industry, the LCA can be divided roughly into three different moments: production, use and end-of-life. This kind on analysis accounts not only for the GHG emissions but also for other effects such as acidification, human toxicity, particulate matter, photochemical ozone depletion and resource depletion.

Some studies [10] report that, taking into account also the production of the car, the GHG positive effect of a BEV depends greatly on the energy mix used for electricity production. Indeed, the construction of a BEV produces 80%

more $kgCO_{2eq}$ than the normal internal combustion engine vehicle (ICEV) [10] (in this case a gasoline standard engine), mostly because of the great energy needed for construction of the battery. During the use, instead, the amount of GHG emissions depends on the electric grid mix, at which the car is charged. For the European average electric mix, the BEV is a better choice after 50000 km. However, if the electric grid mix relies mostly on fossil fuels, e.g. coal, it is possible that the BEV never results convenient from the GHG emissions point of view in comparison to a ICEV [10]. Moreover, the production of batteries provokes damages in terms of acidification, human toxicity, particulate matter, ozone depletion and resource depletion usually greater than the ICEV [10] [11]. Therefore, ICEV in particular equipped with gasoline engines, have the potential to become a relevant factor for the reduction of human footprint on the planet, and, since they are usually cheaper than an equivalent BEV or hybrid electric vehicles (HEV), they will represent an interesting choice for the growing middle class [12].

The greatest amount of GHG emissions in the life of an ICEV happens during the use phase due to the exhaust of combustion products. Therefore, a good solution to reduce or even avoid GHG emissions is to use CO_2-neutral fluid fuels, in order to exploit the lower fingerprint of ICEV production and solve the problem of GHG emissions during use.

Synthetic fuels produced using renewable energies are generally called e-fuels and can contribute to the needed change in the transportation. Among the many different types of e-fuels the most interesting are the liquid ones that can be produced by means of the methanol-to-gasoline process. In this case, the natural resources required are water and CO_2 filtered from air [13]. The key factors to ensure that e-fuels have a potential of reducing GHG emissions is that renewable energy is used and that CO_2 is captured directly from the atmosphere [14]. In this scenario, ICEVs become a very interesting, cheap and less resource-intensive solution towards a carbon neutral transportation [15]. Moreover, e-fuels have the great advantage that can be used also in the already existing engines without any necessary modification, which would “transform” in very limited time and at low cost the already running ICEVs into CO_2-neutral vehicles [16]. Moreover, the already existing infrastructure of fuel stations and pipelines can be adopted for e-fuels and biofuels without changes.

The composition of e-fuels can be defined using a limited number of chemical species [17] and can be precisely determined in order to reduce emissions of ICE [18]. This enables the better design of future ICEs and reduces the emissions of the already running engines [19].

For all these reasons, the ICE used in combination with liquid e-fuels has the possibility to play an important role for the future of transportation for both personal light-duty vehicles and industrial heavy-duty vehicles. It is also important to stress that in the future each technology will be used for the scope that better fits, otherwise there is the risk to force the adoption of technology that is expensive for the consumer and does not benefit the environment. As an example, BEVs can reduce the local emissions and therefore are a good solution for city traffic; however, the environmental impact of BEVs increases with the dimension of the battery [11], i.e. for long range transportation ICEVs fuelled by synthetic fuels are more environmentally sustainable.

Another important role in shaping the future of ICE will be played by the regulations of other pollutant emissions different from GHG gases. While the CO_2 regulations are thought to solve a global problem, pollutant emissions regulations deal with the local quality of air and consequently the health of people. The most relevant regulated pollutants are CO, NO_X, unburned hydrocarbons (HC) and particulate matter (PM). The European Union (EU) has been regulating the emissions of these pollutants since the first Euro emission standard in 1992 [20]. These emission standards had the effect of both challenge the automotive industry and of reducing the exposition of people to harmful pollutants. The homologation procedure of new car models is based on the emission measurement during a driving cycle; up to the Euro 6 standard the test used was the New European Driving Cycle (NEDC), which, however, proved to poorly represent the pollutant emissions in real driving conditions [20]. Therefore, in 2017 the commission regulation (EU) 2017/1154 has been implemented, that requires a real driving emissions (RDE) test for the approval of a new model. Also the NEDC cycle has been replaced with the more challenging World Harmonized Light-Duty Vehicle Test Procedure (WLTP). At the moment the discussion about the following standard emission Euro 7 is on-going, however, it is clear that in the future cars will have to exhaust even less pollutants and more pollutants will be measured during the test [21]. In particular, it is probable that the attention for the cold-start conditions will increase, since those represent the most relevant source of pollutants emissions during an RDE cycle [22] [23] [24].

Therefore, the major challenges that the automotive industry will face in the foreseeable future will be the reduction of GHG emissions and the reduction of pollutants emissions. This will sum up to the need of reducing both costs and time of development, since OEMs are forced to make great investments in other new and strategic fields such as electrification and advanced driver-assistance systems (ADAS).

1.3 Motivation and objectives

Post-oxidation is a strategy that has the potential to deal with some of these problems and that it has not been yet thoroughly investigated and understood. Post-oxidation consists in performing a rich in-cylinder combustion that produces CO and H_2 as exhaust products. The rich combustion products are then completely oxidized in the exhaust manifold by means of oxygen (fresh air, lean EGR, etc.). The oxidation reaction transforms CO and H_2 into CO_2 and H_2O respectively, therefore reducing the emissions, and at the same time raises temperature and enthalpy of the exhaust gases thanks to the heat release rate of the reaction. The temperature increase can be exploited to reduce the time needed for catalyst heating while keeping the overall engine operation close to stoichiometry. Many different types of post-oxidation are possible. Among them, the most common is post-oxidation by means secondary-air injection [25], which consists in using an air pump to inject fresh air in proximity of the exhaust valve. Such strategy proved to be reliable but increases the complexity and cost of the engine. A simpler solution that has been analysed in the following investigation is post-oxidation by means of scavenging. The strategy has been tested on a four-cylinder, turbocharged, direct injection, spark-ignition engine and it consists of a rich in-cylinder combustion followed by a great amount of scavenging due to a very long valve overlap. Fresh air and rich-combustion products mix in the exhaust manifold and start post-oxidation. Moreover, the downsizing of direct injection spark ignition (DISI) engines by means of a turbocharger delays the torque build-up during transient operation (phenomenon also known as turbo-lag). The introduction of RDE measurements increases the need for improved transient engine behaviour while keeping the emissions to a minimum. The turbo-lag origins in the lack of mass flow through the turbine to overcome the rotating inertia. A smaller sized turbine would decrease the rotating inertia but, at the

same time, decreases the engines rated power [26]. One possible solution could be to use a variable geometry turbocharger (VGT), however, the engine becomes more complicated and expensive. Another possibility to increase the mass flow rate through the turbine is to use a long overlap of inlet and exhaust valve lifts. This allows fresh air to flow through the cylinder without participating in the combustion during the scavenging event [27]. Therefore, post-oxidation by means of scavenging has also the possibility to reduce the turbo-lag, while keeping the overall stoichiometric engine operation.

Previous investigations of post-oxidation [25] already pointed out the difficulty to determine the amount of post-oxidation, as well as the most relevant influences. Therefore, the investigation must rely on a coupling of test-bench and 3D-CFD investigations. In the following, the procedure used to investigate post-oxidation by means of scavenging is presented with special attention to 3D-CFD modelling. At first, post-oxidation has been analysed at the test-bench, where detailed measurements have been performed. Afterwards, these measurements have been used to validate two different kinds of 3D-CFD simulations: full engine simulations with the 3D-CFD tool QuickSim [28]; detailed model of the exhaust manifold with chemical reaction mechanism and fine mesh.

2 Fundamentals

Post-oxidation is a chemical reaction triggered by the mixing happening in the exhaust manifold of an ICE. A realistic simulation of post-oxidation requires that both the chemical reactions and the flow field are simultaneously modelled. The computational model should be able to simulate the chemical reactions in the exhaust and to include the complete engine.

The simulation of chemical kinetics must focus on what happens at the very small temporal and spatial scales of the molecular interactions and it is necessary for the determination of the efficiency of post-oxidation, the heat release rate and the correlation of macro parameters, e.g. turbulence and geometry, with local chemical reactions. The simulation of chemical kinetic is usually based on the implementation of chemical reaction mechanisms that are specially developed and validated for specific porpoises. Moreover, it requires a fine discretization of the computational grid and the time-step.

The simulation of the flow field, instead, is necessary for the description of the mixing of gases, local inhomogeneity and local conditions of chemical composition and temperature. The precise description of these effects requires the inclusion in the computational model of the whole engine and the complex phenomena typical of engine operation (e.g. cylinder-to-cylinder interaction, injection, heat release, wall heat exchange, etc.). In this case, the simulation can rely on general equations and models that have already been extensively tested and validated for many engine applications.

It is possible to reproduce in a single model all these aspects, however, it requires a great amount of computational power and time. Therefore, a specific methodology has been developed for the simulation of post-oxidation that is reported in §4. The applied methodology devides the simulation into two steps: the 3D-CFD-full engine simulation and the detailed simulation of the exhaust manifold. The first step focuses on an accurate simulation of the engine operation and the second on the chemical kinetics of post-oxidation.

In the following chapter the fundamentals of chemical reactions kinetics and 3D-CFD simulation are reported.

This chapter will focus only on the application of post-oxidation and is by no means a complete description of the simulations methodology. The interested reader can refer to the specific literature (e.g. [29], [30], [31] and [32]).

2.1 Fundamentals of chemical kinetic simulation

In equation (2.1.1) a general reaction equation is reported, where the chemical species A and B are the reactants and C and D are the products. The factor ν_i relates to the reaction order [30].

$$\nu_A \cdot A + \nu_B \cdot B \overset{k_f}{\rightarrow} \nu_C \cdot C + \nu_D \cdot D \tag{2.1.1}$$

The reaction proceeds consuming the species A and B and producing the species C and D. The parameter that describes the speed at which the reaction proceeds is the reaction rate k_f. The consumption rate of A can be described by equation (2.1.2).

$$\frac{d[A]}{dt} = -k_f [A]^{\nu_A} [B]^{\nu_B} \tag{2.1.2}$$

Where [A] is the concentration of A in mol/m^3. The higher the reaction rate k_f, the faster the decrease of [A]. The decrease of [A] is also proportional to [B] (concentration of B) and [A] itself. The higher the reactant concentrations, the more likely the reactants will have an interaction and will form the products. The reaction orders ν_i describe the change in reaction rate for the different chemical species concentrations involved in the reaction. The overall reaction order in this case is $(\nu_A + \nu_B)$.

The constant k_f is the result of the molecular interactions, which tend to increase as the temperature and the energy of the system increases. Therefore, it is proportional to the temperature and to the overall reaction order. The most common approach to calculate k_f is the empirical modified Arrhenius approach described in the following equation:

$$k = A \cdot T^b \cdot e^{\frac{-E_A}{R_u \cdot T}} \tag{2.1.3}$$

E_A is the activation energy (the minimal energy needed to start the reaction); A is the pre-exponent multiplier and has different meanings if the reacting

species are uni-, bi- or trimolecular reactions. For a bimolecular reaction like the example of equation (2.1.1), A represents the collision rate of molecules, which is a measure of the probability of the reaction [30]. In order to limit the increase of the reactivity, the exponent b of the temperature factor is needed. Otherwise, the reactivity would grow indefinitely with temperature, which is not realistic.

The reaction of equation (2.1.1) can take place also in the opposite direction, i.e. C and D are the reactants and A and B the products, if the conditions are correct. In this case, the reaction rate is the reverse reaction rate k_r. The complete reaction equation is:

$$\nu_A \cdot A + \nu_B \cdot B \underset{k_r}{\overset{k_f}{\rightleftarrows}} \nu_C \cdot C + \nu_D \cdot D \tag{2.1.4}$$

Therefore, the net production or consumption rate of A is the difference of the of the forward and backward reaction rates:

$$\frac{d[A]}{dt} = -k_f[A]^{\nu_A}[B]^{\nu_B} + k_r[C]^{\nu_C}[D]^{\nu_D} \tag{2.1.5}$$

The greater is the consumption rate of A ($-k_f[A]^{\nu_A}[B]^{\nu_B}$) and the lower is the production rate of A ($+k_r[C]^{\nu_C}[D]^{\nu_D}$) the faster the concentration of [A] reduces over time. The smaller the difference between consumption and production of A, the smaller and slower will be the change in concentration of A. Therefore, in specific conditions, it is possible that the consumption equals the production and the concentration of A remains stable in time. This condition is called chemical equilibrium and it is described by the following equation:

$$\frac{d[A]}{dt} = -k_f[A]^{\nu_A}[B]^{\nu_B} + k_r[C]^{\nu_C}[D]^{\nu_D} = 0 \tag{2.1.6}$$

After some simple elaboration, the equation becomes:

$$\frac{k_f}{k_r} = \frac{[C]^{\nu_C}[D]^{\nu_D}}{[A]^{\nu_A}[B]^{\nu_B}} = K_C \tag{2.1.7}$$

K_C is the equilibrium constant and depends on the concentrations of all the species participating to the reaction. As demonstrated in [30], the equilibrium

constant can be expressed as function of partial pressures of each involved chemical species as it follows:

$$K_P = \frac{p_C^{\nu_C} \cdot p_D^{\nu_D}}{p_A^{\nu_A} \cdot p_B^{\nu_B}} = K_C \cdot (R_u T)^{\nu_C + \nu_D - \nu_A - \nu_B} \tag{2.1.8}$$

The equilibrium constant K_P can be calculated using the Gibbs free energy of the involved chemical species, which is a function of the molar enthalpy and molar entropy of each chemical species. The standard values of Gibbs energies are listed in tables. The interested reader can refer to [29] and [30].

With this set of equations and the information about the Gibbs free energy it is possible to define a system that determines the chemical composition at equilibrium for a specific reaction. The dimension of the equation system depends on the number of chemical species that are considered.

The chemical equilibrium is the composition of species of the system if an infinite amount of time is available for the reactions. Since the reactions do not have infinitely fast reaction rates, the actual chemical composition of the system will approach the composition at equilibrium depending on the time available for the reactions. The distance of the actual composition from the one at chemical equilibrium after a given amount of time depends on the reaction rate: the faster the reaction rate, the closer to the chemical equilibrium will be the actual composition.

The reaction rates depend strongly on temperature; in systems with high temperatures, the reactions will progress faster and the final composition will be closer to the composition at equilibrium while in systems with a lower temperature the reaction rates will be lower.

2.1.1 Chemical reaction mechanisms

The application of chemical kinetic to general reacting systems with many species and complex reaction paths is routinely carried out using the chemical reaction mechanisms. In the following section chemical reaction mechanism fundamentals are reported. The discussion will focus on chemical reaction mechanisms for the simulation of combustion and post-oxidation.

The overall oxidation process of fuel and oxidizers can be expressed by a reaction equation in the form of (2.1.1). In order to give a practical example, the oxidation reaction of H_2 will be presented in the following. The overall oxidation of H_2 can be described with the chemical reaction equation:

$$2H_2 + O_2 \rightarrow 2H_2O \tag{2.1.9}$$

The global reaction equation is useful to summerize the overall reaction that is being described. However, the probability that two H_2 molecules hit an O_2 molecule simultaneously and form two H_2O molecules is very low. Such event would require the simultaneos breaking of many chemical bonds and the formation of several new ones. The reaction equation represents the overall oxidation process but not the single, smaller steps that actually happen during the chemical process [29] [30].

The global reaction equation (2.1.9) is the global result of many elementary reactions that take place during the actual kinetic chemistry and that causes the formation of many intermediate species. Indeed the collision of three molecules is less probable than the collision of two molecules. Therefore, it is more probable that only one molecule of H_2 collides with one molecule of O_2 and form HO_2 and H as intermediate species (2.1.10). Moreover, the formation of HO_2 is easier than the formation of H_2O since it requires only one chemical bond to be broken and one to be formed.

$$H_2 + O_2 \rightarrow HO_2 + H \tag{2.1.10}$$

In order to understand the overall oxidation path it is important to be able to determine precisely the formation and consumption of intermediate species generated by elementary reactions.

If an intermediate species has an unpaired electron, it is very likely that it will react with other species and create new chemical bonds. Therefore, these kinds of chemical species are very reactive and called radicals or free radicals. The availability of radicals is connected to the reaction speed in the system. There are four main types of reactions including radicals:

- Chain initiation: when an elementary reaction produces one radical without consuming any;
- Chain propagation: when an elementary reaction produces one radical and consumes one radical;

- Chain branching: when an elementary reaction produces more radicals then the ones it consumes;
- Chain terminating: when an elementary reaction consumes more radicals than the ones it produces.

Chain initiation are fundamental to start the reaction. Chain propagation reactions do not speed up the reaction rate but neither they slow down the reaction rate; in this case the overall amount of radicals remains constant. The chain branching reactions are the ones that speed up the reaction rate by increasing the total amount of radicals available. Finally, the chain terminating reactions reduce the overall amount of radicals and by doing so they reduce the chemical reaction rate [30].

Radicals are fundamentals for many different oxidation processes. In particular, in the case of post-oxidation the availability of radicals is necessary for the oxidation raction of rich combustion products and fuel.

The formation of radicals is strongly dependent on the temperature of the mixture. The higher the temperature, the greater the formation of radicals the the faster the reaction rate. If the temperature is low, less radicals will be produced by means of chain initiating and chain branching reactions and the system will react slowlier. One possibility to speed up the reaction is to increase the amount of reactants. Referring to the equation (2.1.2), A is the general fuel molecule that must react with the radical B; if the system is operated at low temperature, in order to keep k_f high at low temperatures, the concentration of B must be high.

At low temperatures the production of B is low. However, as soon as the reaction starts, there is a certain amount, which raises the temperature of the system, therefore increasing the production of B by means of chain branching reactions. This effect is self-reinforcing and the oxidation proceeds quickly. The time needed to build up the necessary amount of radicals that start and speed up the reaction is called chemical ignition delay [29] [30] and it plays a relevant role also in post-oxidation, as it will be later demonstrated.

The example of equation (2.1.9) is the simplest oxidation reaction possible. Yet, the complete chemical reaction mechanism accounts for more than 20 different elementary reaction [30]. In the case of more complex oxidation reactions, such as fuel or CO oxidation the number of elementary reactions

increases rapidly. Therefore, when choosing the chemical reaction mechanism, it must be payed attention that the necessary reactions are included but the number of other chemical reactions must be limited. The chemical reaction mechanisms must be also validated for the range of boundary conditions of interest.

The structure of a general chemical reaction mechanism, like the ones used in this study (e.g. [33] and [34]) consists of a list of the chemical elements that are involved in the reactions, a list of the elementary chemical reactions and the parameters of the modified Arrhenius approach that are necessary to calculate the forward reaction rate k_f

Moreover, the NASA polynomials (equations from (2.1.11) to (2.1.13)) are necessary for the calculation of thermodynamic quantities. The data includes the value of the parameters $a_1 – a_7$ for each species included in the reaction mechanism. These polynomials are necessary for the calculation of the chemical equilibrium by means of the constant K_p or K_C.

$$\frac{c_p}{R} = a_1 + a_2 T + a_3 T^2 + a_4 T^3 + a_5 T^4 \tag{2.1.11}$$

$$\frac{H^0}{RT} = a_1 + \frac{a_2}{2} T + \frac{a_3}{3} T^2 + \frac{a_4}{4} T^3 + \frac{a_5}{5} T^4 + \frac{a_6}{T} \tag{2.1.12}$$

$$\frac{S^0}{R} = a_1 \ln(T) + a_2 T + \frac{a_3}{2} T^2 + \frac{a_4}{3} T^3 + \frac{a_5}{4} T^4 + a_7 \tag{2.1.13}$$

The number of chemical reaction mechanisms freely available is relatively limited and the reason is that in order to create one mechanism very complex and extensive investigations have to be carried out both in the numerical and for the experimental field. Usually the chemical reaction mechanisms for the oxidation of long-chain hydrocarbons have hundreds of species and many thousands of chemical reactions. This is needed in order to have a high level of generality and be able to simulate many different oxidation processes without the need for simplifications and assumptions. However, the computational time and effort increase drastically. A solution is to reduce the number of species and reactions by choosing the ones that are necessary for the application of interest. In the case of post-oxidation, for example it will be demonstrated that the simulation of long-chain hydrocarbons does not increase the accuracy of the simulation, which allows a drastic reduction of the number of species and reactions. The reduced chemical reaction mechanism is able to

correctly simulate post-oxdation in a lower time and with lower requirements for what concerns computational power. Possible mechanism reduction methodologies are described in [35] and [36].

For the particular application of 3D-CFD simulation to post-oxidation, chemical reaction mechanisms are necessary for the simulation of the reacting fluid. They describe for each time-step the chemical reactions that happen locally in each cell of the computational grid; its consequences in terms of heat release and change in the composition of the fluid are then connected to the flow field. The information about local temperature, composition and pressure in the cell are instead given by the 3D-CFD flow field simulation. The connection between these two models is the flame front where the reactions take place. Post-oxidation, as it will be discussed in detail in §6, is a non-premixed turbulent flame and requires the simulation of both the flow field and the local chemical effects in order to be correctly reproduced.

2.2 Fundamentals of 3D-CFD simulation for ICEs

Starting from the sixties, as computational power started to increase, engine designers use, besides theoretical knowledge and experimental test also computational models. The advantages that the modelling offers are a reduction of time and costs, and a great flexibility and possibility to test different variables. Therefore, the computational models are widely used and will for sure play an essential role in designing the future engines.

The current standard of the so-called virtual engine development consists of three main tools:

- Real working process calculation. It consists in a 0D approach based on fundamental energy conservation equations but it is unable to calculate any kind of temperature or species distribution;
- One-dimensional computational fluid dynamics (1D-CFD). It focuses on the simulation of the engine as a whole and simulates the thermodynamic processes by means of 1D assumptions;
- Three-dimensional computational fluid dynamics (3D-CFD). In this case, the very general flow field is calculated and the geometries of the engines

are discretized by means of a three-dimensional computational grid. In each cell of the grid the conservation equations and the equations of fluid mechanics are solved, ensuring the highest level of accuracy.

2.2.1 Real working process analysis

The real working process is a simple analysis of thermodynamic processes inside the engine. It is based on the energy conservation equation, the mass conservation equation and the thermal equation of state. Since the model is so simple, it can be implemented easily and requires very little calculation power and time. The type of analysis is very useful in order to carry out a first evaluation of the processes taking place inside the engine.

2.2.1.1 First law of thermodynamics (energy balance)

The definition of the first law of thermodynamics has been proposed by Hermann von Helmholtz around the year 1850 and it states: the sum of all energies is constant in an isolated system.

$$Q_B + Q_W + H_I + H_E + H_L + W = 0 \tag{2.2.1}$$

Where Q_B is the fuel heat release, Q_W is the wall heat transfer, H_I is the intake enthalpy, H_E is the exhaust enthalpy, H_L is the enthalpy of the leakage and W the work produced on the piston, considering the whole cycle. The time derivative of the the energy balance describes the changes of internal energy U over time. If $d\varphi$ is the crank angle derivative, the formulation of the energy balance allows the cranck-angle resolved analysis of the whole cycle.

$$\frac{dQ_B}{d\varphi} + \frac{dQ_W}{d\varphi} + \frac{dH_I}{d\varphi} + \frac{dH_E}{d\varphi} + \frac{dH_L}{d\varphi} + \frac{dW}{d\varphi} = \frac{dU}{d\varphi} \tag{2.2.2}$$

2.2.1.2 Mass balance

A similar balance can be carried out for the mass in the cylinder.

$$\frac{dm_C}{d\varphi} = \frac{dm_I}{d\varphi} + \frac{dm_E}{d\varphi} + \frac{dm_L}{d\varphi} + \left[\frac{dm_B}{d\varphi}\right]_{DI} \tag{2.2.3}$$

Where m_C is the mass inside the cylinder, m_I the mass of fresh air entering the volume, m_E the mass of exhaust gases leaving the cylinder, m_L the mass of air due to leakage and blow-by and finally m_B is the mass of fuel in case of direct injection engines.

2.2.1.3 Thermal equation of state

In order to complete the model the equation of state is necessary for the correlation of the thermodynamic variables.

$$p \cdot V = m \cdot R_s \cdot T \tag{2.2.4}$$

For typical ICE applications, the assumption of ideal gas is usually acceptable as the engine is operated in a range of pressures and temperatures, which is far away from the condensation conditions.

The drawback of a real working process analysis (0D simulation) is that it is usually necessary to introduce parameters that must be tuned for each engine operating point, therefore reducing the predictability of the models.

2.2.2 1D-CFD simulation

Real Working Process analysis are usually coupled with 1D-CFD simulations that allow a spatial resolution of the fluid movement on the main direction of the engines. The model usually includes the whole volume of the engine that is afterwards divided into a finite number of sub-volumes that enable the calculation of the flow field in one direction by solving the conservation equations in each volume (continuity, momentum and energy). The combustion process is modelled using phenomenological or quasi-dimensional models and correlations. These models are able to roughly reproduce the most relevant influence of factors such as the geometry of the combustion chamber and of the piston, the in-cylinder flow motion like tumble and swirl.

The 1D-CFD simulation are very interesting for the investigation of transient behaviours like change in rpm or rapid changes in the power output. It is also common to include the model of the turbocharger in order to carry out a complete turbo-matching. The advantage of modelling the whole engine is that

these simulations are able to cover the whole engine map of the engine up to the simulation of complete RDE and WLTP cycles.

The drawback of 1D-CFD simulations is that although they are able to model also complete engine, they are not the right tool to simulate changes in detailes of the geometry (e.g. spray targeting, geometry of the combustion chamber…).

For the specific case of post-oxidation, the 1D-CFD simulation has a too coarse spatial discretization and it cannot simulate the local inhomogeneity, without which the simulation of post-oxidation is not possible. In order to simulate post-oxidation a specific model must be developed, which however needs data for its development and validation. These limitations can be compensated by adopting 3D-CFD simulations.

2.2.3 3D-CFD simulation

The 3D-CFD simulation completes the design process of a new engine. It enables a great level of detail and theoretically does not require neither simplifications in terms of geometry nor semi-empirical models based on tune-parameters for the simulation of complex processes such as mixing and fluid movement in the cylinder. On the downside, however, the needed computational time and power increase greatly in comparison to the other kinds of simulations listed above. Therefore, the application of 3D-CFD simulation to engine design focuses mostly on the description of specific complex behaviours during engine operation, its understanding and tuning.

3D-CFD simulation is based on the discretization of the volume of interest into finite volumes by means of the so-called computational grid or mesh. Each volume is defined as a cell and the centre of the cell is where the discretized Navier-Stokes (NS) equations are solved. The assumption is that, since the analytical solution of the NS equations is available only for a very limited number of applications of little practical interest, the dimension of the computational grid and the discretization schemes permit to calculate a numerical solution of flow field very close to the real one. In the following the fundamental equations of the 3D-CFD simulations are shortly reported, however, it does not intend to be a complete description of the methodology. The interested reader can refer to specific lectures such as [31], [32].

2.2.3.1 Fundamental equations

Using the Euler approach, it is possible to write the conservation equation of a general intensive variable $f(\vec{x};t) = dF/dV$ function of position and time in the form:

$$\frac{\partial f}{\partial t} + div\vec{\Phi}_f = s_f + c_f \tag{2.2.5}$$

The equation (2.2.5) states that a change in time of the intensive variable $\frac{\partial f}{\partial t}$ can originate from a flux through the volume delimited by the surface $\vec{\Phi}_f$, by a source or sink s_f or by long-range processes c_f.

Such general formulation can be applied to the different variables of the CFD problem. If the function $f(\vec{x};t)$ is the density, the source and long-range process terms are zero because mass cannot be created nor can undergo any kind of long-term process and the equation becomes:

$$\frac{\partial \rho}{\partial t} + div(\rho\vec{v}) = 0 \tag{2.2.6}$$

If i species are present in the system, the equation becomes:

$$f = \rho_i = \rho w_i \tag{2.2.7}$$

$$\vec{\Phi}_f = \rho_i\vec{v}_i = \rho_i\left(\vec{v}_i + \vec{V}_i\right) = \rho_i\vec{v}_i + \vec{j}_i \tag{2.2.8}$$

$$s_f = M_i\omega_i \tag{2.2.9}$$

$$c_f = 0 \tag{2.2.10}$$

Where:

- $w_i = m_i/m$ is the mass fraction of the species i;
- The local flow velocity $\vec{v}_i$ is substituted by means of the flow velocity $\vec{v}$ and the diffusion velocity $\vec{V}_i$, which generates a species diffusion mass flux $\vec{j}_i$;
- The source term s_f is the product of the molar mass M_i of the i species and its molar fraction rate ω_i.

Therefore, the conservation equation becomes:

$$\frac{\partial \rho w_i}{\partial t} + div(\rho w_i \vec{v}) + div(\vec{j}_i) = M_i \omega_i \tag{2.2.11}$$

In the case the intensive variable is the specific energy of a fluid, the following consideration can be done:

$$f = \rho e = \rho \left(u + \frac{1}{2} |\vec{v}|^2 + G + h_f \right) \tag{2.2.12}$$

Where u is the internal energy, $\frac{1}{2}|\vec{v}|^2$ is the kinetic energy, G is the gravitational energy and h_f is the enthalpy of formation of the mixture. The energy conservation equation can be defined after making the following considerations:

$$\vec{\Phi}_f = \rho e \vec{v} + \bar{\bar{P}} \vec{v} + \vec{j}_q \tag{2.2.13}$$

$$s_f = 0 \tag{2.2.14}$$

$$c_f = q_r \tag{2.2.15}$$

Where:

- $\vec{\Phi}_f$ is composed by the sum of the convective heat exchange $\rho e \vec{v}$, the energy transport term due to pressure shear stresses $\bar{\bar{P}} \vec{v}$ and energy transport due to heat conduction $\vec{j}_q$;
- It is assumed that there are no energy sources inside the control volume;
- The long-range term c_f is given by the contributions of radiations or magnetic fields.

The conservation equation for energy results:

$$\frac{\partial (\rho h_{tc})}{\partial t} - \frac{\partial p}{\partial t} + div\left(\rho h_{tc} \vec{v} + \vec{j}_q\right) + \bar{\bar{P}} : grad(\vec{v}) - div(p\vec{v}) = q_r \tag{2.2.16}$$

Where h_{tc} is the thermal and chemical contribution, respectively h and h_f:

$$h_{tc} = h + h_f \tag{2.2.17}$$

Finally, the equation for the conservation of momentum can be desumed as follows:

$$f = \rho\vec{v} \tag{2.2.18}$$

$$\overrightarrow{\Phi}_f = \rho\vec{v} \otimes \vec{v} + \bar{\bar{P}} \tag{2.2.19}$$

$$s_f = 0 \tag{2.2.20}$$

$$c_f = \rho\vec{g} \tag{2.2.21}$$

Where:

- $\rho\vec{v}$ is the momentum density;
- $\overrightarrow{\Phi}_f$ is composed by a convective term $\rho\vec{v} \otimes \vec{v}$ and a second-order stress tensor $\bar{\bar{P}}$;
- c_f represents the gravitational contribution $\rho\vec{g}$.

$\bar{\bar{P}}$ is the second-order stress tensor that describes the variation in momentum due to viscous effects $\bar{\bar{\Pi}}$ and the pressure p. The momentum flux results:

$$\overrightarrow{\Phi}_f = \rho\vec{v} \otimes \vec{v} + \bar{\bar{P}} = \rho\vec{v} \otimes \vec{v} + p\bar{\bar{I}} + \bar{\bar{\Pi}} \tag{2.2.22}$$

The resulting conservation equation for the momentum can be formulated as:

$$\frac{\partial(\rho\vec{v})}{\partial t} + div(\rho\vec{v} \otimes \vec{v}) + div(\bar{\bar{\Pi}}) - grad(p) = \rho\vec{g} \tag{2.2.23}$$

2.2.3.2 Turbulence modelling

All CFD simulations of internal combustion engines are in turbulent regime, therefore, the model must be able to represent the effects of turbulence. There are many possibilities to model turbulence, in the following the three most common approaches are briefly discussed focusing on the trade-off of accuracy and computational time. For a more detailed description of the types of simulations, the reader can refer to [31], [32] and [37].

The equations reported in the previous paragraph are able to describe any kind of flow field. The direct discretization and application of these equations is a

well-known technic called direct numerical simulation (DNS). Such application does not require any further model in order to simulate any kind of flow field, both turbulent and laminar. The drawback is that it also requires a very fine discretization of both space and time. This results in a very fine computational grid and a very small time-step of the simulation. The dimensions are characteristic of the fluid flow analysed and are dictated by the dimension of the smallest turbulence eddy; in general an estimation of the grid points N is proportional to the Reynolds number Re:

$$Re = \frac{\rho|\vec{v}|l}{\mu} \tag{2.2.24}$$

$$N \cong Re^{9/4} \tag{2.2.25}$$

Therefore, the dimension of the problem explodes even for the very small geometries reaching calculation times up to many years [31]. Moreover, the level of detail granted by DNS is much greater than what is usually required for virtual engine development.

One of the most important characteristic of turbulence is that, while the large eddies (i.e. whose dimension is around 2 mm) have a shape that can be very different depending on the geometry of the problem, the small eddies are nearly isotropic and have a universal behaviour. The small eddies are also characterized by the smallest time and spatial turbulent scales that make the problem computationally extremely stiff. A possible solution is to filter the small eddies and substitute them with a model, while carrying out a complete description of the large eddies. Such kind of simulation is called large eddies simulation (LES) and it is already been used for some engine applications [38]. However, LES are usually applied to problems in which the domain is limited and the needed level of detail is high, e.g. spray analysis. Indeed, LES are faster than DNS simulations but they still require a very fine computational grid.

The last simulation methodology widely adopted is the Reynolds-Averaged Navier-Stokes (RANS) equations. This methodology allows to use a coarser computational grid and a longer time-step interval. They rely, as the name says, on the averaging of the Navier-Stokes equations and on the division of the velocity contribution into two components: the mean and the fluctuating velocity. This methodology allows the best trade-off of accuracy and computational time for the engine applications, however, the effects of

turbulence must be completely modelled. The most common approach for engine application is the k-ε turbulence model, which is based on two additional transport equations for turbulent kinetic energy (k) and the rate of dissipation of turbulent kinetic energy (ε). The k- ε has been tested on a variety of different kinds of flows with good results, in particular for confined flows, as for the case of ICE.

2.2.3.3 Modelling of working fluid and chemical reactions

Post-oxidation can be modelled as a turbulent non-premixed flame that uses as fuel the rich combustion products, which are in the gas-state, and as oxidizer the fresh air or lean EGR. The modelling of chemical reactions requires that each species that takes part to post-oxidation is modelled. The transport equation of species has already been reported above (equation (2.2.11)), which it is reported also here:

$$\frac{\partial \rho w_i}{\partial t} + div(\rho w_i \vec{v}) + div(\vec{j_i}) = M_i \omega_i \tag{2.2.11}$$

The simulation must solve one transport equation for each species included in the chemical reaction mechanism. This increases the computational power required for the simulation and, as it will be demonstrated, the number of species to be included for the simulation is a fundamental tuning parameter. The greater the number of species the lower the number of assumptions that has to be done for what concerns the boundary conditions of system and the chemical composition of the inflowing mass flow rate. However, the computational time explodes quickly without necessarily increasing the accuracy of the results. Another important factor to be taken into account is that the increase of chemical species, i.e. of transport equations, makes the simulation numerically more unstable, which again could result in not accurate solutions.

Similar adaptations must be carried out also for the other equations [31] [39] [40] [41].

In order to determine the mass source term $M_i \omega_i$ of each involved species, for each cell and time-step the chemical reaction mechanism must be solved. The solution of the chemical reaction mechanism for each cell can become quickly extremely time-expensive [42], therefore, some assumption is necessary in

order to simplify and speed-up the simulation. All the assumption, however, must be verified against experimental evidences.

Since when using RANS equation the turbulence is not directly simulated, the interaction of turbulence with chemical reaction kinectics requires an additional model, commonly known as turbulence-chemistry interaction model. One of the most commonly used turbulence-chemistry interaction models for the implementation of complex chemistry in 3D-CFD simulations is the so-called flamelet model [30], which is more adequate than the Eddy Break-Up model for the simulation of post-oxidation [43].

In both cases, at first it is necessary to implement in the model the chemical reaction mechanism in the form already described (§2.1.1).

The Eddy Break-Up model calculates the mean reaction rate by means of empirical models that assume that it is proportional to the turbulence dissipation rate. As the name suggests, the underlaying physical assumption is that the break-up of turbulent eddies is the limiting factor to the reaction rate. As the turbulence dissipates, fresh reactants mix and react. Numerically it results in the substitution of the kinetic rates by a single turbulent mixing scale. Therefore, the model is usually adopted only for small chemical reaction mechanism (one ore two steps), which would be a strong simplification in the case of post-oxidation.

The flamelet model, instead, assumes that the assumes that a turbulent flame can be approximated as an ensemble of laminar flamelets [44], where flamelets are thin structures where the post-oxidation (i.e. mixing, heat release…) takes place. This model calculates the reaction rate in each cell as function of the local species mass fractions, pressure and temperature. This corresponds to resolve the chemical reaction mechanism for each time-step in each cell. Such modelling increases the computational effort with respect to the Eddy Break-Up model but it is better suited for more complex chemical reaction mechanisms. The model precomputes reactions for representative scenarios and tabulates the relevant quantities before starting the simulation, in order to speed up the solution at each iteration.

At each time-step the chemical state in each cell is integrated from the state (w_i, T, p) to the state $(w_i, T, p)^*$:

$$w_i^* = w_i + \int_0^\tau r_k(\boldsymbol{W}, T, p)dt \tag{2.2.26}$$

Where r_k is the reaction rate as function of vector of the mass fractions ($\boldsymbol{W}$), the temperature (T) and the pressure (p) during the integration time τ.

The source of species molar fraction is then solved as:

$$\omega_i = \rho\left(\frac{w_i^* - w_i}{\tau}\right) \tag{2.2.27}$$

Where ρ is the density.

The application of the flamelet model assumes that the chemical reaction is much faster than the turbulent time-scale. This assumption is known as "fast chemistry" assumption and it is generally considered to be realistic for chemical reactions happening at high temperature (>1000 K).

As the 0D chemical kinetic investigations demonstrated, it is realistic to model post-oxidation as "fast chemistry" because of the very high reaction rates for temperatures higher than 1000 K. Below this temperature, instead, the reaction proceeds very slowly. Therefore, where the conditions for "fast chemistry" simulation does not apply, the chemical reaction of post-oxidation almost stops. The integral of equation (2.2.26) does not predict any change in the composition and the source of species molar fraction remains constant.

The possibility to simulate post-oxidation as a "fast chemistry" process numerically simplifies the problem because it permits to separate the turbulence scales from the chemical scales.

In order to reduce the simulation time, many different numerical solutions have been tested (e.g. [45], [46]). The most efficient and accurate solution is the use clustering [44]: the cells with similar thermal and chemical states are numerically grouped using a number of variables (e.g. temperature, equivalence ratio, etc.); the average chemical state of the group is integrated for each group for each time-step and finally the solutions are interpolated back to the original cells. The advantage of clustering is that the number of clusters increases slowlier that the number of cells. Therefore, for models with great mesh sizes clustering offers a substantial performance improvement.

The validation process of the 3D-CFD methodology will have to validate the choices and assumptions that have been adopted for the modelling of post-oxidation keeping in mind, which are the more sensitive assumptions and sources of errors.

3 Simulation environments

For the following investigation, two different simulations have been performed using two different simulation environments. The full engine simulation have been carried out with the 3D-CFD tool QuickSim [28], which was specifically designed for the simulation of ICEs, while the simulations of the detailed model of the exhaust manifold with the chemical reaction mechanism has been performed on the commercially available, general-purpose-tool Star-CCM+.

3.1 3D-CFD tool QuickSim

QuickSim is a 3D-CFD code based on Star-CD that has been developed over the last 20 years at the Research Institute of Automotive Engineering and Vehicle Engines Stuttgart (Forschungsinstitut für Kraftfahrwesen und Fahrzeugmotoren Stuttgart - FKFS) and at the Institute of Automotive Engineering (Institut für Fahrzeugtechnick Stuttgart - IFS) by the University of Stuttgart.

The main characteristic is to use ICE-adapted and tuned computational models, which allow for coarser meshes compared to traditional 3D-CFD approaches without sacrificing the quality of the simulation. As a result, the computational effort for a simulation is minimized (2 hours for a complete operating cycle of the full engine model on a 20 cores CPU). The typical time scale of different investigation approaches is showed in Figure 3.1.

The strategy adopted in QuickSim has two major advantages: it allows to include in the simulation domain the complete engine and the calculation of several consecutive engine operating cycles in a very competitive time frame. Therefore, the simulation starts from a first estimation of flow field and thermodynamic conditions and at first performs a small transient from the initial conditions to the stable ones. The length of the transient depends on the engine operating point being simulated and on peculiarities of the model; usually after 5-10 cycles the transient is concluded and the user-defined initial conditions do not affect any longer the flow field [28].

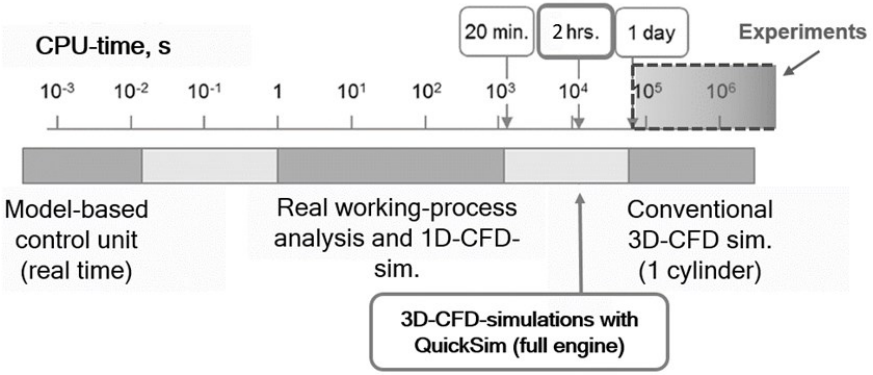

Figure 3.1: Comparison of QuickSim time scales with experiments and conventional simulation techniques

A crucial aspect in 3D-CFD simulations is the influence of boundary conditions on the result of the simulation. Boundary conditions are required for the description of the fluid conditions at the boundary of the control volume. The type and dimension of the control volume determines the kind of boundary conditions needed and the assumptions that has to be made for their generation. In the case the simulation domain concentrates only on the cylinder plus intake and exhaust channels, the boundary conditions can be either measured at the test bench or calculated using a 1D-CFD simulation. The problem is that both types of boundary conditions allow only for a uniform distribution of the variables such as temperature and species on the inlet surface. However, the fluid flow in the cylinder head cannot be usually considered uniform over the section because of the many complexes phenomena that tipically occur in these volumes: mixing, three-dimensional flow, heat exchange with the walls, fuel vaporization, backflows from the cylinder, pressure waves…

As it will be discussed, the correct representation of these phenomena is of major interest for the simulation of post-oxidation. In order to reduce the effect of assumptions at the boundary conditions, QuickSim usually expands the simulation domain to include the full engine, if needed a 0D turbocharger model [47] can be implemented. Thanks to this approach, the boundary conditions are pure (or humid) air at ambient pressure and temperature, without any particular three-dimensional flow (Figure 3.2), therefore drastically reducing the assumptions on boundary conditions.

This approach enables for a simplification of the simulation methodology because it requires less input data from the test-bench and the required information for boundary conditions is the standard evaluation that is carried out for test-bench operation, e.g. indicating pressure, injection timing, valve timing…

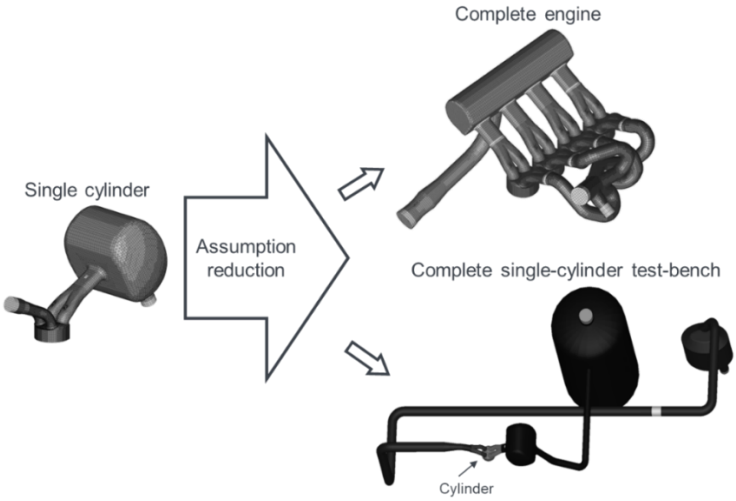

Figure 3.2: QuickSim approach to engine simulation

QuickSim can simulate variations of the following parameters without any particular limitation:

- Engine layout: cylinder number and disposition, combustion chamber geometry (also opposed piston), intake and exhaust manifolds, air-box, throttle valve position, injection system (direct injection, port fuel injection, single point injection…) with arbitrary spray targeting and geometrical disposition.
- Combustion: spark-ignition, compression ignition, homogeneous charge compression ignition (HCCI, [48] [49]) and spark-assisted compression ignition SACI.
- Fuel type: gasoline, diesel, compressed natural gas (CNG), biofuels and e-fuels [50].

- Valve timing, cranckcase configuration (connecting rod, cranck radius, piston wrist pin) or free piston kinematics.
- Two or four stroke engines.

Once the engine layout is completed, the simulation approach allows for flexibility in geometry and strategy changes.

3.1.1 Thermodynamic description of working fluid

As already mentioned above (§2.2.3), the precise description of the working fluid requires the definition of all the chemical species, which requires the definition of one additional partial differential equation for each species, increasing drastically the computational time. This approach is useful if the target of the simulation is to reproduce exactly the chemical reactions in the fluid and will indeed be used for the detailed simulation of post-oxidation. For the full engine simulation, however, such approach is usually overdetailed and the computational effort is not justified by the increase of accuracy. The goal of the full engine simulation is to be able to simulate all the most relevant phenomena inside the engine reducing the assumptions at the boundary conditions and reducing the simulation time. Therefore, QuickSim adopts a system of few scalars in order to divide the working fluid into groups of interest. Such a system is able to simulate accurately the real working fluid while simplifying the model and saving computational time.

The scalars represent thermodinamically fresh charge, EGR (burned gas of the previous cycle), burned gas and water [51]. Figure 3.3 schematically shows the composition of a general 3D-cell during combustion. A detailed description of each scalar can be found in [28].

Post-oxidation requires the introduction of an additional scalar called “air-burn-plus”. The scalar “air-burn-plus” is present only in the burned gas and its chemical composition is of fresh air (O_2 and N_2). It is calculated in cells where the burned gases have a local A/F ratio greater than stoichiometry. In these conditions, there is some still fresh air that is separated from the exhaust gases by means of the “air-burn-plus” scalar, which is equivalent as having a lean lambda in the burn region. The “air-burn-plus” is necessary for the simulation of the mixing of rich exhaust gases with oxygen present in the exhaust gases for further oxidation.

This approach allows to directly quantify:

- The composition of the burned gas;
- The amount unburned fuel flowing to the exhaust manifold;
- The mass of air in the exhaust gas.

More details are available in [28] [50] [52].

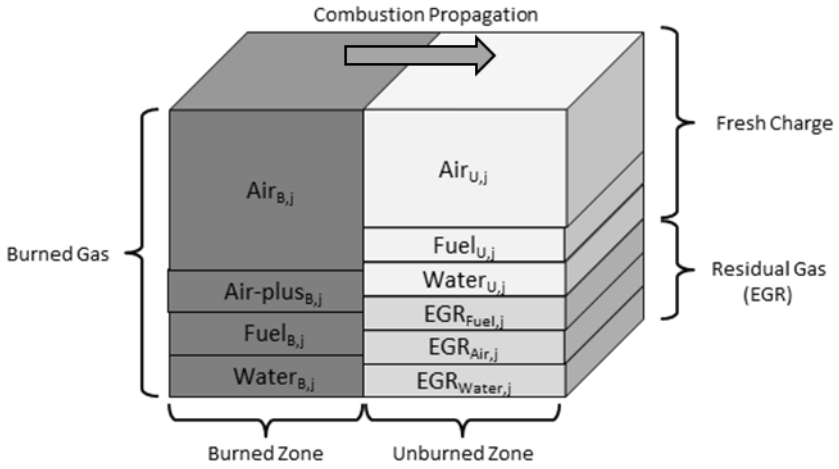

Figure 3.3: Scalar composition in the 3D-CFD cell of QuickSim

The system of ten scalars implemented in QuickSim permits to define indirectly in each cell the final chemical composition of the gases. The coupling between the scalars and the chemical species is done by means of a look-up table, called caloric, which is specific for each fuel and is calculated before the simulation. In the caloric, the chemical composition is calculated as function of temperature, pressure, λ_{EGR}, λ_{FRESH}, amount of egr, amount of water and amount of air-burn-plus. The calculation is carried out using a chemical reaction mechanism and assuming that at low temperatures the chemical composition is "freezed", i.e. all reactions stop [28]. Some of the caloric values are reported in Figure 3.4, Figure 3.5, Figure 3.6 and Figure 3.7. It can be seen that the compositions of burned gases change as function of lambda, temperature and pressure. For the application of post-oxidation, the majority of the investigated engine operating points are characterized by low

temperature, rich conditions and low pressure at exhaust valve opening (EVO). In these conditions, the caloric predicts great amounts of CO and H_2 and very little O_2. It can be seen that post-oxidation, because of the rich combustion that takes place inside the cylinder, lacks of O_2 for the complete oxidation of CO and H_2. This problem is solved by the fresh air from scavenging. There is also a limited amount of NO, whose effect on post-oxidation will be later on investigated.

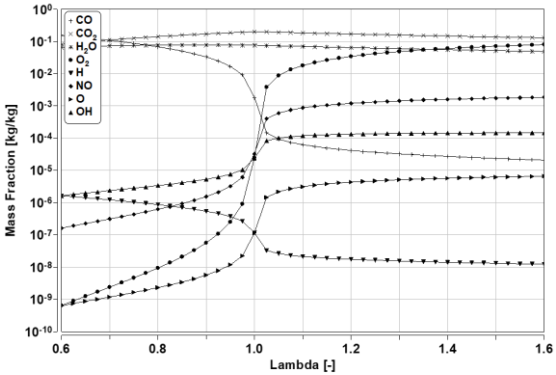

Figure 3.4: Burned gas composition for a combustion of SuperPlus98 at 1 bar, 1700 K and for different values of lambda

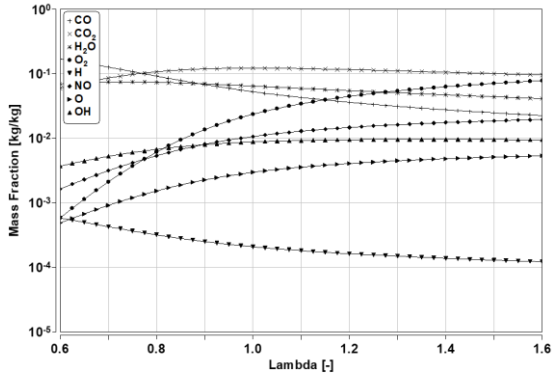

Figure 3.5: Burned gas composition for a combustion of SuperPlus98 at 1 bar, 2700 K and for different compositions

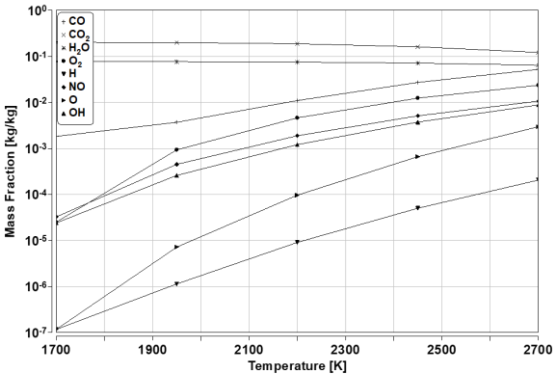

Figure 3.6: Burned gas composition for a combustion of SuperPlus98 at 1 bar at stoichiometry and for different temperatures

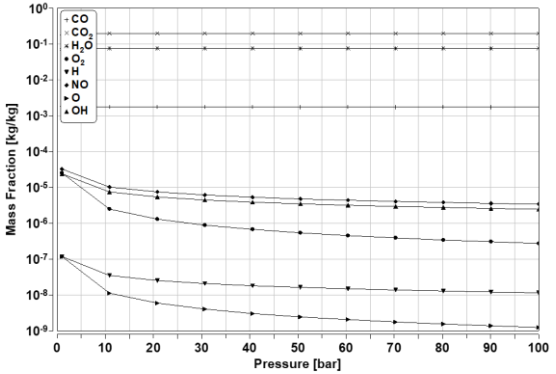

Figure 3.7: Burned gas composition of SuperPlus98 at 1700 K and stoichiometric conditions for different values of pressure

This approach has the advantage to rely on 3D-CFD simulation for the mixing and on a detailed look up table for the local composition of the gases; therefore, it allows a fast and yet precise calculation of the chemical composition of the fluid without the direct implementation of the chemical reaction mechanisms in the simulation, which would increase drastically the calculation time. This approach has been widely adopted during the investigation of post-oxidation and it proved to be able of great accuracy.

3.1.2 Combustion modelling

From the computational point of view, the combustion can be extremely expensive [29], [30]. The detailed simulation of the fuel requires the calculation of hundreds of different species and thousands of chemical reactions. Moreover, for the simulation of ICEs such level of detail is not necessary. Therefore, in QuickSim has been implemented different combustion models dedicated to the application of ICEs and based on the heat release law [28], [50]. Such models do not simulate the chemical reactions but only the heat release of the combustion as function of the thermodynamic conditions and the local composition. These models are specific to the type of fuel that has been used in the simulation and rely on the information provided by the caloric:

- Spark-ignition: the combustion starts with a heat release at the spark-plug, then a flame front propagates through the combustion chamber;
- Self-ignition: the model can detect the volumes where the gases are in self-ignition conditions and start there a local combustion (e.g. HCCI, knocking);
- Diffusive flame: in this case there is no moving flame front and the chemical reaction rate is determined as function of the diffusion velocity of the species involved.

In QuickSim is also present a post-oxidation model that has been described in §10, when it has been validated and improved using the results of the investigation.

The following investigation has been performed on a DISI engine. Therefore the combustion model for spark-ignition combustion and self-ignition have been used. The approach in QuickSim for the simulation is to reproduce the turbulent flame assuming that it behaves like a laminar flame that is wrinkled by turbulence. Therefore, for the simulation, the tool uses information about the laminar flame speed in the same thermodynamic conditions of the cell and for the same composition, plus a wrinkling factor that multiplies the laminar flame front so that its surface resumes the one of the turbulent flame front (Figure 3.8).

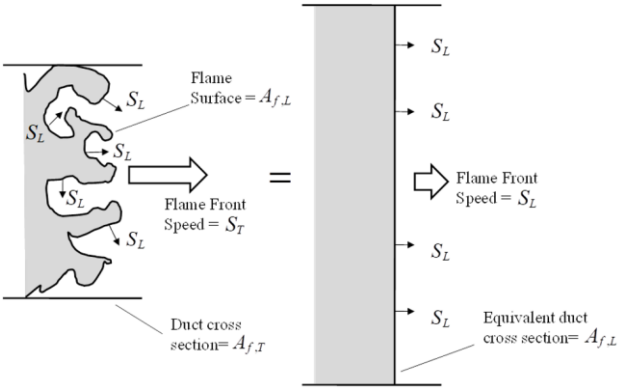

Figure 3.8: Schematic representation of the flame propagation by means of a wrinkling factor [28]

The wrinkling factor, which links the laminar and the turbulent flame speed, is defined as:

$$K = \frac{A_{f,L}}{A_{f,T}} = \frac{S_T}{S_L} \tag{3.1.1}$$

Where:

- $A_{f,L}$ is the area of the flame front in the laminar case;
- $A_{f,T}$ is the area of the flame front in the turbulent case;
- S_T is the flame front speed in the turbulent case;
- S_L is the flame front speed in the laminar case.

The value of the wrinkling factor is determined using correlations that are deduced from empirical and theoretical investigations. The model adopted in QuickSim has been proposed for the first time by Weller [53] and has been adopted for wide range of validated cases in the field of internal combustion engines. The model calculates locally the value of the wrinkling factor and couples the information with local thermodynamic conditions. This information determines the local laminar flame speed, which then is multiplied by the wrinkling factor for the calculation of the turbulent laminar flame speed.

The calculation of the laminar flame speed depends on the thermodynamic variables, such as temperature and pressure, local mixture composition, local amount of water, local amount of EGR and chemical composition of the fuel as shown in (3.1.2).

$$S_L = f\left(\lambda, p, T_U, \lambda_{EGR}, w_{EGR,U}, w_{WATER,U}\right) \tag{3.1.2}$$

It is possible to calculate the value of the laminar flame speed by means of semi-empirical correlations like the one from Gülder [54], however, it has been proven, that these correlations are precise for a limited interval of air/fuel ratio and for standard fuels.

A better precision for the calculation of the laminar flame speed requires the use of detailed chemical reaction mechanisms in order to correctly simulate the fuel composition. Therefore, the computational time required is very high. The solution adopted in QuickSim is to implement the laminar flame speed as a look-up table, where its values are stored as function of the variables reported in (3.1.2). The simulation enters the table with the local values of the variables and reads the value of laminar flame speed.

The look-up tables for the laminar flame speed are calculated separately as part of the simulation pre-processing and must be loaded in the simulation directory. Together with the information of laminar flame speed also the ingnition delay is modelled.

The look-up tables are specific for each fuel. The process for the production of laminar flame speed and ignition delay values starts with the definition of the fuel surrogate. Real fuels are composed of thousends of species and its composition can change during the year and because of the origin of the fuel or the process it underwent. Moreover, the analysis of the fuel is expensive and time consuming. For all these regions, usually the precise composition is not available and the fuels are better characterized as function of specific paramters such as CHO composition, density, LHV, A/F ratio, RON, MON… It has been widely demonstrated that, if these parameters are similar, different fuels behave in a similar way during the engine operation.

The same principle can be exploited for the simulation of fuel from a numerical point of view. In this case the problem is not only that the real composition of the fuel is usually unknown, but also that numerically it would be not possible to include all the species in a chemical reaction mechanism. The solution is to

use a limited amount of species to meet some, if not all, the most relevant properties of the fuel. The species that are chosen must represent the main chemical groups that compone gasoline [52] [55] like those listed in Table 3.1.

Table 3.1: Most representative chemical species used for gasoline surrogates

N-alkanes	n-heptane, n-pentane
Iso-alkanes	iso-octane, iso-petane
Olefines	2-methyl-2-butene, cyclopentene
Aromatics	Toluene, benzene
Cycle-alkanes	Cyclohexane, cyclopentane
Oxygenates	Ethanol, ETBE

There are different possibilities to define the composition of the fuel surrogate [39] [56] [57]. The first and most simple methodology is to use iso-octane and n-heptane to compone a mixture who meets the RON of the simulated fuel. This kind of mixture is called primary reference fuel (PRF) surrogate. However, other properties, such as density, volatility or LHV, can result to be very different from the real value. Therefore, more chemical species are added to the mixture. Typically, another solution is to add Toluene to the mixture and the mixture is called TRF surrogate. Generally a mixture of these three components is not enough to reproduce the complete spectrum of properties of a fuel that are necessary for an accurate engine simulation, in particular in the case of special fuels such as e-fuels, oxygenated fuels or competition fuels. Therefore, more chemical species are included in the surrogate definition, which requires the use of a larger chemical reaction mechanism, which again increases the calculation time.

In QuickSim a similar approach is used, which however integrates the system of scalar used for the description of the working fluid [50]. The look-up tables are calculated starting with the definition of the fuel surrogate that accurately matches the relevant fuel characteristics. Then the values of laminar flame speed and ingnition delay are calculated using 1D/0D chemical simulations in Cantera and finally are stored in look-up tables that are loaded in the simulation.

3.1.3 Spray modelling

The simulation of spray must be accurate in order to reproduce correctly the engine behaviour because of the many effcts it has on the flow field, on turbulence, on the temperature and density of the fresh charge and on the pollutants formation.

The complete description of the physical phenomena that take place during the injection process (e.g. flow of the liquid inside the injector, cavitation inside the injector, primary and secondary break-up, evaporation…) is very complicated and requires a lot of computational resources. Many studies have used 3D-CFD simulations to precisely describe the injection process [58] [38]. However, those studies usually focus only on the injection process and are based on LES simulations.

In QuickSim it has been preferred to model the spray by means of some submodels, which are able to reproduce the most relevant aspects of fuel injection in a simpler and yet accurate way. More detailed can be found in [51] and [59].

The fuel movement inside the injector is not reported and at the beginning of the injection for each nozzle the droplets are initialized in a cone-shaped volume. The droplets are characterised with a specific mass, volume and velocity. The volume of the droplet is determined using a Rosin-Rammler distribution of the diameters; velocity and density of the droplets, instead, are function of the injection pressure and characteristics of the fuel.

In QuickSim it is possible to define as many injector nozzles as necessary and each of them has a defined direction. In this way, it is possible to reproduce all kind of spray targeting.

3.2 Detailed simulation using 3D-CFD commercial tool STAR-CCM+

The second step of the investigation of post-oxidation consists in the detailed simulation of the phenomena taking place in the exhaust manifold. For this kind of simulation it is necessary to implement a chemical reaction mechanism

directly in the simulation. This is more easily implemented in the commercially available 3D-CFD tool Star-CCM+, which is already well validated for several similar applications. For the simulation of post-oxidation a model has been set-up by analysing which models are necessary.

An overview of the models is reported in Table 3.2.

Table 3.2: Overview of the models implemented in Star-CCM+

Flow	Turbulent – unsteady RANS equations
Turbulence	Realizable K-ε Two-Layer
Wall treatment	Two-Layer all y^+ wall treatment
Fluid	Multicomponent gas
Equation of state	Ideal gas
Chemistry	Laminar flame concept

The flow is turbulent because of the very high velocities of the mass flow rates during the exhaust strokes. Moreover, inside the exhaust manifold the interaction of the different cylinders keeps the gases moving with high velocity also in the time between the exhaust strokes. For the simulation of turbulence, the RANS have been chosen because of the lower computational effort that they require. In addition, the RANS equations represent the most tested approach to the simulation of ICEs and do not require a very fine time-step.

The Realizable K-ε is a stable and widely tested model for the turbulence in confined spaces. In the model the Realizable K- ε model has been chosen, which, in comparison to the standard approach, it has at least the same accuracy and in general increases the reliability. The Realizable approach uses a new transport equation for the turbulent dissipation and further refinements for some self-adjusting model coefficient. The name “Realizable” refers to the ability of the model to respect the mathematical constraints on the normal stresses.

The turbulence modelling relys also on a two-layer approach. Such approach tries to better reproduce the transition from the region near the walls with low Re numbers and the completely developed turbulent flow at high Re numbers. This modelling uses the value of Re_y ($Re_y = y\sqrt{k}/\nu$, where y is the distance

from the wall) as a method to devide the boundary layer into the two regions described above. In the fully turbulent region, the modelling remains the same of the standard approach, while in the viscous region there are some adaptations to the length scale, rate of dissipation and eddy viscousity. In order to smoothly connect these two regions, a blending formula is used to evaluate the eddy viscousity.

The wall treatment requires particular attentions because its modelling must take into account also the form of the computational grid. Walls are generally a critical aspect of the simulation since they are the source of the boundary layer, which is essencial for the flow field, but also difficult to reproduce.

On the wall generally the condition “no-slip” for the velocity is applied, i.e. the fluid does not posses any velocity and therefore the Re number is zero. In the completely developed turbulent flow, instead, the Re number is high. Between these two extreme situations, there is the boundary layer, where the transition of Re numbers, flow type and velocity profile take place. The boundary layer is generally devided into three different sublayers, which are characterized by the shape of the velocity profile, which is the result of the interactions at a microscopic level of the inertia and viscous forces. Close to the wall the viscous forces dominate and create an almost laminar region called viscous sublayer. Moving from the wall towards the fully developed turbulent flow, there is a so-called log layer layer where the viscous effects are equal to the turbulent ones. Between the viscous and the log layers there is the buffer layer, where the transition between the two takes place.

The modelling of these effects relies on the application of a so-called wall treatment model that is usually based on algebraic equations that reproduce the distribution of velocity, temperature and turbulence quantities. These equations are applied on the near-wall cells of the computational grid.

The dimension of the boundary layer, however, depends on characteristics of the fluid flow such as the velocity in the completely developed turbulent flow and the geometry of the problem. Therefore, in the case of post-oxidation it is probable that the dimension of the boundary layer changes during one engine operating cycle because of the pulsations of the flow field inside the exhaust manifold. The pulsations cause the conditions in the near-wall cells to change during the engine operating cycle, i.e. a general approach for the wall treatment. The “all-y^+” wall treatment allows the simulation of very different

types of flow simulations. In the model is adopted together with a Two-layer approach, that is required by the choice of the turbulence simulation.

The implementation of the chemical reaction mechanism required the choice of a multicomponent gas as working fluid. This model allows the representation of each species present in the chemical reaction mechanism, their interaction and mixing.

Considering the pressures and temperatures typical of post-oxidation, the assumption of ideal gas as equation of state is realistic and permits the correct simulation of the mixture while limiting the computational time. The ideal gas assumption means that the density of the gas is calculated as function of temperature and pressure using an ideal gas law.

Finally, as already discussed in §2.2.3, the simulation of the chemical reaction mechanism is based on the laminar flame concept. This allowed for the implementation of chemistry in the simulation.

4 Simulation pre-processing

In this project, the focus is the analysis of post-oxidation taking place in the exhaust manifold of a four-cylinder direct injection engine with turbocharger. Post-oxidation is obtained by means of a rich in-cylinder combustion followed by scavenging of fresh air from the intake to the exhaust manifold during the long valve overlap. In the exhaust manifold the fresh air from scavenging and the exhaust gases of the rich combustion mix and react increasing temperature and enthalpy before the turbine [60], if the conditions of temperature and mixing are available.

The methodology adopted to analyse this phenomena has been described in the previous chapter and consists of two different 3D-CFD simulation. In this chapter, the methodology is applied to the practical problem analysed in this project.

The whole simulation part has been coupled to the work at the test-bench carried out by the researchers at the Chiba University [61], which provided the detailed data necessary for the validation of the simulation methodology and the boundary conditions. The investigations at the Chiba University also tested many different operating conditions and selected the most interesting ones, therefore concentrating the numerical effort on selected engine operating points. The cooperation enabled also a constructive feedback from the simulation to the test-bench.

The analysed engine is a four-cylinders, direct injection, turbocharged spark ignition engine. The group at the Chiba University has provided the geometry of the engine in the form of a CAD. The most important characteristics of the engine are reported in Table 4.1.

The engine is representative of many engines currently available on the market, which makes the investigation interesting for the application of post-oxidation to already existing engines.

Bore and stroke are typical of the so-called “square engines”, where the bore-to-stroke ratio is close to the unity (in this case is equal to 0.98), which is a common compromise between efficiency and power. The resulting compression ratio is in line with a good standard technology.

The engine is equipped with a twin variable valve timing control that allows to freely change the valve timings both for intake and exhaust valves. The valve lift, however, remains fixed.

Table 4.1: Engine general information

Engine general information	
Bore [mm]	79.7
Stroke [mm]	81.1
Compression ratio [-]	10.5
Cylinders [-]	4
Displacement [l]	1.618

4.1 Full engine model

The first model to be developed is the full engine model for the simulation in QuickSim. This model can be seen in Figure 4.1 und Figure 4.2.

The model is implemented as described in the previous paragraphs (§3.1). A recap of the most relevant models is reported in Table 4.2.

The mesh of the full engine model includes:

- The air-box and intake pipes;
- The four cylinders;
- The exhaust runners.

The mesh is composed by more than 400 000 cells. An important geometrical feature is the 10 cm adaptor (Figure 4.1) placed between the engine's head and the exhaust four-in-one runner. This feature was needed at the test-bench for the installation of sensors and it has been carefully reported also in the 3D-CFD model because, as it will be demonstrated, has an important influence on the mixing in the exhaust.

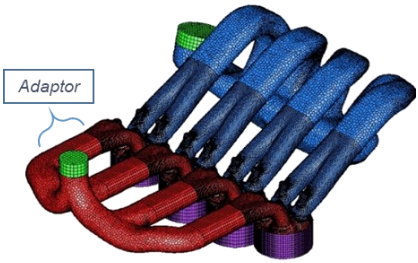

Figure 4.1: Full engine model

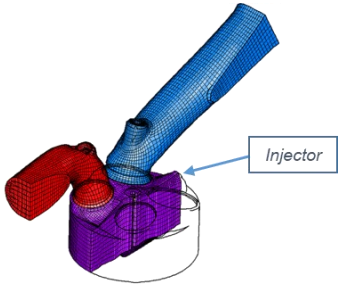

Figure 4.2: Cylinder (violet), intake channels (blue) and exhaust channel (red)

Table 4.2: Overview of QuickSim models

Simulation methodology	Multiphase RANS
Multiphase flow	Euler / Lagrange
Turbulence	k-ε
Combustion – flame propagation	Two-zone Weller model adapted to GDI-combustion for spark-ignition flame propagation
Time step Δt	Variable: 0.25°CA – 0.5°CA

The advantage of QuickSim is that there is no need for a further refinement of the mesh because there are many specifically for ICE designed models that can simulate all the most important phenomena that take place during the engine operation. Therefore, it is possible to simulate with the same amount of cells a much bigger volume and hence to move the boundary conditions away from the cylinders. Since each boundary condition consists of an assumption about the status of the fluid in a particular position, the more general the condition (e.g. ambient conditions, pure air), the smaller is the degree of the assumption that has to be done and the less affected are the phenomena of interest.

The boundaries of the model are, for what concerns the inlet of the model, before the air-box just after the throttle valve (Figure 4.1); the outlet, instead, is placed on the exhaust side of the engine, just before the volute of the turbine. For the full engine simulation, the following boundary conditions are necessary:

- Inlet: pressure profile before the air-box (after the throttle valve) and temperature in the same position; both conditions can be obtained either from experimental measurements at the test-bench or from GT-Power simulations;
- Outlet: pressure profile before turbine inlet either from the test-bench or from GT-Power simulation;
- Injection: amount of fuel, timing of the injection, position of the injector and spray targeting.
- Valve timing: valve profile

Once that the boundary conditions are implemented, it is possible to carry out the simulation of the engine operating point without further adjustments of the simulation. The full engine simulation in QuickSim includes all most relevant engine phenomena described before (§3.1).

4.2 Detailed model of the exhaust system

The target of the fine mesh model is a detailed description of the physical and chemical phenomena taking place in the exhaust manifold during the engine cycle. For this reason, the simulated volume is reduced to the exhaust manifold, the mesh refined and the model built in the commercial software Star-CCM+, which includes the possibility to implement and easily change a chemical reaction mechanism.

The computational mesh is reported in Figure 4.3; it consists of the exhaust manifold from the exhaust valves up to the turbine volute including the 10 cm adaptor between cylinder head and the four-in-one exhaust runner. The complete model is discretized with more than 2.2 mln cells.

The mesh is composed mostly of hexahedra and particular attention is paid to achieve a uniform structure. The turbine geometry is not available and therefore it is not possible to simulate neither the geometry of the blades nor their movement. Nevertheless, the geometry of the volute of the turbine has been included; this has remarkably improved the stability of the simulation by moving further away the outlet boundary conditions. Since in the model the turbine is not included, there are no pressure and temperature drops after the volute. During the simulations, it has been assumed that the results are reliable up to the turbine inlet (red dotted line in Figure 4.3) because afterwards the geometric simplifications become too important. This, as it will be demonstrated, is a good compromise of accuracy and geometrical simplifications.

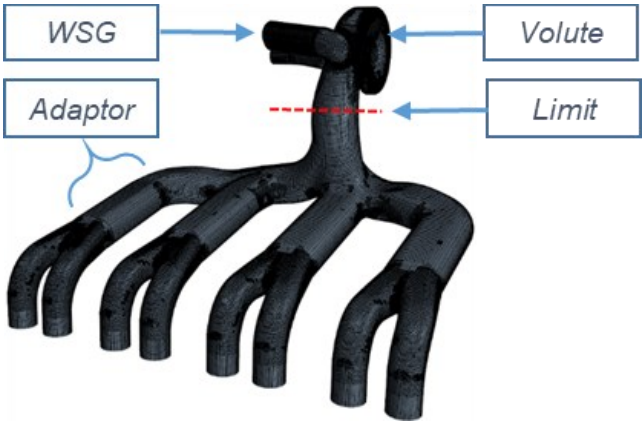

Figure 4.3: Fine mesh model of the exhaust manifold

The information needed for the boundary conditions is transferred from the full engine 3D-CFD simulation described before. The advantage of the coupling of these two types of simulations is that the model behaves realistically, taking into account all the complex phenomena explored in the full engine.

The information needed for the boundary conditions are:

- Temperature signal at the exhaust valves;
- Pressure signals at the exhaust valves;

- Mass flow rates through the valves;
- Species mass fractions at the exhaust valves;
- Pressure signal at the outlet.

The crank-angle-resolved boundary conditions are defined at each exhaust valve. The outlet boundary condition is placed after the turbine volute and consists of a constant pressure specification due to the lack of more precise data. During the tuning of the simulation against experimental data, it has been necessary to include the wastegate valve in the model.

The fluid is modelled using the unsteady RANS and the standard k-ε model for the simulation of turbulence as introduced above (§3.2).

4.3 Implementation of a reaction mechanism

The last step of the preparation of the simulation is the implementation and test of different reaction mechanisms in the detailed model of the exhaust manifold in Star-CCM+.

The choice of the reaction mechanism depends on the definition of the species and reactions that are needed during post-oxidation. A detailed analysis has been carried out by means of 0D simulations in Cantera [62].

The result of the analysis is the selection of the reaction mechanisms reported in Table 4.3.

The detailed mechanism Polimi_1412_detailed has the greatest amount of species and reactions and is able to simulate also the oxidation of long-chain hydrocarbons, typical of gasoline surrogates. The Polimi_1412_H2/CO reaction mechanism is a reduced reaction mechanism specifically designed for mixtures of hydrogen and CO, which makes it particularly interesting for post-oxidation because the most relevant species and reactions are reported while many unnecessary reactions and species are excluded, therefore drastically reducing the computational effort. The Polimi_1412_H2/CO-NOx mechanism is the same of the Polimi_1412_H2/CO mechanism, in which the most relevant reactions for NOx formation have been included, therefore the CPU-time increases and it must be demonstrated if the additional reactions are indeed

important for post-oxidation. The Polimi_1412_ H2/CO-NOx is the only reaction mechanism in the list that includes the reactions for NOx formation. The Polimi_1412_detailed reaction mechanism is the most general and validated of the mechanisms, hence it will be used as a reference for the first tuning of the model.

Table 4.3: Selection of reaction mechanisms

Mechanism	Species	Reactions	Source
Polimi_1412_detailed	156	3465	[63]
Polimi_1412_H2/CO	14	33	[64]
Polimi_1412_ H2/CO-NOx	32	173	[64], [65]

In order to test these reaction mechanisms, a dedicated model and simulation have been set up. The simulation has been carried out in Star-CCM+ with a smaller geometry (mesh around 400k cells): a simpler, more stable simulation capable of isolating the effect of each variable while representing a realistic condition. The model is reported in Figure 4.4.

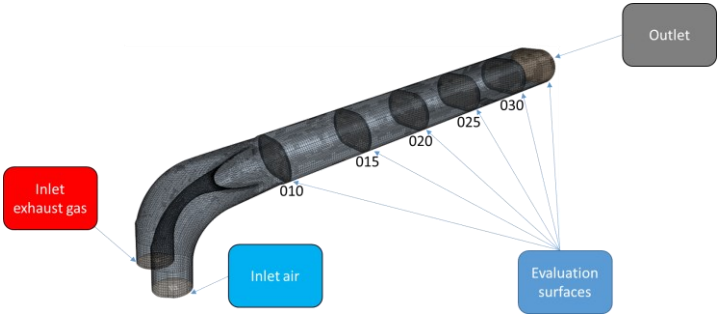

Figure 4.4: Model for reaction mechanism validation

The geometry is taken from exhaust channels and adaptor of cylinder 1 of the detailed model. The adaptor has been prolonged until the total length of the model is the same of that of the real geometry up to the turbine. It has been chosen to carry out a stationary simulation in order to reduce the numerical instabilities, speed up the test and better isolate the effects of the different variables. This choice was very much forced by the need to test also the

detailed reaction mechanism in a realistic time frame and under different conditions.

Since the post-oxidation is triggered by the mixing of exhaust gases and fresh air from scavenging, exhaust gases of rich combustion and fresh air enter into the model separately through the two inlets of the computational grid (exhaust channels). In the model have been added a series of surfaces at which all the most important variables are evaluated. The boundary conditions are reported in Table 4.4.

Table 4.4: Boundary conditions for mechanism validation

	MF [kg/s]	CO [kg/kg]	CO_2 [kg/kg]	H_2 [kg/kg]	H_2O [kg/kg]	N_2 [kg/kg]	O_2 [kg/kg]
Ex. gases	0.012	0.04	0.17	$8*10^{-4}$	0.08	0.71	-
Air	0.012	-	-	-	-	0.77	0.23

The composition of the exhaust gases is calculated with a 0D simulation in Cantera of a combustion with $\lambda_{CYLINDER}$ equal to 0.8. The temperature of intake air is kept constant at 360 K as well as the mass flow rate at both inlets of the models. At the outlet is imposed a constant pressure condition.

For the sensitivity analysis, the temperature of exhaust gases and the pressure of the system has been varied for all the three reaction mechanisms choosing the most interesting conditions for post-oxidation. This test serves to understand the level of approximation introduced using the reduced mechanisms as a function of the computational time.

In Figure 4.5 is reported the heat release rate from chemical reactions in the whole volume of the simulation for different temperatures of the rich combustion products at the inlet 1. The temperature of fresh air is kept constant. The pressure of the system is constant at 1.4 bar.

The Polimi_1412_detailed and Polimi_1412_H2/CO reaction mechanisms give exactly the same results for all the simulated points. The two reactions mechanisms predict the start of post-oxidation by a temperature greater than 1000 K. By 1025 K the first heat release is taking place, but it is very limited; after 1400 K the heat release remains constant.

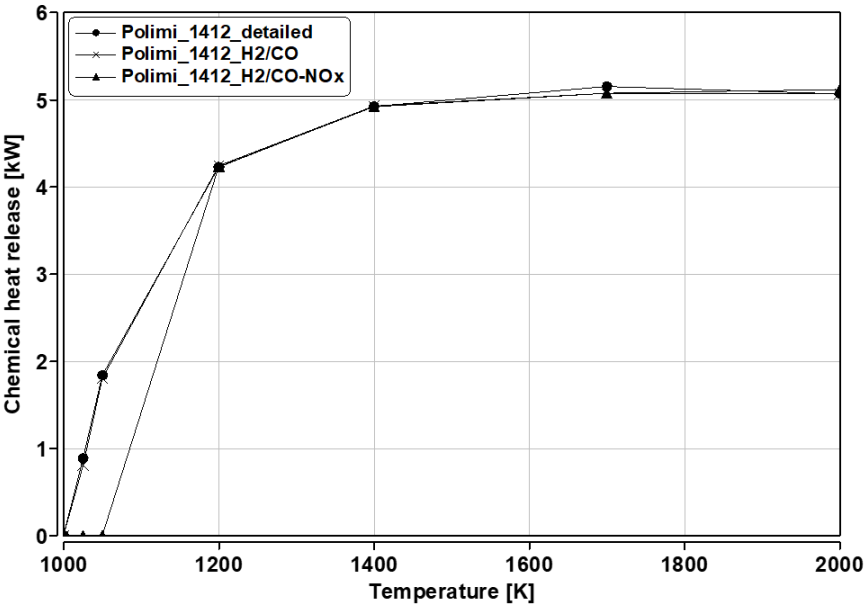

Figure 4.5: Temperature sensitivity

On the other hand, the Polimi_1412_H2/CO-NOx reaction mechanism predicts for the points at 1025 K and 1050 K no heat release. From the point at 1200 K on, all the reaction mechanisms predict the same heat release rate for post-oxidation. The different behaviour of the Polimi_1412_H2/CO-NOx reaction mechanism is probably due to the interaction of the NOx formation with the oxidation of CO, since the simulation of NOx is the only difference between the two simulations. In particular, NO during rich combustion slows down the reactions while in lean conditions speeds up the oxidation [62]. In this case, it is probable that the local conditions at which the post-oxidation starts are rich and therefore the Polimi_1412_H2/CO-NOx reaction mechanism predicts no start of post-oxidation at low temperature.

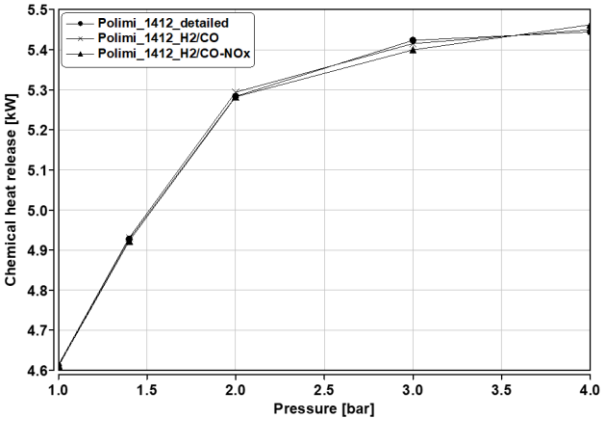

Figure 4.6: Pressure sensitivity

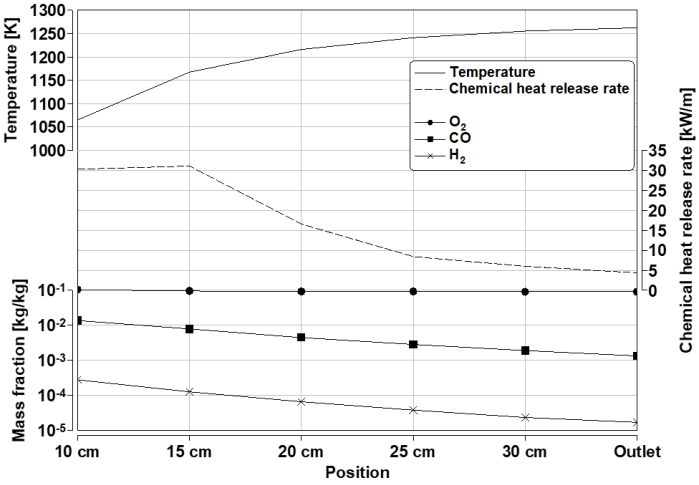

Figure 4.7: Spatial distribution of post-oxidation variables for the case at T_{INLET} =1400 K, p = 1.4 bar and chemical reaction mechanism Polimi_1412_detailed

For the pressure sensitivity analysis it has been kept a constant temperature of 1400 K and the pressure has been variated from 1 bar to 4 bar. Due to the high temperature, the effect of NOx is in this case negligible. There is a good agreement among the three reaction mechanisms for all conditions and it can

be seen an increase in heat release as the pressure increases. This is because the pressure favours the reactions with decrease of the number of molecules [30], which is the case of post-oxidation.

The analysis so far shows that both reduced mechanisms have a good agreement with the detailed reaction mechanism and that the implementation in the 3D-CFD model has proved to give realistic results.

In Figure 4.7 it is reported how some fundamental variables are distributed inside the model starting from 10 cm after the inlets of the model (exhaust valves) up to the outlet. Each value is the average calculated on the surfaces reported in Figure 4.4. It can be seen that there is a steep increase of temperature up to 25 cm and then the temperature settles around 1250 K. The chemical heat release rate on the surface has a peak around 15 cm and then decreases sharply. This explains the temperature increase up to 25 cm and why it later on settles around 1250 K. The heat release rate on the surface relies on the availability of both oxidizer and fuel. In this case, the oxidizer is O_2, present in fresh air, and the fuel molecules are H_2 and CO. The amount of H_2 is very limited from the beginning and decreases quickly around 15 cm. Also CO decreases mostly around 15 cm, where the greatest amount of heat release rate is taking place. In the last part of the model, i.e. from 20 cm up to outlet, the conditions of temperature are still very good for post-oxidation, yet the heat release rate is limited as well as the temperature increase. Also for what concerns the composition there is still a limited amount of CO and H_2 that can be oxidised by the great amount of O_2 still available. However, this does not happen because the reactants are not in contact and remain separated in "clouds". This can become a problem if the goal is to completely oxidize the rich combustion products; as it will be showed later, this is a characteristic of post-oxidation and in general of turbulent non premixed flames: the limiting factor is the mixing.

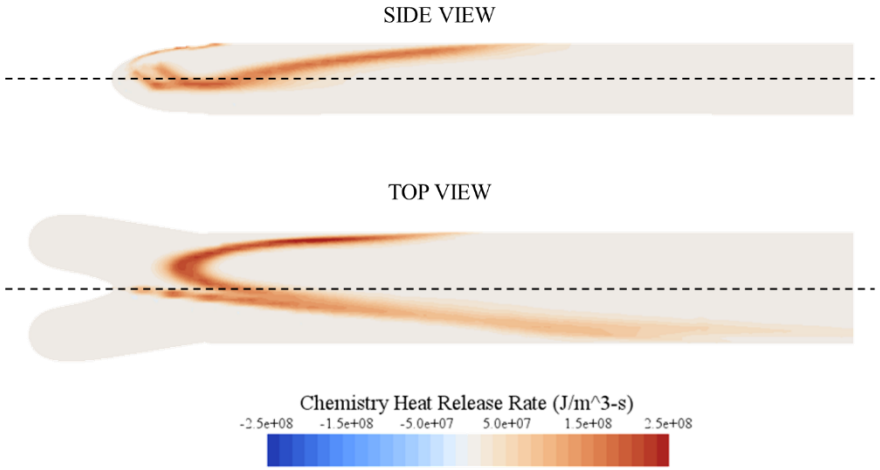

Figure 4.8: Chemical heat release rate in the model

Figure 4.8 can give an interesting explanation of the limit of mixing that is happing inside the model. Both the side and the top view show that the highest heat release rate takes place very close the point where the two flows of hot combustion products and fresh air are brought together by the geometrical features close to the surface at 10 cm. The greatest part of the heat release rate takes place on the side of the hot combustion products where the temperature conditions are better for the start of post-oxidation. In this area, the two fluxes mix and react. However, as the pipe proceeds, the difference in temperature and density of the two fluids limits the mixing and the two flows separate. Therefore, there is only a limited interface, where the post-oxidation reaction can happen.

In Figure 4.9 the streamlines of the fluid are reported; it can be seen that the difference in temperature and density between the two mass-flow-rates of fresh air and hot combustion products limits the overall mixing in the model.

These effects are extremely important for the simulation of post-oxidation and play an important role in more complex simulations.

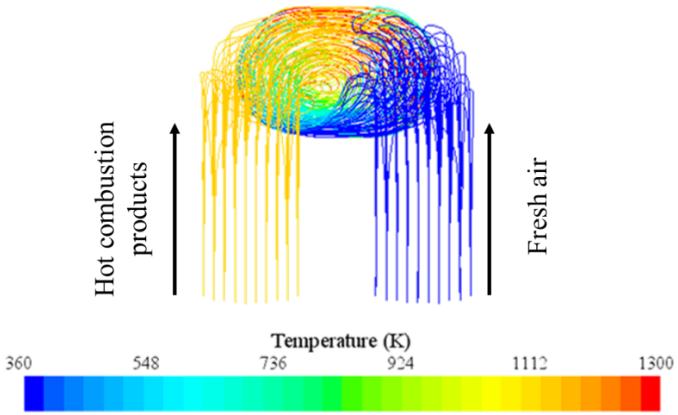

Figure 4.9: Fluid streamlines in the model seen from the front. The colour refers to the temperature of the fluid

The simplified model was therefore able to reproduce well the interaction of the flow field with the composition of the fluid and the chemical reaction mechanism.

Another very important aspect that must be taken into account is the time needed for the simulation for each reaction mechanism in the same conditions. These results will deeply influence the choice of the mechanism to be used in the detailed 3D-CFD model of the exhaust manifold. It is necessary to find the trade-off between accuracy and time needed for the simulations. During the tests has been used a computer with 16 cores and 16 Gb of RAM. The parameter used to measure the computational effort is the time elapsed for one iteration during the simulation of the same model in the same conditions with different reaction mechanisms.

In Figure 4.10, the time needed for one iteration is reported as function of the number of species of the reaction mechanism. The simulation time increases almost linearly with the amount of species. Indeed, for example, the Polimi_1412_detailed mechanism has 5.2 times the number of species of the Polimi_1412_H2/CO-NOx mechanism and the simulation takes 5 times longer for each step. The ratio is not so precise also for the case of the Polimi_1412_H2/CO mechanism but still very close to linear: the Polimi_1412_detailed model has 11 times more species but it takes 8.4 times longer each iteration.

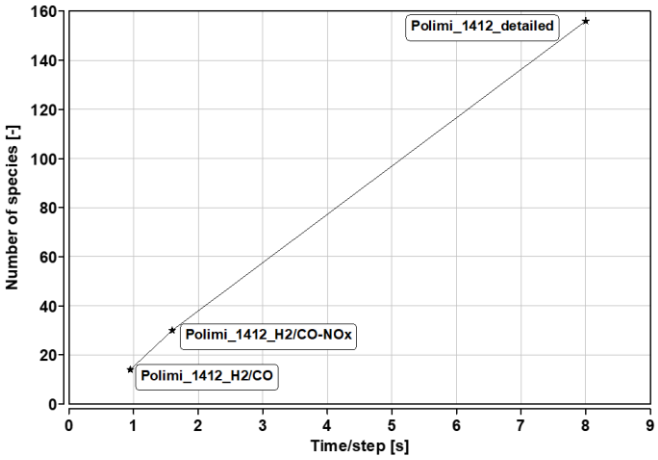

Figure 4.10: Comparison of time per iteration among different reaction mechanisms

Considering that the simulation of one cycle of the detailed model of the exhaust manifold with the Polimi_1412_H2/CO reaction mechanism takes almost one day, it means that it would take for the Polimi_1412_detailed mechanism 8.5 days and 1.7 days for the Polimi_1412_H2/CO-NOx mechanism. Moreover, for each engine operating point at least three engine cycles are simulated. This means that, in these conditions, a single simulation takes with the Polimi_1412_detailed reaction mechanism almost one month (26 days), which is, of course, not acceptable.

Since the results in of the Polimi_1412_detailed mechanism are the same of the ones of the Polimi_1412_H2/CO mechanism in all the tested conditions, the Polimi_1412_detailed mechanism has been excluded because the computational time escalates without increasing accuracy.

However, this might seem a strong assumption to exclude the Polimi_1412_detailed reaction mechanism due to the fact that the simulation, on which it has been tested, is very simplified and in steady state, therefore not representing the more complex conditions of the engine operation. To address this question, a further test has been performed with the detailed model of the exhaust manifold and the Polimi_1412_detailed chemical reaction mechanism (§7).

The Polimi_1412_H2/CO-NOx mechanism has also been excluded because the time needed for a simulation would be too high. It remains open the question if the effect of NOx of slowing down the reactions at low temperatures is of practical interest in the conditions of post-oxidation. It will be later on demonstrated (§7) that this is not the case.

These open questions, i.e. the application of the detailed reaction mechanism and the influence of NOx during post-oxidation, are investigated in §7 thanks to the availability of a HPC cluster.

With the choice of the reaction mechanism Polimi_1412_H2/CO with 14 species and 33 reaction the pre-processing of the simulation is completed and the simplified model is no longer needed. The simulation methodology that is going to be tested and validated from now on is composed of the following steps:

- Full engine simulation with the 3D-CFD tool QuickSim;
- Detailed simulation of the exhaust manifold in Star-CCM+ with fine mesh, reaction mechanism and boundary conditions from the full engine simulation.

The target of following step is to validate this methodology against experimental data of the test-bench.

5 Simulation validation

The validation of the 3D-CFD simulation consists in applying the simulation methodology to engine operating points that has been already analysed at the test bench and for which data are available. If there is a good agreement of measurements and simulations, it is assumed that the methodology works, that it is capable of reproducing post-oxidation and that it can be used for the simulation of other engine operating points.

Since post-oxidation is a complex phenomenon that cannot be directly measured, the validation must rely on indirect measurements of post-oxidation (e.g. temperature and composition of the exhaust gases). The validation process is composed of two mayor parts: at first, the full engine simulation must match the data from the test-bench; then the boundary conditions from the full-engine model must be applied to the detailed simulation that must undergo a dedicated validation.

The validation process is focused on two engine operating points, which are representative of the typical application of post-oxidation in the exhaust manifold by means of scavenging air:

- Low rpm;
- Low boost pressure;
- Great valve overlap (90°CA);
- Great amount of scavenging air.

These engine operating points have been chosen because of the availability of detailed data for the validation process.

All the experimental data are coming from the experimental work done at the test-bench at the Chiba University [61].

5.1 Full engine simulation

Two different engine operating points have been simulated and compared to experimental data in order to test the quality of the full engine simulation; both engine operating points are at 1600 rpm and are characterized by a great valve overlap of 90°CA (Figure 5.1 and Figure 5.2):

- Torque = 150 Nm; imep = 12.4 bar (low load);
- Torque = 180 Nm; imep = 14.9 bar (high load).

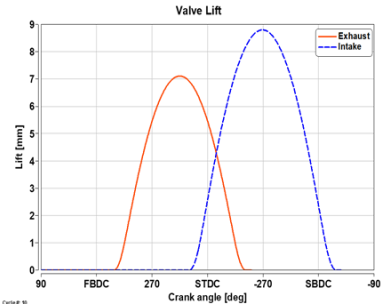

Figure 5.1: Valve overlap

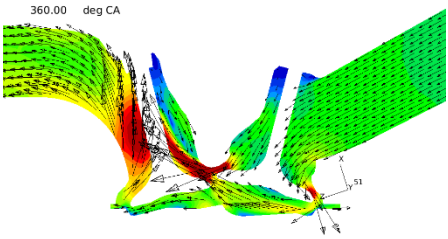

Figure 5.2: Flow field during scavenging

In both cases the simulation (Figure 5.3 and Figure 5.4) shows a very good agreement with experimental measurements. In particular, the in-cylinder pressure signal is for the simulation very close to the measured pressure from the test-bench during the whole cycle.

For the low load case, the pressure at ignition point (IP) is slightly lower than the measurement, which could be caused by a slightly different temperature at the intake boundary condition. However, such deviance is acceptable because in the range of experimental uncertainty in measuring the temperature of the intake air or the air mass flow rate. The pressure peak is in both cases well matched in terms of both timing and pressure.

Both engine operating points are characterized by a late IP in order to keep high the temperature of the in-cylinder gas at the opening of the exhaust valve.

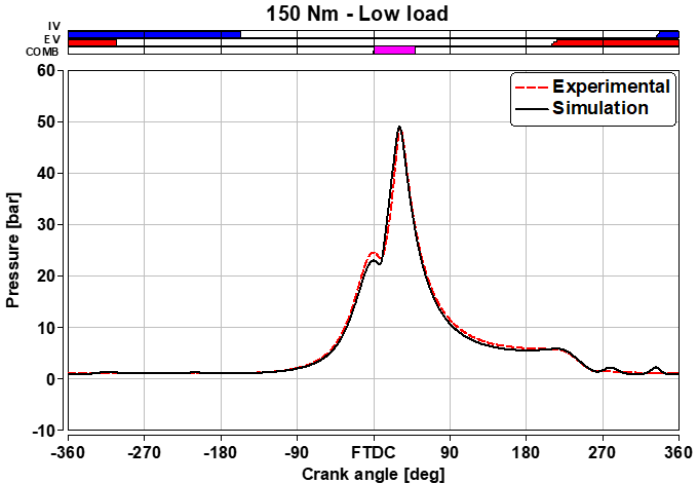

Figure 5.3: In-cylinder pressure. Experimental measurements against simulation data – 150 Nm

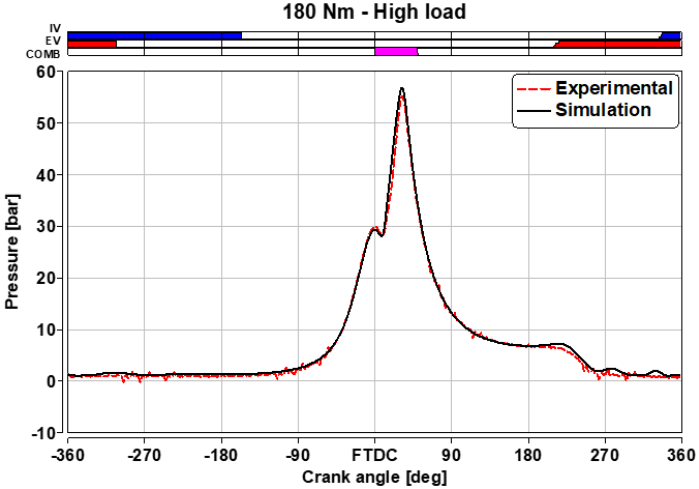

Figure 5.4: In-cylinder pressure. Experimental measurements against simulation data – 180 Nm

Some of the most relevant parameters of engine operation are reported in Table 5.1 and show an overall very good agreement with measurements at the test-bench.

Table 5.1: Tuning of full engine model against experimental data

	Low load		High load		Error	
Variable	**Test Bench**	**Sim.**	**Test Bench**	**Sim.**	**150 Nm**	**180 Nm**
Imep [bar]	12.4	12.2	14.9	14.6	2 %	2 %
P_max [bar]	50	48	55	55.5	4 %	0.9 %
Air Cons. [kg/h]	123	119	171	173	4 %	1%

Thanks to the good agreement of the two engine operating points with measured data, the full engine model has been considered adequately tuned. The advantage is that there is no need for tuning of the single engine operating point: once the parameters are defined for one engine operating point, the model will be able to simulate also different conditions.

For the others engine operating points it has been always controlled the quality of the simulation by comparing it with experimental measurements, if available, or GT-Power results of the same engine operating point with a calibrated model.

5.1.1 Scavenging analysis

Fresh air necessary for post-oxidation is brought into the exhaust manifold by means of scavenging, which is possible thanks to the positive pressure drop across the valves during the valve overlap. In Figure 5.1 is reported the valve lift used in both engine operating points. Since the engine has the possibility to regulate the valve timing but not the valve lift, in order to centre the scavenging on top dead centre (TDC), the opening of the exhaust valve has been delayed. The resulting valve overlap is extremely long (90°CA) causing the complex interaction of intake and exhaust manifold and making the engine very sensitive to pressure pulses propagating inside the pipes (Figure 5.5 and Figure 5.6). In Figure 5.2 is reported the flow field during scavenging for

cylinder 1 of the high load engine operating point. The relatively high boost pressure creates an important mass flow rate of fresh air from the intake directly into the exhaust. The picture is also a good example of how the great valve overlap connects the exhaust system to the intake: both valves are still open and the lift is still high (3 mm for the intake and 5.5 mm for the exhaust); the volume of the cylinder is very small because the piston is at TDC. In these conditions pressure waves and gases move easily through the whole engine because the cylinder does not act as a plenum volume independent of the pressure waves in the intake and exhaust. The boost pressure plays a fundamental role to keep the direction of scavenging constant; a low boost pressure or high-pressure peaks from the exhaust cause inversion of the mass flow rates.

In Figure 5.5 and Figure 5.6 the pressure patterns in the engine during the scavenging of cylinder 1 are reported for the two different engine operating points analysed as an example to clarify why this strategy makes the whole engine operation very delicate and sensible to pressure patterns. In the pictures there are numbers that refer to six events that will be analysed for both engine operating points.

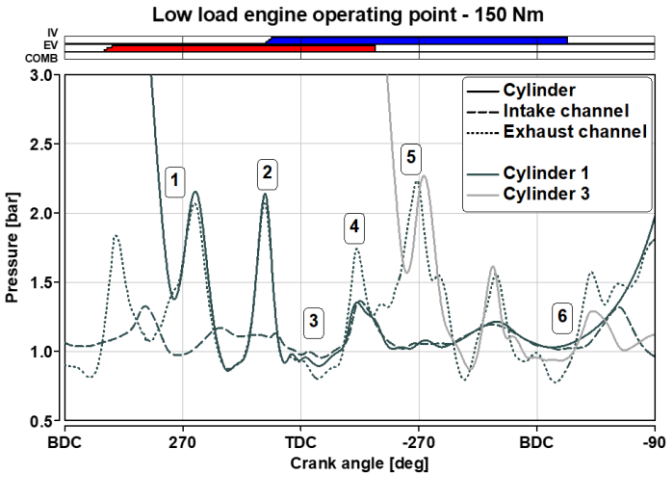

Figure 5.5: Pressure patterns in the engine during scavenging of cylinder 1 – Low load

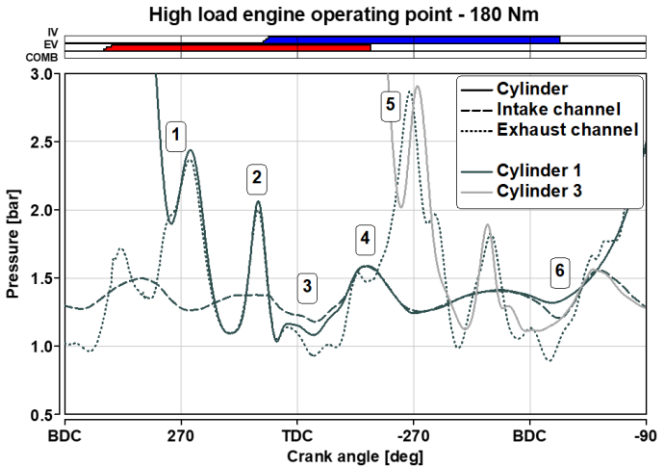

Figure 5.6: Pressure patterns in the engine during scavenging of cylinder 1 – High load

The first event (1) is the exhaust of cylinder 1 that causes the pressure in the cylinder to drop and rises the pressure in the exhaust channel creating a pressure wave that propagates in the exhaust manifold. This first event is very similar in the two cases but for the low load the pressure peak is slightly lower, due to the lower pressure in the cylinder at EVO.

The second event (2) is a high-pressure peak in the exhaust channel and cylinder very close to the intake valve opening (IVO), which inverts the mass flow rate through the exhaust valves causing a backflow from the exhaust into the cylinder. This is probably due to the reflection of the pressure wave of the exhaust in the volume of the exhaust manifold.

In point (3) scavenging is taking place and the pressure patterns is very well suited for the mass flow rate from the intake to the exhaust. In both cases the pressure in the intake channel is higher than the pressure in the cylinder and in the exhaust channel. In the high load case this effect is extremely evident because of the higher boost pressure.

However, at the end of scavenging (4) there is a steep pressure rise in the exhaust channel, in the cylinder and consequently in the intake channel. This is due to the exhaust of the following cylinder, in this example is cylinder 3. In the low load case the effects of this pressure wave propagation cause the

inversion of the pressure drop across the valves, with a higher pressure on the exhaust side. The inversion of the pressure drop is due to the low boost pressure. In the high load case this effect is not as evident: the pressure in the exhaust channel never becomes higher than the pressure in the intake thanks to the higher boost pressure.

In the point (5) the exhaust valves of cylinder 1 are closing and the exhaust of cylinder 3 continues. From this moment on the pressure inside cylinder 1 is determined by the boost pressure, therefore we will focus on pressure signals inside the cylinder and in the intake channel.

The last interesting point is (6): at this moment the intake valves of cylinder 1 are about close, the piston has already surpassed BDC and is now moving upwards. The movement of the piston creates a pressure increase due to the inertial effects of the mass of air in the cylinder that coincides with a low pressure in the intake channel. Therefore, once again the pressure drop across the intake valves inverts, which causes a backflow from the cylinder into the intake channel. This effect can be seen in both engine operating points.

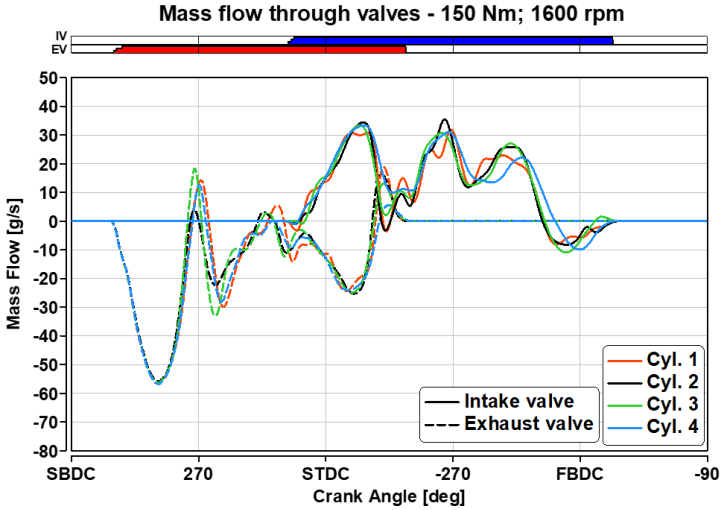

Figure 5.7: Mass flow rate through the valves – low load case (positive → flowing into the cylinder)

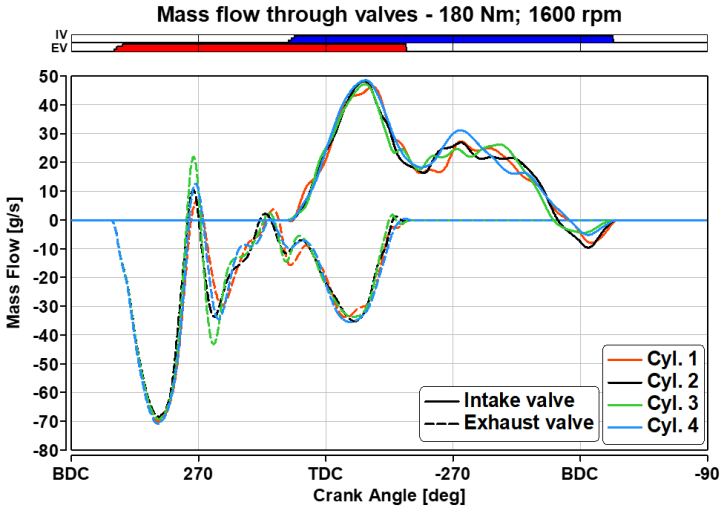

Figure 5.8: Mass flow rate through the valves – high load case (positive → flowing into the cylinder)

The advantage of a full engine 3D-CFD simulation is that the contribution of each single cylinder can be precisely determined. In Figure 5.7 and Figure 5.8, the mass flow rates through the valves for each cylinder for both cases are reported.

In both engine operating points during the valve overlap there is a great amount of fresh air flowing from the intake into the exhaust. In the low load case, close to exhaust valve closing (EVC) there is an important backflow from the exhaust into the cylinder and from the cylinder into the intake manifold. This is due to pressure waves propagating in the exhaust manifold determined by the exhaust of the following cylinder (point (4) in Figure 5.5) as already discussed; at the beginning of the exhaust event a great mass flow exits the cylinder and creates a pressure front that travels across the exhaust manifold and reaches the other cylinders. One of the cylinders still has the exhaust valves open and is concluding the scavenging phase, which is characterised by low mass flow rates of fresh air and relatively low pressure. Due to the low boost pressure of the low load engine operating point, the pressure peak causes an important backflow from the exhaust into the cylinder.

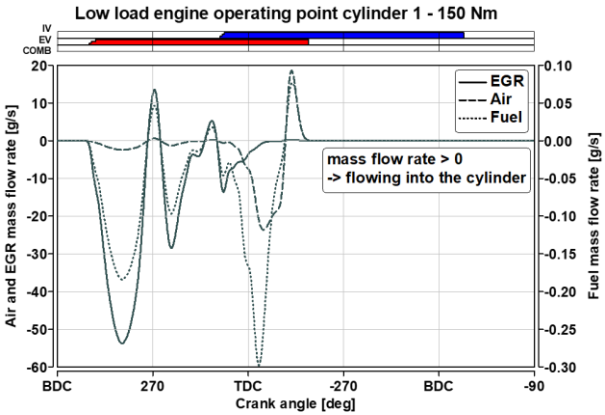

Figure 5.9: Species mass flow rates through the exhaust valves. Air and EGR are reported on the left y-axis and fuel on the right y-axis

In Figure 5.9 it is possible to see how the simulation quantifies, what species is the backflow composed of. First of all, it is possible to see how during the scavenging the mass of EGR (burned gases of the previous cycle) that flows through the exhaust valves into the exhaust system rapidly decreases and is substituted by fresh air. Moreover, the model predicts that the backflow at the end of the valve overlap is mostly composed of fresh air that has been previously pushed into the exhaust by scavenging and accumulated close to the exhaust valve in the form of a cloud. Such air pocket is then during the backflow partially pushed back into the cylinder.

Also a small amount of fuel in the gas state flows to the exhaust. The mass flow rate of fuel is always very limited and has two different sources: the unburned mixture from the cylinder and the fresh mixture that accumulates in the intakes channels due to the backflow before intake valve closing (IVC), when fresh mixture is pushed back into the intake system by the movement of the piston. Indeed, the peak of fuel mass flow rate through the exhaust valves happens at the beginning of scavenging, i.e. the first air flowing to the exhaust has a certain amount of fuel that can be quantified.

In this case, the backflow does not increase the amount of EGR inside the cylinder, which could influence the combustion. The backflow reduces also the amount of fresh air in the exhaust manifold; however, as it will be demonstrated later, this effect does not affect post-oxidation significantly

while reducing the air consumption, which has the advantage of keeping the engine operation closer to stoichiometry. The pressure peak propagates also in the intake manifold due to the open valves. The effect on the other cylinders is on the intake side less relevant because the great volume of the air-box absorbs partially the pressure wave [66].

This is also a good example of how pressure waves propagating from the exhaust may cause two major problems that are difficult to control during engine operation and that cause numerical problems for the simulation:

- Pressure waves may cause a backflow so big that pushes a great amount of air out of the cylinder back into the intake manifold. If the boost pressure is not high enough, the cylinder filling is poor and the amount of air in the cylinder does not allow for combustion due to the extremely rich $\lambda_{CYLINDER}$.
- It is possible that, in case of very high pressure peaks, during backflows an important amount of burned gases flows back into the cylinder before EVC, forcing them to participate to the next combustion. This can raise the amount of internal EGR above the limit that the engine can support for combustion. This is not the case of the low load engine operating point because of the great scavenging that happened just before the backflow. The backflow consists in this case of fresh air and there is no internal EGR in the combustion chamber. However, it is possible that in engine operating points with lower scavenging the amount of internal EGR inside the cylinder increases.

The mass flow rates through the valves in the high load engine operating point have a different pattern due to the higher boost pressure. Indeed, in this case, the scavenging is extreme and there is no backflow close to EVC. The engine operation is more stable because the boost pressure is able to counteract the pressure from the exhaust system. The mass flow rates across the valves are more stable and the effect of pressure waves is less evident.

5.1.2 Lambda analysis

Both engine operating points are characterized by a backflow from the cylinder into the intake manifold short before intake valve closing (IVC). This

backflow is due to the fact that IVC happens around 10°CA after bottom dead centre.

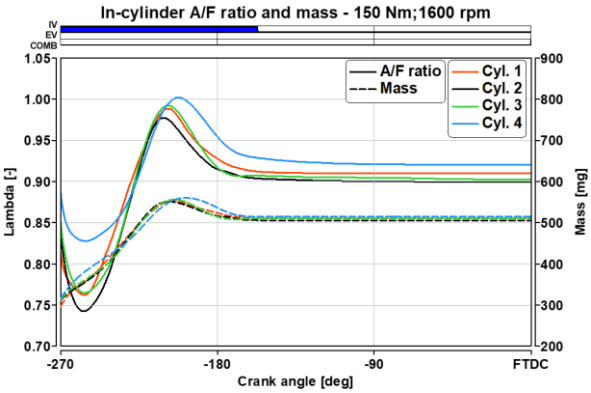

Figure 5.10: Air fuel ratio and in-cylinder mass – Low load

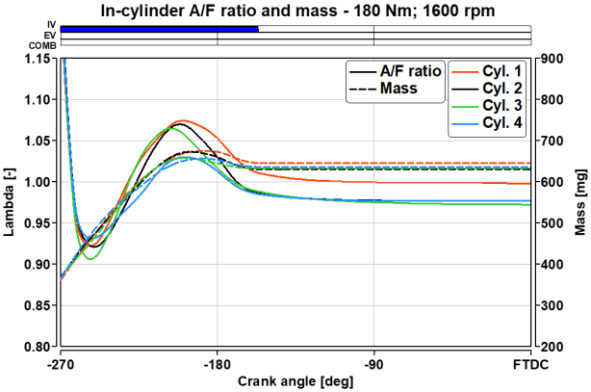

Figure 5.11: Air fuel ratio and in-cylinder mass – High load

During the final part of the intake, the piston is moving upwards and pushing some air back into the intake system with its movement. The boost pressure and the pressure patterns in the intake system are not enough to overcome the piston movement. Therefore, there is a mass flow rate from the cylinder into the intake manifold. Since at this moment the injection is already completed and most of the fuel is already vaporized and mixed, the backflow brings some fresh mixture into the exhaust manifold. This fresh mixture accumulates close to the intake valves and at the following cycle it flows directly to the exhaust

during scavenging (Figure 5.9). This fresh mixture is a possible source of tail hydrocarbons (THC) that may cause emission problems. It is necessary that these THC are completely oxidized during post-oxidation, which is a quite complicated target to reliably achieve. In Figure 5.10 and Figure 5.11 it can be seen that the backflow causes in both cases a reduction of the in-cylinder air mass and a change of $\lambda_{CYLINDER}$ that in both cases shifts towards richer values because during the backflow more fresh air than fuel flows to the intake manifold.

Another important parameter to be analysed is the in-cylinder mixture formation. In Figure 5.10 and Figure 5.11 the value of in-cylinder lambda is reported. For both engine operating points there are differences in the mixture formation among the cylinders. This is due to the different amount of air in the cylinders, which is again the effect of complex pressure wave patterns in the whole engine. Since a very small variation in the in-cylinder mixture formation has an important effect on the amount of CO and H_2 that are available for post-oxidation and therefore on the resulting heat release, the cylinder-to-cylinder difference must be taken into account during the simulation.

Both engine operating points have a rich in-cylinder mixture ($\lambda_{CYLINDER}$), which means that there is not enough air to completely oxidize the fuel. Therefore, the oxidation reaction (combustion) is interrupted before the fuel is completely oxidized to CO_2 and H_2O. The combustion products will therefore contain CO and H_2, which are the most stable intermediate products of the oxidation reaction and which have still a relevant heating value [30]. Post-oxidation is mostly fuelled by the oxidation of these two species [62]; therefore, their availability is a necessary condition. The parameter that permits to control the amount of CO and H_2 is $\lambda_{CYLINDER}$: theoretically the lower the $\lambda_{CYLINDER}$ the higher the amounts of CO and H_2 available for post-oxidation. In practical application, there is a limit of $\lambda_{CYLINDER}$, below which the combustion becomes too unstable for engine operation. A second important limit is for $\lambda_{CYLINDER}$ equals to stoichiometry or greater: in this case the combustion is complete and the amount of CO and H_2 are too low to start the post-oxidation.

The in-cylinder average $\lambda_{CYLINDER}$ in the low load case is 0.90, which means that the in-cylinder mixture is quite rich and the amount of CO and H_2 in the exhaust gases is relevant. The differences among the cylinders in the low load case are due to the different mixture formation process; in particular, cylinder

4 has a slightly better filling, therefore more fresh air in the cylinder and a mixture closer to stoichiometry. It can be expected that cylinder 4 has a lower heat release from post-oxidation in comparison to the other cylinders.

In the high load case, instead, the mixture inside the cylinder is closer to stoichiometry ($\lambda_{CYLINDER}$ 0.98), therefore there is less CO and H_2 available and a limited post-oxidation. Also in this case there are important differences among the cylinders; cylinder 1 in particular has a stoichiometric mixture in the cylinder, which means that theoretically the exhaust products cannot trigger the post-oxidation. These consideration, however, apply only to a global analysis, while locally the mixture conditions can be very different.

Table 5.2: In-cylinder mixture distribution for the high load engine point

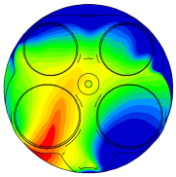	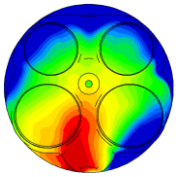	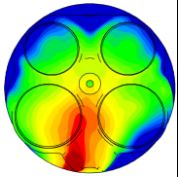	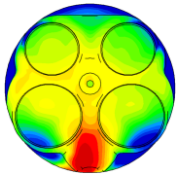	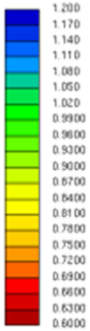
Cylinder 1	Cylinder 2	Cylinder 3	Cylinder 4	Lambda

The values reported in Figure 5.10 and Figure 5.11 assume that the amounts of air and fuel inside the combustion chamber are perfectly mixed together. However, mixture formation is a complex process that depends on many different parameters like in-cylinder charge motion, turbulence production, injection timing, injection targeting, etc. Therefore, the in-cylinder mixture formation can be very different between two engine operating points and even among different cylinders in the same engine operating point.

The analysis of the local distribution of the fuel in the cylinder is carried out by means of the parameter λ_{LOCAL}, which represents the mixture in one particular point of space, i.e. in one cell.

As an example, in Table 5.2 are reported the in-cylinder mixture distributions for each cylinder at firing top dead centre (FTDC) for the high load engine operating point. The distributions are very different among the cylinders; generally there is a volume underneath the injector that has a very rich λ_{LOCAL} = 0.6, i.e. a small volume that is locally very rich. This volume is surrounded by increasingly leaner mixtures and at the walls of the cylinders there is generally a very lean mixture (λ_{LOCAL} = 1.2). The description of local mixture distribution is fundamental for the simulation of post-oxidation and the advantage of a 3D-CFD simulation is that it enables not just for a qualitative description but also a quantitative one.

5.1.2.1 Lambda Map

In order to quantify the inhomogeneity inside the cylinder, a tool called Lambda-Map has been developed in QuickSim taking advantage of the fact that the 3D-CFD simulation defines for each time step and each cell of the grid the mixture. At each crank angle the volume of the combustion chamber is calculated and the local air-fuel ratios are grouped into different bins within the current volume. For each crank angle then the percentage of the cylinder volume at a certain lambda can be identified. This map is useful to analyse the evolution of the mixture inside the cylinder and to evaluate the composition and amount of exhaust gases.

In Figure 5.12 it can be seen, as an example, the mixture distribution of cylinder 1 of the high load engine operating point. At the end of injection (around -270°CA) a limited volume has a very rich lambda while the remaining volume has a very lean mixture. During the compression, the fuel mixes and the homogenization increases. Nevertheless, at FTDC there is still an important dispersion of λ_{LOCAL} around the stoichiometric value, i.e. there are lean and rich volumes inside the cylinder. In particular, although the overall in-cylinder mixture has a $\lambda_{CYLINDER}$ = 0.98, 40% of the volume at FTDC has a lean mixture (λ_{LOCAL}>1.05) and less than 15% of the volume is in very rich conditions with a λ_{LOCAL}<0.85. This means that the mixture formation is incomplete. The explanation is the very low tumble and therefore turbulence inside the cylinder in combination with the injector targeting, which are characteristic of high load and low load engine operating points.

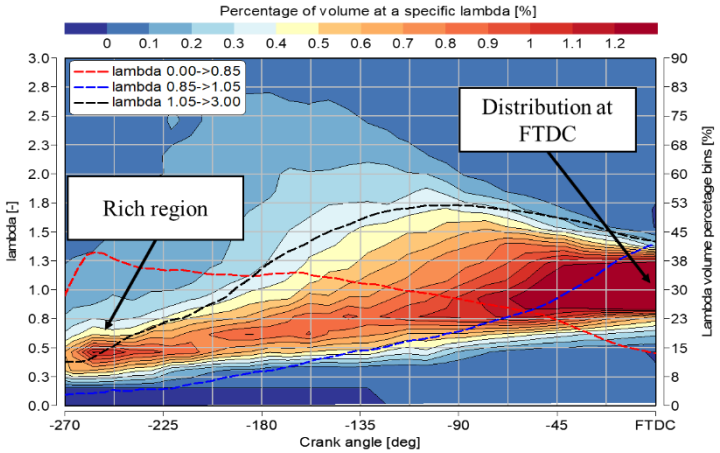

Figure 5.12: Lambda-Map of cylinder 1 in the high load case

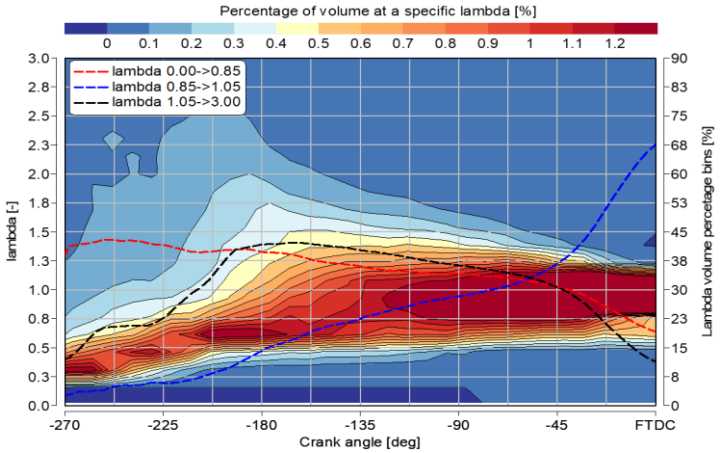

Figure 5.13: Lambda map of cylinder 1 in the low load case

The same analysis has been carried out for the low load engine point (Figure 5.13). The same processes can be highlighted also here. In this case, however, there is a better homogenization of the fresh charge at FTDC.

In Figure 5.14 the distributions at FTDC are compared for cylinder 1 in the two engine operating points. The distribution in the low load case is more

homogeneous and the peak in distribution is for richer in-cylinder mixture. Moreover, the low load engine operating point has a smaller peak in the distribution for $\lambda_{LOCAL} = 0.6$, meaning that there is a small volume in very rich conditions that will produce great amounts of CO and H_2. Finally, the mixture distribution ends for values of the mixture that are stoichiometric and lean; lean volumes represent a small part of the total distribution and store fresh air that can be used for the oxidation of the rich mixture of exhaust gases.

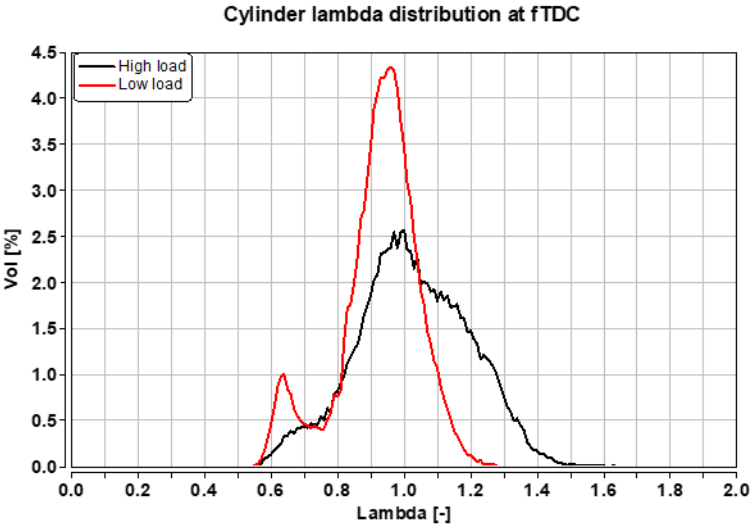

Figure 5.14: Lambda distribution at FTDC for low load and high load engine operating points

The distribution of the high load engine operating point, instead, is much more disperse and has a lower peak, which means that the homogenization is less effective. There are important parts of the combustion chamber in lean or even very lean conditions. The peak in the distribution corresponds to a mixture very close to stoichiometry and its absolute value is much lower than that of the low load engine operating point. Therefore, the greatest part of the cylinder is in stoichiometric and lean conditions, which reduces the amount of CO and H_2 produced because in these volumes there is oxygen available to complete the oxidation of the fuel. Moreover, the lower peak of the distribution means that generally the homogenization in the cylinder is less complete.

These two examples demonstrate that the information of $\lambda_{CYLINDER}$ is important and can serve as a first approximation of the amount of CO and H_2, but it must be completed with the Lambda-Map analysis, which gives an information also about the λ_{LOCAL}.

5.1.2.2 Charge motion analysis

The cylinder-to-cylinder differences of tumble and turbulence give reason for the differences in mixing patterns in the cylinders (Figure 5.15 and Figure 5.16). Tumble is a structured rotational flow on a cylinder axial plane generated during the intake process. Tumble continues during the compression stroke and, as the volume of the combustion chamber decreases, increases in intensity. The tumble motion dissipates into turbulence, which reaches its maximum around fTDC. The higher turbulence increases the gas motion and the flame speed. As a result, the combustion duration decreases, which can be exploited to increase the efficiency of the engine.

Tumble is the result of different parameters. The greatest influence is due to geometrical features of the engine such as the shape of the intake channels, the form of cylinder roof, the angle of the intake valves, the shape of the piston etc. The injection strategy and the injection targeting can also be used to create a tumble movement in the cylinder. The spray targeting must point in the direction of the tumble motion, which is easily achieved with a lateral direct injection, as for the analysed case. The injection timing must be phased in order to maximize the effects of the injection, i.e. when the spray targeting allines with the tumble motion. For the case of interest, this happens for a late injection during the compression stroke. However, such strategy has not been adopted because it has been preferred to use an early injection that exploits the evaporation of the fuel to cool down the charge, increase it density and achieve a better cylinder filling.

The tumble number quantifies the intensity of the tumble motion and is an important parameter for engine development: the higher the tumble the number, the faster is the rotation of the charge in the combustion chamber. A too high tumble can cause a blow-off of the flame, i.e. the flame propagation is slower than the gas movement and the combustion results in a misfire. A too low tumble number usually causes a very slow combustion and an incomplete mixture formation. A normal value for tumble number for SI engines at low rpm is between 2 and 3.

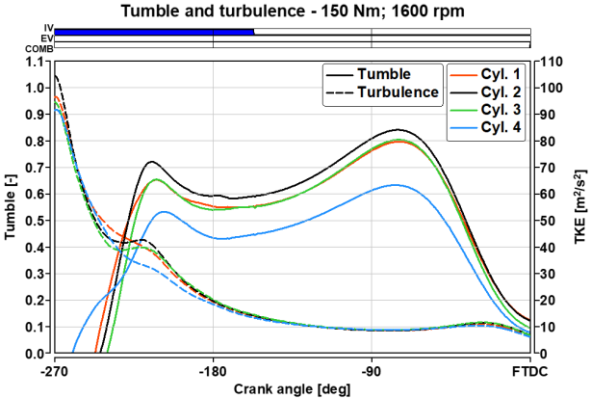

Figure 5.15: Tumble and turbulence in the cylinder – Low load case

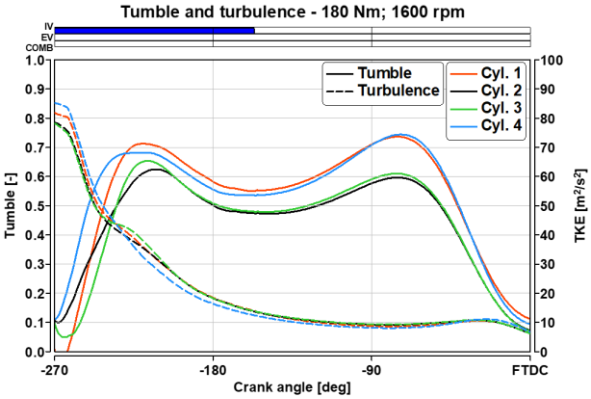

Figure 5.16: Tumble and turbulence in the cylinder – High load case

As expected, in the analysed cases the behaviour of each cylinder changes as a consequence of the engine operating load.

In the two analysed cases tumble results very low because during the intake phase the mass-flow rates through the intake valves do not have enough energy to accelerate the mass inside the cylinder. Therefore the tumble movement remains limited and consequently also the turbulence. This condition has many effects, among which the most interesting are: an incomplete homogenization of the charge inside the cylinder, a slow combustion and therefore a high temperature of the exhaust gases at EVO.

5.1.2.3 Global lambda analysis

The inhomogeneity in the cylinder ensures that during the combustion it is possible that the flame encounters volumes with a local value of lambda that differs from the overall average value. There are two major possibilities:

- Volumes with a rich mixture where the combustion cannot completely oxidize the fuel and CO and H_2 are formed, which can later on participate to post-oxidation in the exhaust manifold.
- Volumes with a stoichiometric mixture or lean mixture where fresh air remains available for the post-oxidation as well as there might be the formation of pollutants such as NO.

Thanks to the full engine simulation, the local inhomogeneity is taken into account and the information is implemented in the detailed simulation of the exhaust manifold in the form of boundary conditions.

The air to fuel ratio of the total engine (λ_{ENGINE}) must be considered when analysing the engine operation during post-oxidation. It can be easily calculated as the ratio of the total air consumption and the total fuel consumption divided by the stoichiometric value of the specific fuel. Since the target of the post-oxidation strategy is to enable scavenging, i.e. turbolag reduction, without causing any efficiency losses at the three-way-catalyst (TWC), λ_{ENGINE} must be very close to stoichiometry.

In Figure 5.17 (first column), it is reported the overall air consumption for the two engine operating points. This general indicator is composed by the sum of:

- Volumetric air consumption, i.e. the air consumption due to the air trapped in the cylinders;
- Scavenging air consumption, i.e. the air flowing directly to the exhaust manifold during scavenging without participating to the combustion.

For both engine operating points there is a certain amount of scavenging air, as expected. The air consumption is much higher for the high load case due to the higher boost pressure; scavenging air represents almost the 30% of the total engine air consumption because for the whole period of valve overlap there is positive pressure difference. In the low load case, instead, the percentage of

scavenging air to the total air consumption is around 17%. The amount of scavenging is in both cases very high and has the scope of making oxygen available in the exhaust manifold.

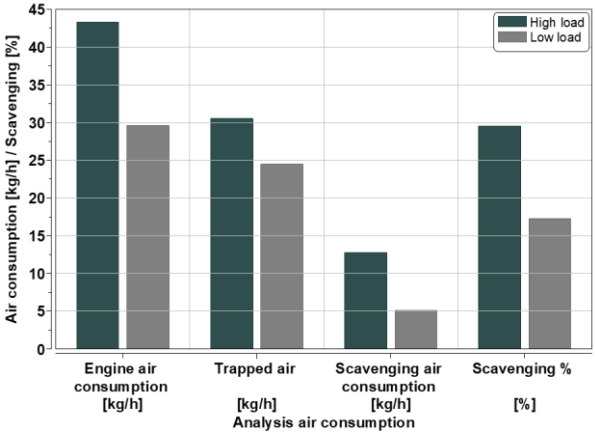

Figure 5.17: Air consumption analysis

The second important parameter for post-oxidation is the in-cylinder lambda ($\lambda_{CYLINDER}$), which has to be lower than stoichiometric in order to produce CO and H_2. In Figure 5.18, it can be seen that for both cases the mixture in the cylinder is slightly rich. Finally, in Figure 5.18 are reported the values of the overall engine operation that should be as close to stoichiometry as possible. Due to the high scavenging and the $\lambda_{CYLINDER}$ close to stoichiometry, the high load engine point has a λ_{ENGINE} = 1.32, which is too lean and may cause efficiency losses at the TWC. The low load engine point, instead, has a λ_{ENGINE} = 1.03, which is a very good result because ensures a stoichiometric operation and the best conditions for post-oxidation.

The tuning of the engine operation for post-oxidation, as it has been demonstrated, is very complicated. For the correct definition of $\lambda_{CYLINDER}$ and λ_{ENGINE} a fine equilibrium of valve overlap, boost pressure and injected fuel must be found. The low load case is very well calibrated. The high load case, instead, requires further tuning. For the sake of the validation of the 3D-CFD simulation methodology, both engine operating points are used. In a second step a more detailed optimization is used, in order to keep λ_{ENGINE} as close to stoichiometry as possible.

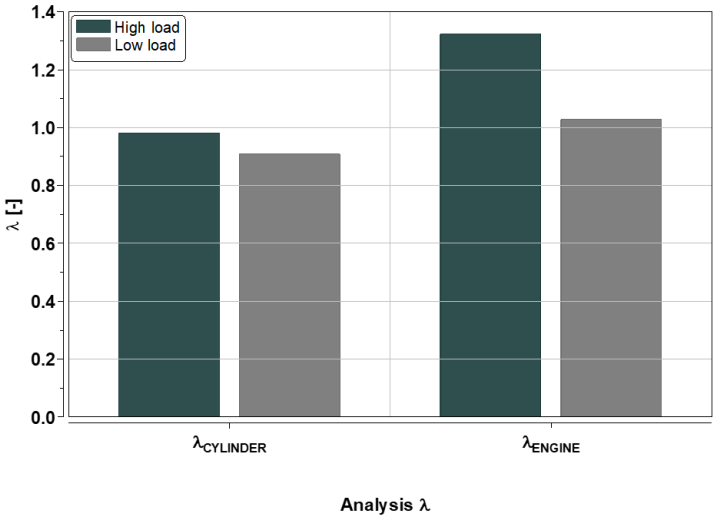

Figure 5.18: Lambda analysis

The full engine simulation has a very good agreement with experimental data and gives a deep insight in the most important phenomena of engine operation. The analysis based on these simulations pointed out that both engine operating points are well set for the operation in post-oxidation conditions.

These results have been used to define the boundary conditions for the detailed model of the exhaust manifold.

5.2 Detailed model of the exhaust manifold

The two engine operating points described in the previous session have been simulated also using the detailed model of the exhaust manifold. This model has the advantage of being able to simulate the chemical reactions that are taking place inside the exhaust manifold. For each engine operating point, the boundary conditions have been controlled and then at least three engine cycles have been simulated in order to reduce the influence of guessed initial conditions.

The validation process tests the ability of the simulation to match data from the test-bench. For the validation, the following data are available from the investigations at the test-bench:

- Pressure signals before the turbine;
- Temperature measurements;
- Species concentration measurements.

These three types of measurement are a way to test the model ability to make predictions for all the most relevant phenomena of post-oxidation. If the agreement of experimental data with the simulation is satisfactory, the whole simulation methodology is validated.

5.2.1 Pressure signals before the turbine

Pressure signals are measured at the test-bench before the turbine inlet in the position indicated with “limit” in Figure 4.3. In order to make a realistic comparison, it is possible to introduce in the computational grid of the simulation a virtual sensor exactly in the same position of the test-bench that evaluates at each iteration the pressure of the fluid.

In Figure 5.19 and Figure 5.20 is reported the comparison between the measured and the simulated pressure signals before the turbine.

The low load case shows a very good agreement with the experiments by matching the timing and the amplitude of pressure peaks. There are some differences in the pressure fluctuations around 1 bar, which are probably due to the fact that the model is limited to the exhaust manifold and lacks the complete interaction with the cylinders and the intake manifold. Such simplification changes the pressure wave patterns causing the mismatching of pressure signals. Since the agreement proved to be good throughout the cycle, this first validation step is successful.

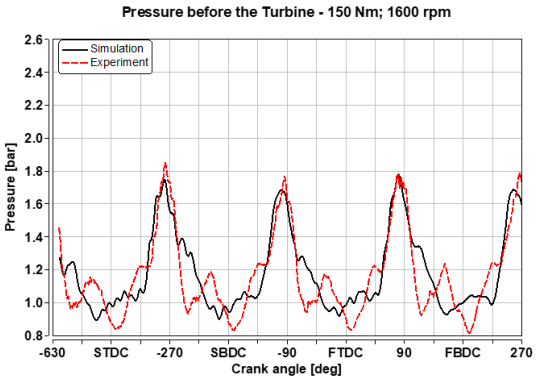

Figure 5.19: Pressure signal before the turbine – low load case

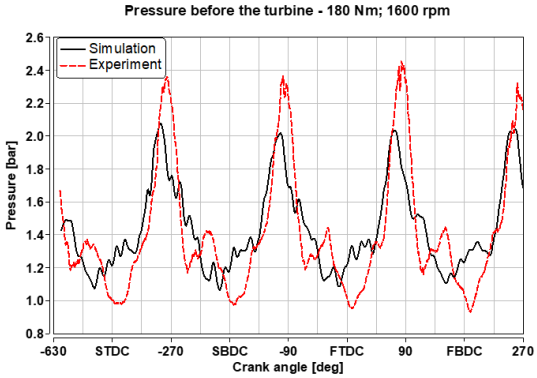

Figure 5.20: Pressure signal before the turbine – high load case

In the high load case, instead, the pressure peaks are underestimated while the timing of pressure peaks is correctly matched. This can be explained with the geometrical simplifications that have been necessary for the preparation of the model. In particular, the absence of the turbine plays a crucial role. However, the overall agreement is good: the timing of pressure peaks is matched correctly as well as the minima and the average value of pressure. Therefore, the validation can be considered also in this case successful. The lower pressure peaks in the simulated case may be an indication that the mass flow rates in the model tend to flow away a bit faster than in the real engine operation because of the lack of backpressures. The simplifications

introduced, however, do not change drastically the pattern of the pressure waves and the flow field inside the exhaust manifold.

A possibility to improve the accuracy of the pressure signal could be to use other approaches to simulate the turbine. An example could be the implementation of a 0D model of the turbocharger.

5.2.2 Temperature measurements

An important indication of post-oxidation is the increase in gas temperature before the turbine due to the reactions that are taking place inside the exhaust system. Therefore, temperature has been measured in five different positions at the test-bench using thermocouples. In order to carry out a meaningful comparison of experimental data and simulation, it is important to take into account the differences between the two types of investigation.

In the simulation it is possible to introduce inside the computational grid punctual simulation sensors, i.e. grid points that evaluate at each iteration the temperature of the fluid. It is fundamental to match in the simulation the same position of the thermocouple at the test-bench. In Figure 5.21 the punctual simulation sensors are reported inside the mesh.

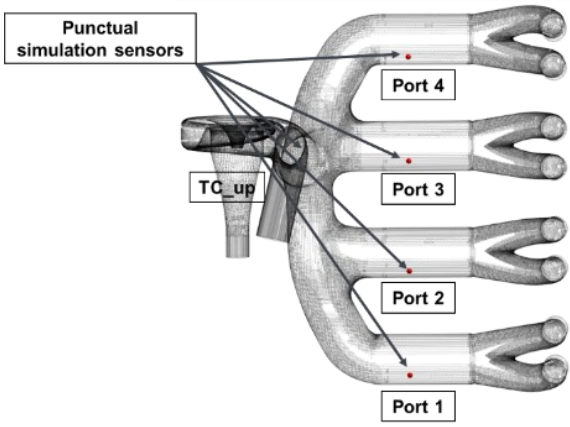

Figure 5.21: Position of punctual simulation sensors. Top view of the detailed mesh of the exhaust manifold

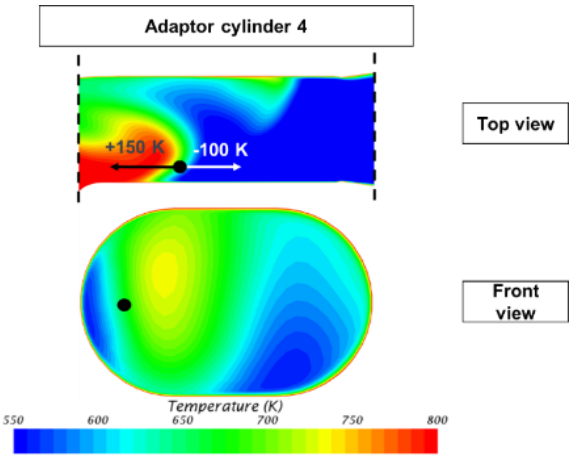

Figure 5.22: Temperature in the adaptor of cylinder 4 in the high load engine operating point

There are four thermocouples in the 10 cm adaptor tract and one before the turbine. While before the turbine there is a better mixing of gases and the distribution of temperature across the section of the pipe is more uniform, the position of the sensors in the adaptors is particularly crucial because in this zone the mixing is not effective and there are great gradients of temperature and species concentrations. An example can be seen in Figure 5.22. During the engine operation, the fresh air coming from scavenging gathers close to the exhaust valves and in the adaptor and forms a cold non-reactive cloud. In the four-in-one pipe of the exhaust manifold, instead, hot gases mix and post-oxidation starts. Therefore, the thermocouples placed in the adaptor are during the majority of the cycle in a position where in a few centimetres distance the thermodynamic and chemical conditions are completely different. For this reason, the position of the thermocouples has been accurately checked and copied from the position at the test-bench.

Another important factor to be considered in order to make a correct validation is the behaviour of real thermocouples.

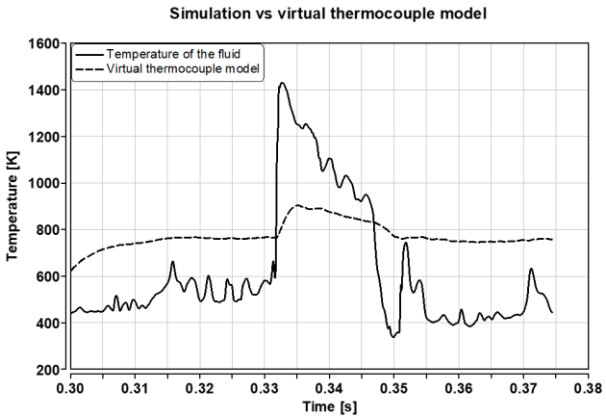

Figure 5.23: Difference between temperature of the fluid and virtual thermocouple sensor

The differences between the real thermocouple and the grid point, where the temperature evaluation is carried out, are that the grid points do not have a defined volume, therefore nor thermal inertia neither radiative heat exchange. The grid points do not have a specification of the material, therefore cannot account for the contact heat exchange. A comparison that neglects these effects cannot give realistic results because the temperature signal at the test-bench is not able to measure the exact fluid temperature. The real effects of the thermocouple consist in: thermal inertia due to the mass of the element; radiative and conductive heat exchange with the walls; convective heat exchange with the gases. Heat exchange depends strongly on the physical shape of the thermoelement, which must be reproduced accurately. Moreover, these effects are not in steady state, since the fluid around them is continuously moving.

In order to take into account the effects of real sensors, a model of a virtual thermocouple sensor has been developed following the work presented in [67]. The solution implemented consists in a numeric model that uses both thermodynamic data from simulation and information about the dimensions and materials of the real thermocouple. The application of this model on the position “Port 4” during the high load case can be seen in Figure 5.23.

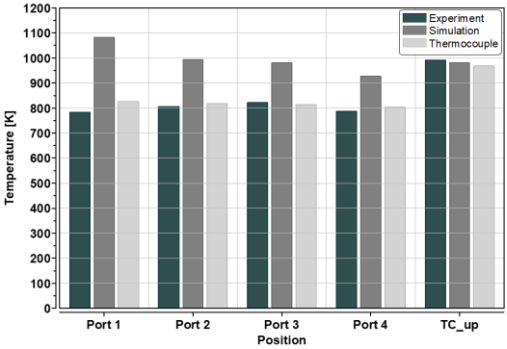

Figure 5.24: Temperature measurements and simulated values – low load

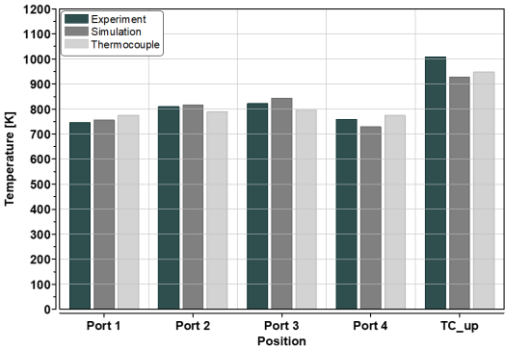

Figure 5.25: Temperature measurements and simulated values – high load

The effect of the virtual thermocouple model is to smooth the temperature signal that becomes almost constant, which is much more similar to the temperature signal of the measurements at the test-bench.

The results are reported for all positions in Figure 5.24 and Figure 5.25: for each position is reported the experimental value (Experiment), the mass flow average temperature of the fluid (Simulation) and the value after the implementation of the model of virtual thermocouple sensor (Thermocouple).

For both cases, the implementation of the virtual thermocouple model increases the agreement of simulated values with the experimental ones. In the low load case, the virtual thermocouple model increases definitely the accuracy for the sensors positioned in the adaptor because the simulation tends

to overestimate the very hot gases that flow during the exhaust stroke. In the high load case the benefit of the virtual thermocouple model is less evident.

In general, the low load case has higher temperatures, because of the lower scavenging, therefore lower amount of fresh air gathering in the exhaust and less cooling effect. The high load case, instead, has much higher mass-flow rates through the valves that cool down the exhaust manifold. In both cases, there is an increase of temperature between the adaptor and the TC_up position, due to both post-oxidation and the greater amount of hot gases that flows through the point.

It is also interesting that there are in the experiments differences among cylinders and that the patterns are fitted well by the simulation. Such cylinder-to-cylinder differences are due the flow field in the exhaust manifold and the amount of energy liberated by post-oxidation by each cylinder, which is related to the mixture formation inside the cylinder. Therefore, to match the differences among cylinders means that the simulation is able to precisely reproduce many complex and interconnected phenomena, which have an effect on post-oxidation. It is also a proof that the information transfer from the full-engine simulation to the detailed model of the exhaust manifold is working properly.

Finally, the simulation matches very accurately the experimental values, therefore making the validation successful. Another important result of this analysis is the importance of understanding the different characteristics of measurements and simulations in order to make a realistic comparison.

5.2.3 Species concentration measurements

The most delicate validation has been carried out using detailed data from the test-bench of molar concentrations of the most relevant species. At the test bench has been used a MEXA system for the measurement of molar concentrations of CO_2, O_2 and CO.

The measurements have been carried out also in this case inside the adaptor. As for the temperature measurements, it is fundamental to match the position where the measurements have been done at the test-bench. Indeed, the limited mixing in the adaptor and the formation of clouds of fresh air close to the exhaust valves and in the first part of the adaptor create steep gradients of

species concentrations with on the one side fresh air and on the other exhaust gases. In Figure 5.26 the positions can be seen, where the experiments have been carried out; these are exactly in the regions where the interfaces between fresh air and exhaust gases are and where the fluid mostly fluctuates during the engine cycle. This phenomenon is in the high load case extremely evident due to the great amount of scavenging.

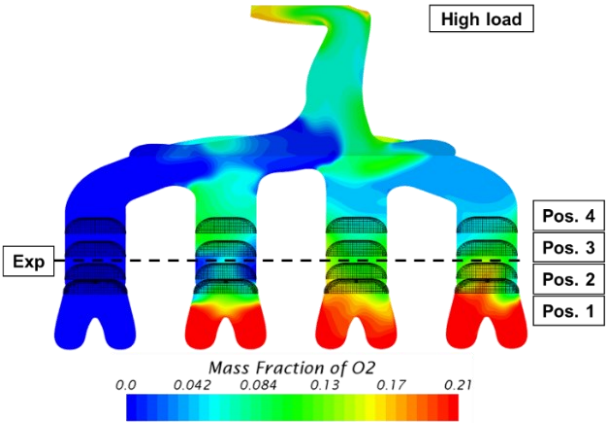

Figure 5.26: O_2 distribution in the exhaust manifold positions of measurements in experiments and in the simulation

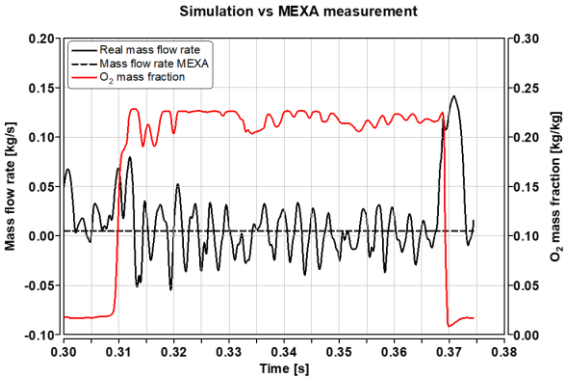

Figure 5.27: Comparison of real mass-flow rate across one surface and MEXA measurements

The evaluation of species concentrations in the simulation is not punctual, as for the temperature, but it consists of the average value on each surface at each iteration of the simulation. The evaluation has been carried out not only on the surface closest to the experiments (Pos. 2) but in four different positions for each adaptor in order to give an idea of the species gradients in the adaptor.

Also for this validation it is important to mimic the measurement method used in the experiments in order to have a meaningful comparison. MEXA measurements use a constant mass-flow-rate, which is completely different from the real mass-flow-rate across the surface. An example can be seen in Figure 5.27 where the real mass-flow-rate across one surface in the adaptor is compared with a theoretical mass-flow-rate of MEXA. In the diagram it is also reported as an example the concentration of O_2 on the same surface. The simulation predicts a mass-flow-rate around zero for most of the engine cycle, which means that the fluid is oscillating around the surface due to pressure waves propagating in the exhaust. Only at the end of the cycle there is one single event with very high positive mass-flow-rate, which means that the exhaust of the cylinder just happened and the exhaust gases are being pushed towards the turbine. The O_2 concentration starts with very low values, i.e. the surface is inside a cloud of exhaust gases, then rises to a value of 23% kg/kg that means that the fresh air from scavenging has reached the surface. The fresh air is pushed away by the following exhaust of the cylinder, which in this case happens at the end of the cycle.

If the average species concentration is calculated using the real mass of each species that flows across the surface, the long period with low and often negative mass-flow-rate and high oxygen mass fraction will have little relevance. On the other hand, the period with high mass-flow-rate and low amount of oxygen will be more relevant because most of the mass flows during the exhaust of the cylinder. MEXA measurements, instead, due to the constant mass-flow-rate, overestimate the period with high amount of oxygen and underestimate the exhaust period with very limited amount of oxygen resulting in an overestimation of the amount of oxygen. Therefore, it is important to reproduce this effect before comparing the results of the simulation with those of experiments. The constant mass-flow-rate measurement can be numerically simulated starting from the standard evaluation of the simulation by means of some simple elaboration. In Figure 5.28, Figure 5.29, Figure 5.30 and Figure 5.31 are reported the results concerning the low load case.

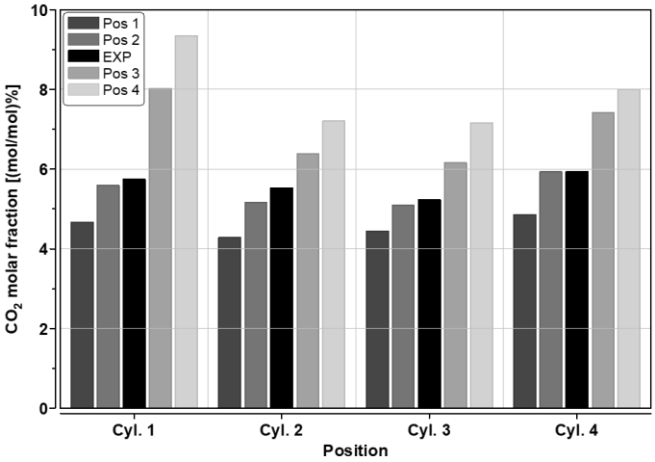

Figure 5.28: CO_2 measurements – low load

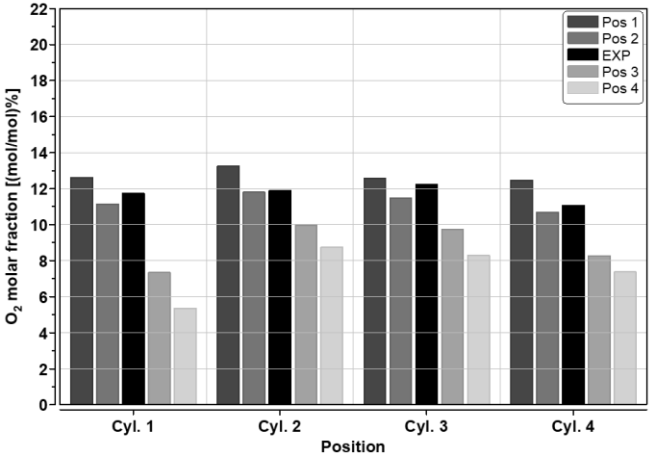

Figure 5.29: O_2 measurements – low load

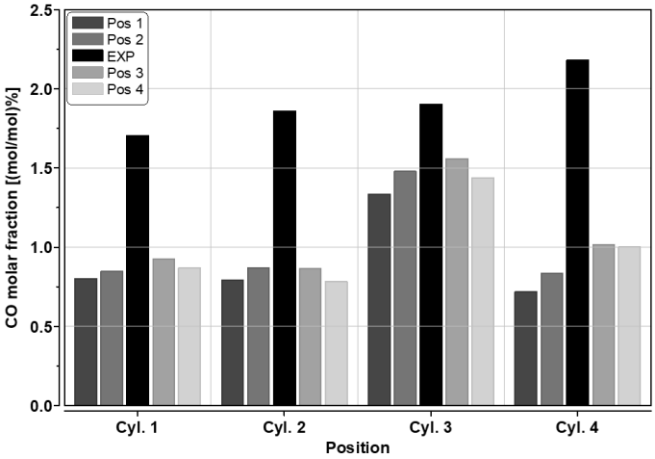

Figure 5.30: CO measurements – low load

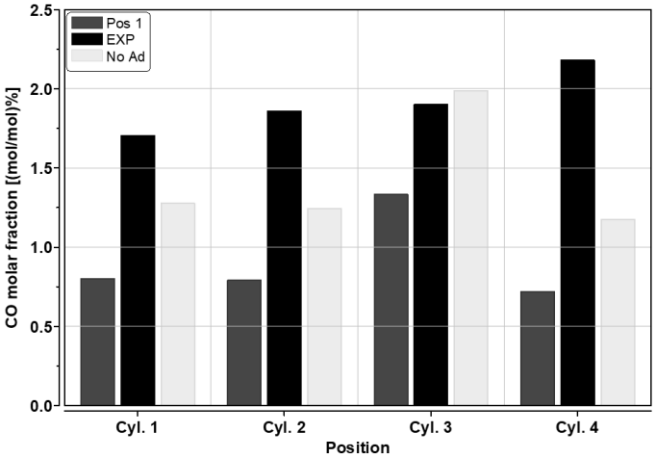

Figure 5.31: CO measurements assuming a non-adiabatic wall – low load

In each adaptor, are reported the results for the four surfaces used for the evaluation. The experimental measurements are the black columns between Pos. 2 and Pos. 3. The position of the black columns is where the sampling at the test-bench have been carried out.

Considering the low load engine operating point, the values both from measurements and from the simulation do not match the expetations for this engine operating point. The overall engine operation for the low load case is very close to stoichiometry, therefore, as reported in Table 5.3 and Figure 5.32, after a combustion in ideal and stoichiometric conditions, the molar fraction of CO_2 in the exhaust gases should be 13 mol%; moreover, there shouldn't be neither O_2, nor CO. In the measurements, instead, the molar fraction of CO_2 is less than 6 mol% and the amount of CO is around 1.5 mol%. In order to have a similar amount of CO_2, it would be necessary a $\lambda_{CYLINDER} = 0.7$ (in ideal conditions). Also the amount of oxygen differs substantially from the ideal conditions. In order to have 10 mol% of O_2 like in the measurements, it would be necessary a combustion with $\lambda_{CYLINDER} = 1.3$. None of this happens for the low load engine operating point, as already discussed, and these results can be explained thanks to the performed simulations.

The simulations demonstrated that the presence of CO in the exhaust manifold is due to the rich in-cylinder combustion performed with a $\lambda_{CYLINDER} = 0.9$. In second place, although the engine overall operation is stoichiometric, there is fresh air flowing into the exhaust during the scavenging event. The reason for such high molar fraction of oxygen is that the position, where the experiments are sampling, is the same, where the gradients between the fresh air clouds and the combustion products are. Therefore, the sampled exhaust gases are greatly diluted with fresh air. On top of this, the MEXA measurement uses a constant mass-flow-rate that, as already demonstrated, overestimates the amount of oxygen during one cycle. The simulations are therefore fundamental to understand the frame in which the measurements have been performed and provide a logical explanation of the results.

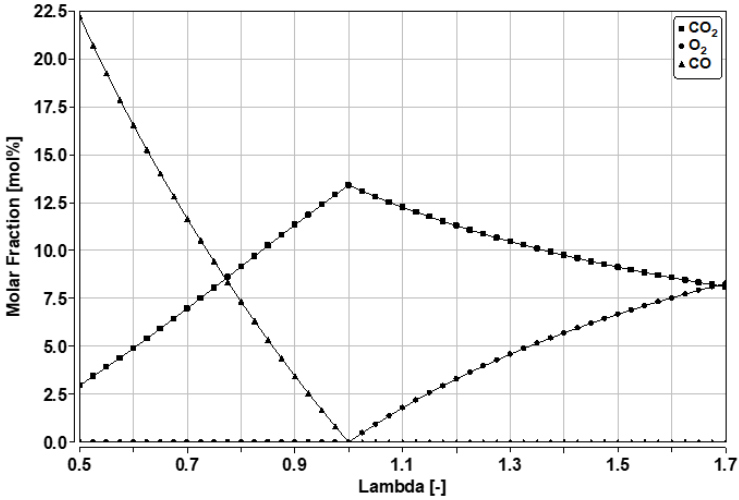

Figure 5.32: Molar fraction of relevant species after an ideal combustion

Table 5.3: Composition of exhaust gases of combustions with different air-fuel ratios

λ [-]	CO_2 [mol%]	O_2 [mol%]	CO [mol%]
0.7	6	0	11
1	13	0	0
1.3	10	5	0

For CO_2 and O_2 measurements there is a very good agreement in all sampling positions. The best agreement is for Pos. 2 for all cylinders, because this surface is the closest to the sampling point. When moving from Pos. 1 to Pos. 4 there is an increase in CO_2 and a decrease in O_2, which is an expected result because the evaluation surface is moving from the exhaust valve towards the turbine (Figure 5.33). Therefore, Pos. 1 will be in the middle of the fresh air cloud with high molar fraction of O_2 that dilutes CO_2. In Pos. 4, instead, the surface is closer to the four-in-one exhaust runner that acts as a mixing volume before the turbine where all adaptors come together and hot exhaust gases stagnate. In this region, the molar fraction of O_2 is much lower than in Pos. 1 and the molar fraction of CO_2 increases thanks to the diminished dilution with

fresh air from scavenging. Still, the CO_2 reaches at most 8 mol%, which is still a very low value, which suggests that also in this position the amount of dilution air is important.

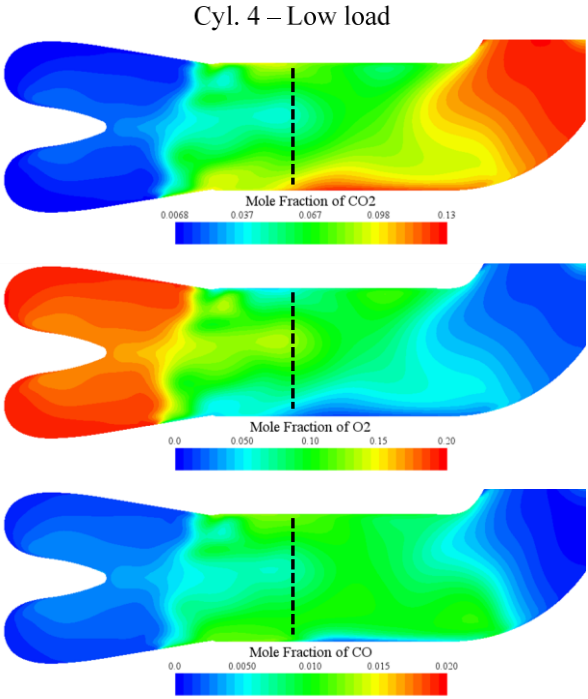

Figure 5.33: Mole fraction gradients in cylinder 4 – low load case

Concerning CO (Figure 5.30), instead, the agreement is less precise between experimental data and the simulation. It has to be noted that the molar fractions are for CO much lower than for the other species. Therefore, a small absolute difference in the amount of CO causes a great relative difference of molar fractions. This makes the simulation and the experiments very sensitive to assumptions and simplifications. A second factor for the difference between experiments and simulation is the rate of post-oxidation. Indeed, since CO is consumed exclusively during post-oxidation, a reaction rate too high before the sampling point could lead to an underestimation of CO. The most important parameter that influences the reaction rate is the temperature of the gases, which is the result of the boundary conditions and the thermal condition

at the walls of the model. Since the boundary conditions come from the full engine simulation, they can be considered reliable, because of the good agreement of full engine simulations with experimental data. The only left possibility is the thermal condition imposed at the walls of the model. For the first simulations, the assumption of adiabatic walls has been adopted. However, in real engine operating conditions this assumption is not realistic.

In Figure 5.31 is compared the result at Pos. 2 of the simulation with adiabatic walls with the one assuming a fixed temperature at the walls of 700 K in the same position. The last simulation matches better the experimental results confirming that the simulation with adiabatic walls overestimates the reaction rate of post-oxidation. A further tuning of the model is not desirable for many reasons:

- The absolute error in CO is very limited;
- Although the comparison is based on the mimic of the measurements method used at the test-bench, there is a number of assumptions that could introduce small differences, which in the case of very limited absolute values of CO have a great impact;
- The tuning consists in a modification of boundary conditions, e.g. numerical increase of the amount of CO that enters the volume, that cannot be based on experimental evidences, since the full engine simulation demonstrated a very good agreement for the most relevant parameters;
- The geometrical simplifications introduced in the detailed model of the exhaust manifold probably play a more relevant role than boundary conditions;
- The introduction of tuning parameters makes the simulation methodology less flexible;
- The perfect match of experimental measurements is not realistic also due to the cycle-to-cycle variability and experimental accuracy.

Overall, the agreement of simulation and experimental data is very good and the validation can be considered to be satisfied.

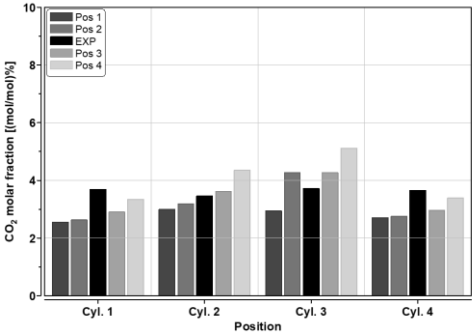

Figure 5.34: CO_2 measurements – high load

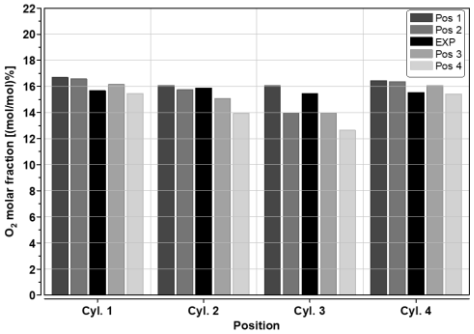

Figure 5.35: O_2 measurements – high load

The same comparison is carried out also on the high load engine point, which is characterized by a much greater amount of scavenging.

In Figure 5.34 and Figure 5.35 are reported the results for CO_2 and O_2 measurements. The values of molar fractions can be explained using the same demonstration used for the low load case. In the high load case, however, the dilution of exhaust gases by means of fresh air from scavenging is even more extreme: the molar fraction of CO_2 is even lower and the one of O_2 is higher than the ones in the low load case, meaning that the amount of fresh air in the adaptor is higher. In this case, there is a much lower gradient in O_2 from Pos. 1 to Pos. 4, which is due to the fact that there is a greater amount of fresh air

also very close to the four-in-one exhaust runner. This can be seen for example in Figure 5.26, where the surface 4 is inside a fresh air cloud.

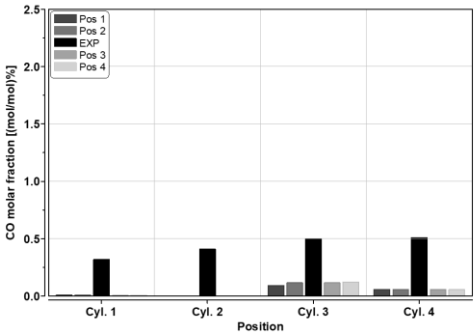

Figure 5.36: CO measurements – high load

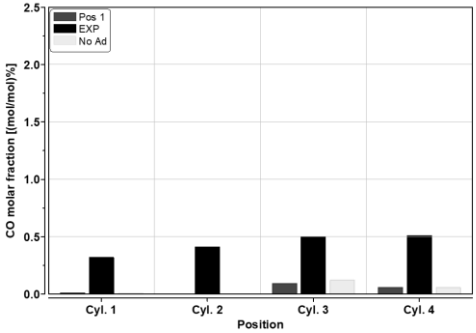

Figure 5.37: CO measurements assuming a non-adiabatic wall – high load

Also in this case, there is a very good agreement of experimental data and the simulation for CO_2 and O_2, which proves that the simulation is able to reproduce correctly the most relevant phenomena.

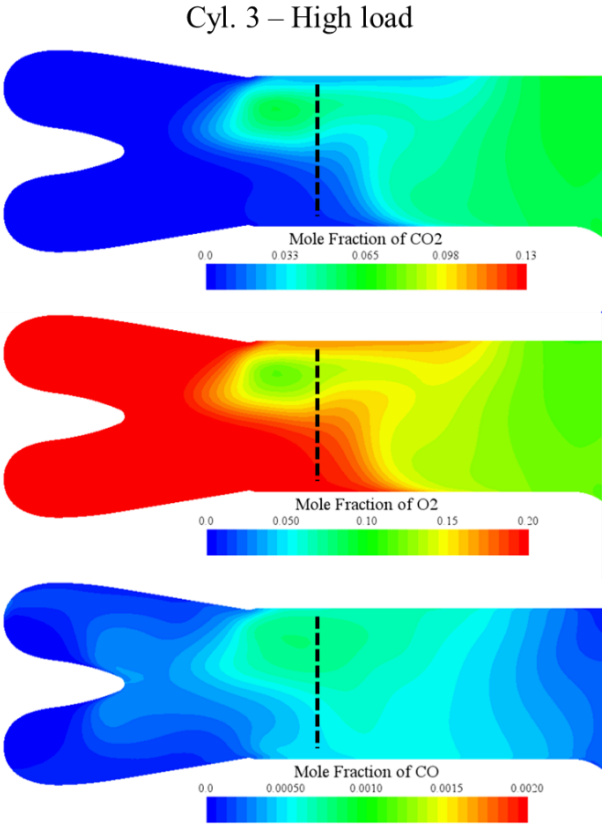

Figure 5.38: Mole fraction gradients in cylinder 3 – high load case

The molar fraction of CO is lower than the one in the low load case due to the in-cylinder mixture very close to stoichiometry (Figure 5.38). This makes the comparison even more delicate and sensitive to simplifications and assumptions. Similarly to the low load case, the simulation predicts a lower amount of CO at the sampling point (Figure 5.36) with some extremes at cylinders 1 and 2 where the simulation predicts virtually no CO. Also in this case, an explanation could be the assumption of adiabatic walls. In Figure 5.37, however, the comparison shows that the substitution of the assumption of adiabatic walls with a fix temperature of 700 K has little or no benefit for this engine operating point. One factor that could cause the lack of CO are the boundary conditions from the full engine simulation. However, at the

boundary conditions the average CO mole fraction is 2 mol%, which is theoretically enough. What's more, the full engine simulation proved to be very well validated and for the low load case provided reliable boundary conditions, therefore it is unlikely to be the origin of the inaccuracy. Another factor is the extreme scavenging event that is typical of this engine operating point and that, if only a bit overestimated, could cause a dilution of exhaust gases that has a great impact on species like CO that are present in very small quantities. The geometrical simplification of excluding the turbine in the simulation may have more effect on the simulation of this engine operating point because the backpressures are lower and therefore probably the mass flow rates are overestimated. Finally, the error is extremely limited in absolute values, which makes the results overall realistic.

The simulation showed a very good agreement with experimental data from the test-bench, therefore the validation of the detailed simulation can be also considered successful. Moreover, the simulation is able to give a detailed and realistic explanation of the results from the test-bench.

With this final step, it has been possible to demonstrate that the methodology used for the simulation of post-oxidation in the exhaust manifold is reliable and that both the full engine simulation and the detailed simulation of the exhaust manifold are capable of giving a deep insight in the phenomena that characterize post-oxidation.

The following steps will be to use this methodology of 3D-CFD simulations to describe post-oxidation and to investigate other operating conditions.

6 Description of post-oxidation

Based on the validation of the simulation methodology (§5), the following chapter uses the engine operating points analysed in order to describe post-oxidation.

6.1 General aspects

Post-oxidation consists in the oxidation of rich combustion products with fresh air taking place inside the exhaust manifold.

The definition of the composition of the exhaust gases is the first important step. Since the in-cylinder combustion happens in rich conditions, the most relevant species will be: N_2, H_2O, CO_2, CO and H_2. Due to inhomogeneity of the mixture inside the combustion chamber, also O_2 is probably present, though the overall rich combustion conditions. These components make up for more than 98% of molar fraction in these conditions and for 95% of the total energy that enters the exhaust manifold during the exhaust stroke. The remaining energy and mass is composed mostly by unburned fuel that was not completely oxidised during combustion. In rich combustion conditions, it is possible that a certain amount of hydrocarbons remain unburned after the combustion. These hydrocarbons flow to the exhaust manifold and there they can participate to post-oxidation.

From the point of view of the simulation, in order to model long-chain hydrocarbon oxidation, it is necessary to implement a detailed reaction mechanism into the detailed model of the exhaust manifold. The detailed chemical reaction model, as already investigated in §4.3, increases by at least a factor 10 the computational resources needed for the simulation. Therefore, in this project, the simulation with a detailed reaction mechanism has been limited to one engine operating point, which will be analysed in the following chapter (§7), and to the exhaust manifold. For all the other engine operating points, the unburned hydrocarbons have been neglected, which is a realistic assumption as it will be demonstrated below.

Out of the six most relevant species listed above, the following three are the main reacting ones: CO, H_2 and O_2. CO and H_2 are present in the exhaust gases, while O_2 is present in the fresh air coming from scavenging. The separation of reactants excludes the possibility of premixed post-oxidation with a flame front travelling across a mixture [30] [29].

Exhaust gases and fresh air are during most of the cycle separated in clouds. The mixing of exhaust gases and fresh air takes place at their interface between two clouds. The mixing is very limited during most of the cycle; only during the exhaust stroke of a cylinder the mixing increases and the reactants are brought in contact.

The second requirement for post-oxidation is a temperature high enough to start the reactions. The oxidation reactions for CO and H_2 need a temperature of least 1000 K. The gas temperature is usually during the cycle too low to start post-oxidation. However, the hot combustion products that enter the exhaust manifold during the exhaust stroke, reach usually such temperature.

Like all the chemical reactions with reduction of the number of moles, also for post-oxidation an increase in the pressure of the system speeds up the reaction. The pressures in the exhaust manifold have peaks around 1.4 bar during the exhaust events.

Therefore, from a chemical point of view, post-oxidation is a non-premixed reaction that takes place in a thin layer where the reactants mix and react [30] [29]. In particular, since post-oxidation happens almost exclusively during the exhaust stroke when the hot exhaust gases are pushed at high velocity through the fresh air causing a great mixing, post-oxidation can be considered a non-premixed turbulent reaction.

The parameters that influence the post-oxidation are:

- Temperature: at least 1000 K;
- Mixing of the reactants: combustion products and air;
- Pressure.

6.2 3D-CFD analysis

The validation concluded in the previous chapter demonstrates that the simulation can recreate the measurements of the test bench. Therefore, it is possible to use the results of the simulations in order to investigate post-oxidation. In the following the results of the simulaitons of the engine operating points already described as “low load” and “high load” are reported. The results refer to the detailed model of the exhaust manifold that uses the boundary conditions from the full-engine simulation.

The best conditions for post-oxidation are during the first part of the exhaust when mass-flow-rates at high speed of hot combustion products are pushed into the exhaust manifold (Figure 6.1, Figure 6.2, Figure 6.3 and Figure 6.4). In proximity of the exhaust valve, the hot rich combustion products find a cloud of fresh air stagnating there. During the first part of the exhaust stroke there is a strong mixing of the reactants at the interface that triggers post-oxidation. Afterwards, fresh air from scavenging flows into the exhaust manifold at low speed during the valve overlap and accumulates close to the exhaust valve, therefore ensuring the oxygen availability for the exhaust for the following cycle.

In the reported pictures, there is a thin layer where most of the chemical heat release from post-oxidation takes place. This thin layer has temperatures around1300 K, relatively low O_2 and high CO mass fractions. These are indeed the perfect conditions for post-oxidation. Interestingly, there are other areas with similar conditions of CO, O_2 and mixing, e.g. adaptor of cylinder 3, in which, however, there are no reactions going on because of the much lower temperature around 600 K.

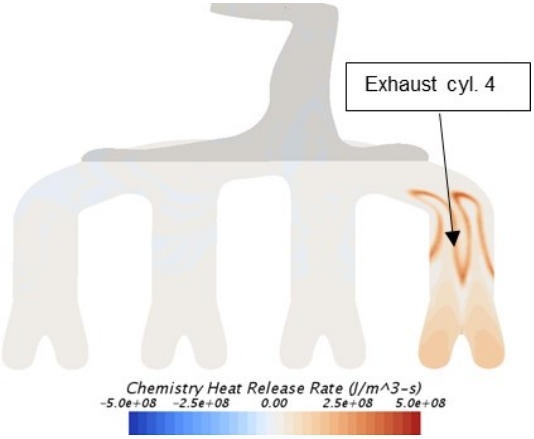

Figure 6.1: Local heat release rate from post-oxidation during the exhaust of cylinder 4 – high load

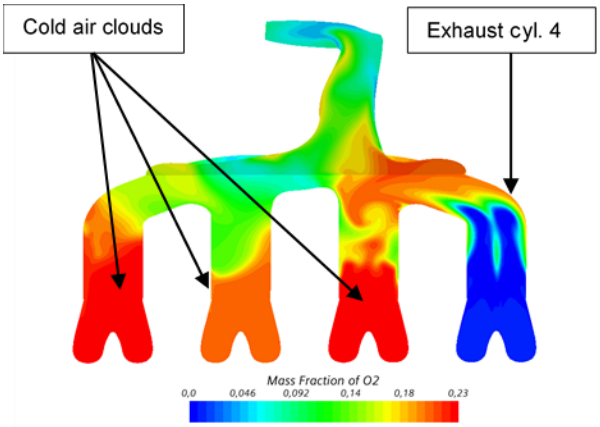

Figure 6.2: O_2 distribution in the exhaust manifold during the exhaust of cylinder 4 – high load

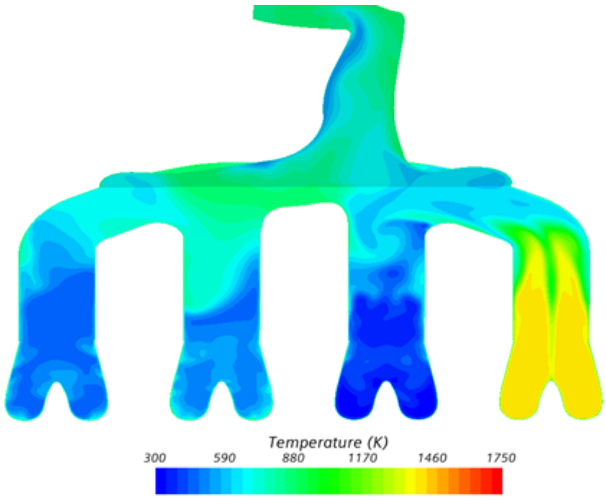

Figure 6.3: Distribution of temperatures in the exhaust manifold during the exhaust of cylinder 4 – high load

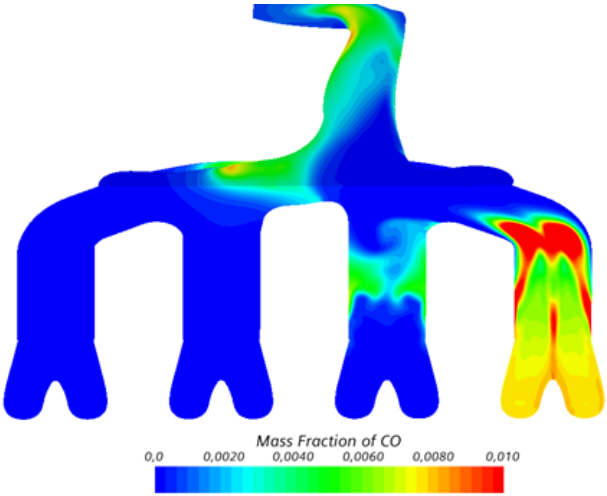

Figure 6.4: CO distribution in the exhaust manifold during the exhaust of cylinder 4 – high load

The regions with lower temperature originate at the end of the exhaust stroke, when the temperature is lower, due to scavenging, and the mixing less

effective because of the lower speed of the gases. In these conditions post-oxidation cannot start.

The heat release takes place also behind the thin layer. However, most of the fresh air has already been pushed away by the first front of rich combustion gases. Therefore, though the high mixing and temperature, post-oxidation is limited. In these conditions, the O_2 availability from the in-cylinder inhomogeneity that the Lambda-Map (Figure 5.12; Figure 5.13) pointed out could help to carry out the reactions.

During the remaining part of the cycle, the influence of the exhaust gases on the interfaces between fresh air and rich combustion gases of other cylinders is limited because of the low mixing and the impossibility to raise the temperature.

The "clouds" of gases are very difficult to mix because of the 10 cm of adaptor between the head of the engine and the four-in-one exhaust manifold. A stronger mixing takes place in the four in one runner, however, in both engine operating points, the simulations show that there are non-mixed gases flowing into the turbine (Figure 6.7 and Figure 6.8).

The high load case has an extremely low post-oxidation, which is due to the following factors:

- $\lambda_{CYLINDER}$ too close to stoichiometry (0.98), therefore low amounts of CO and H_2 that enter the exhaust manifold;
- Excessive scavenging, therefore too much cold air entering the exhaust manifold that causes a cool down of the whole volume and blocks the post-oxidation reactions.

In the low load case, instead, the heat release is greater and more constant thanks to the higher temperature in the exhaust manifold, due to the lower amount of cold air entering the exhaust manifold during scavenging and the greater amount of CO and H_2 that enters the volume.

The differences among the cylinders can be seen in Figure 6.5 and Figure 6.6. In the high load case cylinder 2 makes no post-oxidation because of a better in-cylinder mixture homogenization and an A/F ratio close to stoichiometry. This represents an example of failure of the post-oxidation: mixing and temperature can be considered to be almost the same of the other cylinders but

there is no heat release because $\lambda_{CYLINDER}$ is too close to stoichiometry and there is not enough CO and H_2 to start post-oxidation.

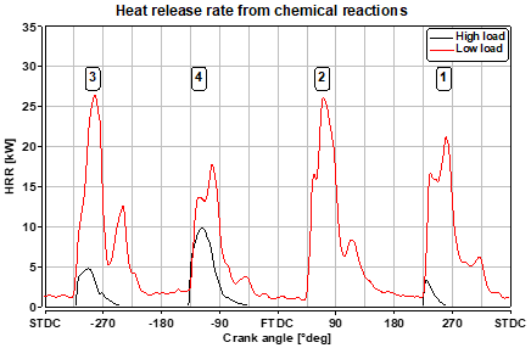

Figure 6.5: Heat release rate from post-oxidation. Numbers refer to cylinder exhausting

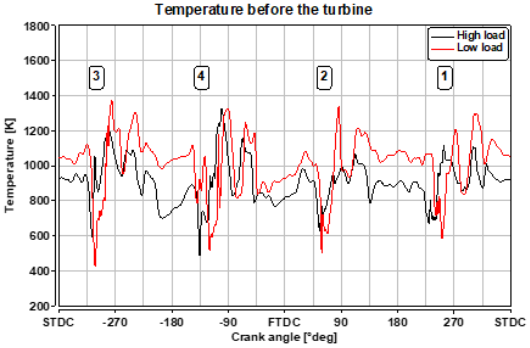

Figure 6.6: Temperature before the turbine. Numbers refer to cylinder exhausting

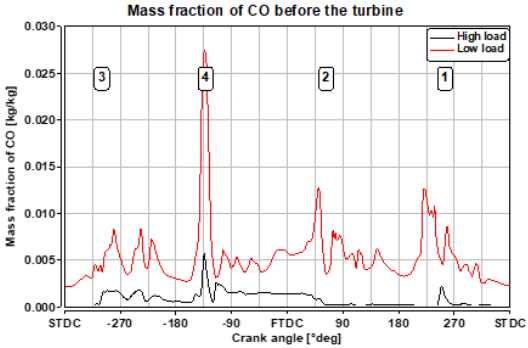

Figure 6.7: CO mass fraction before the turbine. Numbers refer to cylinder exhausting

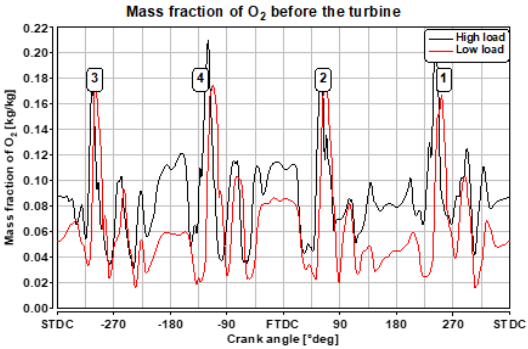

Figure 6.8: O_2 mass fraction before the turbine. Numbers refer to cylinder exhausting

When considering Figure 6.7 and Figure 6.8 it can be seen that, although CO is very limited in the high load case, there is almost always a certain amount of it flowing to the turbine without reacting. The explanation is that the mixing of gases is a very delicate process and there are always certain volumes of reactants that remain separated from fresh air. A second effect is the mixing that happens at low temperature. In this condition, although the local chemical composition is acceptable for post-oxidation, the temperature is too low to start the reactions. Consequently, there are volumes where fresh air and reactants are well mixed together but the reaction cannot start and the non-mixed gases flow to the turbine.

In the low load case, in the composition of the exhaust gases there is much more CO and less O_2. Even though the low load engine operating point has an overall engine operation very close to stoichiometry, that would theoretically preserve the three way catalyst operation from efficiency losses, the simulation predicts that the combination of mixing and temperature distribution in the exhaust manifold is not enough for the complete homogenization and oxidation of the mixture.

This is a general aspect of post-oxidation during our investigation: with the given geometry, the mixing of gases before the turbine is not complete. This characteristic has been observed in all engine operating points that have been analysed, so it is probably a common feature of post-oxidation and shall be taken into account during the strategy design. The incomplete oxidation does not always correspond to an incomplete mixing: there are volumes of already mixed gases that flow to the turbine. The problem is that the mixing happened at too low temperatures. A temperature increase in the exhaust manifold is difficult to achieve. Therefore, the only solution to reduce the amount of non-oxidised gases is to increase the interface of hot combustion products and fresh air while the temperature is still high. A possible way to achieve it, is the study and development of a geometry of the exhaust system characterized by better mixing of gases at high temperatures. An example is provided in §9.2.

6.3 Temperature increase

One of the most relevant effects of post-oxidation is the temperature increase due to the heat release from chemical reactions. The quantification of this temperature increase is very interesting for applications of post-oxidation in different strategies, e.g. heating of the TWC.

One advantage of 3D-CFD-simulations is the possibility to separate the effects of different phenomena. In this case, by deactivating the chemical reactions, it is possible to quantify the differences that are due exclusively to the post-oxidation reaction. In order to investigate this point, the detailed simulations of the exhaust manifold have been run again without activating the chemical reaction mechanism. The simulations use the same boundary conditions, i.e. the starting full-engine simulation is the same. These simulations are then compared with the simulations where post-oxidation is active.

Apart from the lower temperature of the exhaust manifold, there are also smaller differences in the flow field and in variables such as the velocity field and density between the simulations with and without chemical reaction mechanism activated. Such differences, however, are secundary and do not change much between the two cases.

For this investigation, the high load and low load engine operating points have been simulated without chemistry. In order to have a bigger sample and be able to make some inference, further three engine operating points have been simulated both with and without active chemical reactions. These engine operating points have been used also for the mapping of post-oxidation and are analysed below in greater detail (§8). This paragraph focuses instead on the correlation of heat release and temperature increase. The most relevant parameters are reported in Table 6.1: the names of the last three engine operating points refer to the names used for the mapping of post-oxidation (§8); HR is the heat released in the exhaust manifold by post-oxidation; temperatures are measured before the volute of the turbine (T_3); T_{AVG} is the average temperature during one cycle; T_{MAX} is the maximal temperature during one cycle.

Table 6.1: Engine operating points for the investigation of effect of chemical reactions.

	Rpm 1/min	Imep bar	Overlap °CA	HR J/cyc	ΔT_{AVG} %	ΔT_{AVG} K	ΔT_{MAX} %	ΔT_{MAX} K
High load	1600	14.88	90	62.67	1.92	17	9.75	118
Low load	1600	12.34	90	490.90	15.58	137	7.44	95
2	1600	14.99	60	554.22	18.07	189	18.54	227
3	1200	13.15	60	268.88	5.62	59	7.63	94
4	1200	15.06	60	575.41	10.16	104	9.04	124

The engine operating points have different characteristics of imep, overlap, rpm and boost pressure in order to have a wider and more varied sample to analyse. All engine operating points reported, apart from high load, have an overall engine operation very close to stoichiometry (§8).

Engine operating point 2 is very similar to high load in terms of imep and they are both at 1600 rpm. However, engine operating point 2 has a lower overlap that limits scavenging in order to achieve an overall stoichiometric engine operation.

Engine operating points 3 and 4 have a lower rpm and a valve overlap limited to 60°CA. The engine operating point 3 has an imep similar to low load while the case 4 is similar to high load.

The sample is therefore composed by an example of the most relevant engine operating points for post-oxidation.

The most interesting effect of post-oxidation is the increase of T_3, i.e. the temperature before the turbine. This temperature has a limit around 900°C (1200 K) due to materials [68]. On the other side, the temperature increase can be used intentionally to heat up the gases in the exhaust manifold if needed, e.g. during a cold-start operation.

All temperatures reported in Table 6.1 are measured before the turbine volute. For each engine operating point the temperature increase due to post-oxidation is reported for both the average temperature during the cycle and the maximal temperature. The temperature increases are very different among the simulated engine operating points. There is a clear and logic correlation between the heat released by post-oxidation and the temperature increase (Figure 6.9), both relative and absolute: the greater the heat release, the greater the temperature increase.

It is interesting to compare the high load case and the engine operating point 2:

- Similar imep and same rpm;
- High load has a very low heat release, therefore a limited temperature increase (17 K);
- Engine operating 2 has a very high heat release, therefore a great temperature increase (104 K).

The correlation of heat release and temperature increase is almost linear for the investigated engine operating points (the linear regression has a r^2 value of 0.74), however, it is possible that for a further increase of heat release the engine operation becomes more complicated due to the very rich in-cylinder

A/F ratio required. Moreover, the mixing in the exhaust manifold must increase in order to oxidize the greater amount of CO and H_2 entering the volume. Therefore, it is possible that the mixing in the exhaust manifold represents a limit to the maximum heat release.

Temperature increase can reach almost 190 K, which makes post-oxidation a very interesting strategy for conditions like catalyst heating and cold start, when the gases in the exhaust manifold must be heated up quickly. Heat release is controlled mainly by means of a trade-off of scavenging and in-cylinder A/F ratio; indeed, the high load case has a great scavenging but a $\lambda_{CYLINDER}$ very close to stoichiometry (0.98), which results in a very low heat release.

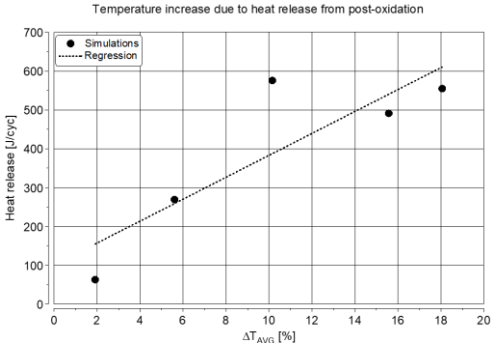

Figure 6.9: Correlation between heat release and temperature increase due to post-oxidation

The problem of post-oxidation is that also the maximum temperature, i.e. the highest temperature peak during one cycle, increases as post-oxidation increases. The increase of maximum temperature has only a limited correlation with the increase of average temperature but for some engine conditions the temperature increase can be very high (230 K). In Table 6.2, it can be seen that the maximum temperature with post-oxidation is usually above the limit of materials. However, these are very short temperature peaks (55°CA, i.e. 5.7 ms at 1600 rpm) and the average value is almost always below that limit.

The average temperatures (Table 6.2) depend not only on post-oxidation but also on more complex phenomena such as scavenging, ignition point and A/F ratio.

Table 6.2: Temperatures before the turbine (T_3)

	w/ Post-ox.		w/o Post-ox.	
	T_{AVG} K	T_{MAX} K	T_{AVG} K	T_{MAX} K
High load	905	1329	889	1210
Low load	1013	1376	877	1280
2	1231	1449	1043	1330
3	1129	1494	1025	1222
4	1112	1321	1053	1227

For example, the low load case has a very low average temperature, even though the heat release and the temperature increase are high. This is due to the great amount of scavenging that cools the exhaust manifold; indeed, the average temperature in the case without post-oxidation is 877 K, which is almost 100 K lower than the other cases excluding high load. The difference is mostly due to the greater scavenging that cools the exhaust manifold. Other engine operating points with lower scavenging start post-oxidation with a higher average temperature before the turbine. These engine points have the same spark advance of high load and low load. The most relevant difference is the valve overlap: the points with great valve overlap have a greater scavenging and therefore the temperature in the exhaust remains lower even when post-oxidation takes place. If other parameters such as IP are considered, there is the possibility to develop a more precise a reliable engine strategy for post-oxidation.

In conclusion, post-oxidation is a non-premixed reaction that is triggered by the exhaust stroke of each cylinder. It depends mostly on temperature and mixing of the reactants. The heat release peaks during the exhaust of each cylinder and then declines rapidly. The characteristics of each peak depend mostly on phenomena taking place inside the cylinder such as mixture formation and air-fuel ratio of the mixture.

Post-oxidation has the capability to increase the temperature in the exhaust manifold by 19% in some cases, which make it a strategy interesting for operating conditions that require to heat up the exhaust gases quickly.

7 Simulation of post-oxidation with detailed reaction mechanisms

In order to investigate the influence of assumptions made by using a reduced chemical reaction mechanism in real engine condition, a series of simulations with a detailed chemical reaction mechanism have been carried out. Such simulations have been made possible by the availability of a High Performance Computer (HPC) cluster at the IFS.

7.1 Simulation set-up

The reaction mechanism chosen for the simulations is the Polimi_1412_detailed (Table 4.3) with 156 species and 3465 reactions. The reaction mechanism has the capability to simulate both CO and H_2 oxidation as well as the oxidation of long-chain hydrocarbons used in gasoline surrogates [63].

The simulation of the detailed model of the exhaust manifold implementing the reaction mechanism Polimi_1412_detailed is numerically extremely challenging and requires a very stable engine operating point in order to give realistic results. The instability is due to the need of the 3D-CFD tool to solve one additional transport equation for each species [31] [32]. The dimension of the numerical problem becomes rapidly very big and the determination of fundamental variables, such as density and temperature, more sensitive to numerical instabilities.

Many engine operating points have been tested and it has been chosen the one, whose simulation proved to be particularly stable. The engine operating point is characterized by:

- Load: 174 Nm
- Rpm: 1200 1/min
- Valve overlap: 60°CA

- λ_{ENGINE}: 1
- $\lambda_{CYLINDER}$: 0.91

The engine operating point is very similar to the ones investigated up to now: low rpm, rich in-cylinder combustion, long valve overlap and high boost pressure that pushes fresh air directly to the exhaust, where post-oxidation takes place at the exhaust of each cylinder.

The analysis that follows focuses on the influence of the assumptions made on the boundary conditions. The adoption of a reduced chemical reaction mechanism requires some simplifications concerning the chemical compositions of the inflowing chemical species. The target of this investigation is to test if such simplifications are acceptable, keeping in mind the need for a trade-off of accuracy and computational time.

The simulation campaign has been carried out gradually by changing at each step only one assumption in order to precisely track the changes in the results with the changes in the setting of the simulation. For all simulations, the flow field and temperature distribution are very similar because the mass flow rates and temperature boundary conditions are the same; therefore, the changes can be consider to affect mostly the chemistry of the simulation.

The following analysis is composed of five different simulations. The type of boundary conditions and name of each simulation are reported Table 7.1.

Table 7.1: Simulations for the detailed reactions mechanism analysis

Name	Reaction mechanism	Boundary conditions
Detailed	Polimi_1412_detailed	No HC
Reduced	Polimi_1412_ H2/CO	No HC
Detailed_HC	Polimi_1412_detailed	HC: gasoline composition
Detailed_Tol	Polimi_1412_detailed	HC: Toluene
NOx	Polimi_1412_ H2/CO-NOx	No HC

The most relevant investigated assumptions are:

- The use of a reduced reaction mechanism instead of a detailed one;

- The influence of long chain hydrocarbons on post-oxidation;
- The influence of NOx reaction path on post-oxidation.

7.2 Analysis of the simulations

In the first test, the exact same simulation has been performed with the reduced reaction mechanism and with the detailed reaction mechanism. The simulations are called Detailed and Reduced. The two models have the same boundary conditions and the same settings, the only difference is the chemical reaction mechanism that, in the first case, is the detailed one and for the second simulation is the reduced one. Since the reduced reaction mechanism can simulate only the oxidation of CO/H_2 mixtures, the boundary conditions in this case neglect the influence of HC. The simulation Reduced has the same setting of the other simulations investigated so far, which proved already to have a good accuracy and represents the standard whose accuracy is tested.

The target of this test is to see the influence of a detailed reaction mechanism using the same boundary conditions of the reduced reaction mechanism. To analyse this assumption the simulations “Detailed” and “Reduced” shall be now compared. In Figure 7.1, it can be seen that the heat release rates of these two simulations is very similar during the whole cycle; only in the second and the third peak the Reduced simulation predicts slightly higher heat release rates. This could simply be due to little differences in the turbulence or temperature patterns of the flow field between the two simulations that could speed up the reaction in the Reduced case. In Figure 7.2, the total heat released during one cycle is reported; the difference between the first two cases is in absolute values 12.5 J/cyc, which corresponds to the 1.7% of the total heat release, therefore, the two simulations have a very good agreement. In Figure 7.3, it is possible to see that also the temperature signal before the turbine inlet is very similar in the two cases and only around 90°CA there is a small overshoot of the Reduced simulation, which can be explained with the higher heat release rate at the same exhaust event. Finally, the Reduced simulation predicts slightly less CO that flows to the turbine (Figure 7.4), which can again be explained with the slightly higher heat release rate. For what concerns the other parameters (Table 7.2) there is always a very good agreement. In Table 7.2 masses refer to the amount of each species flowing to the turbine during

one cycle. HR_{max} is the maximum possible heat release considering the amount of energy entering the system. PO-rate is the rate of post-oxidation calculated as the ratio of the heat released in the whole volume of the detailed model during one cycle and HR_{max}.

This first comparison demonstrates that, when using the same boundary conditions without HC, the use of a reduced reaction mechanism does not introduce any significant difference with respect to the adoption of a detailed chemical reaction mechanism. It is therefore proven that, in these conditions, the use of the detailed chemical reaction mechanism does not change substantially the results of the simulation.

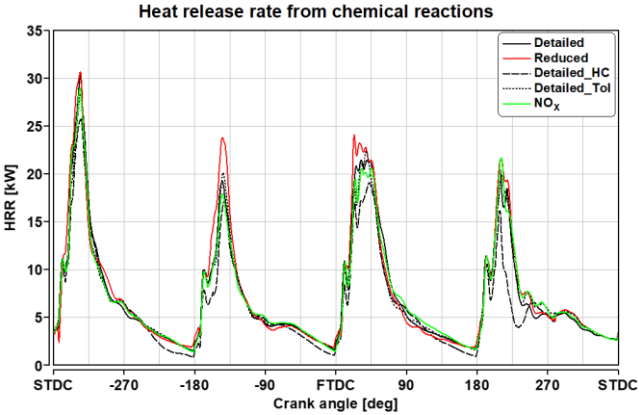

Figure 7.1: Heat release rate from post-oxidation in the whole detailed model of the exhaust manifold

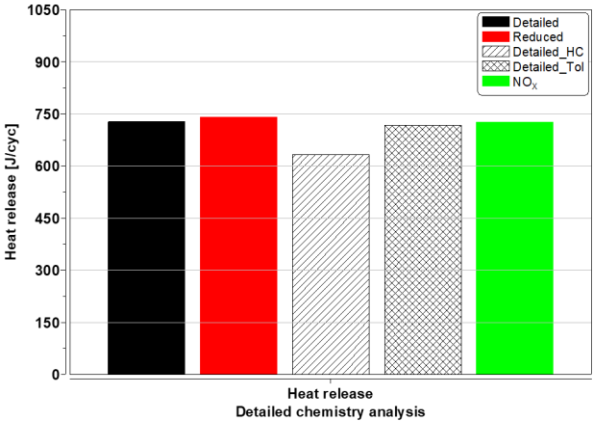

Figure 7.2: Heat release in the exhaust manifold during one cycle

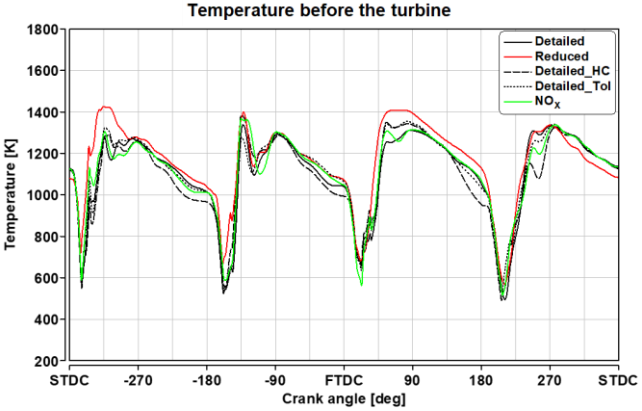

Figure 7.3: Temperature before the turbine in the whole detailed model of the exhaust manifold

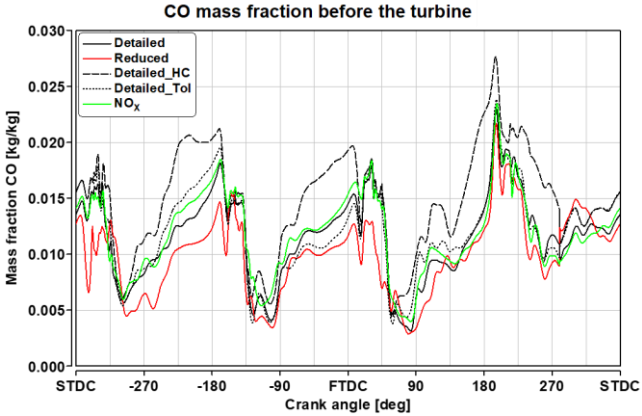

Figure 7.4: CO mass fraction before the turbine in detailed model of the exhaust manifold

To answer the question if the influence of HC must be considered for the simulation of post-oxidation, new boundary conditions have been produced. The full engine simulations always report a certain amount of unburned fuel that flows into the exhaust manifold (Figure 5.9). This information has been up to now neglected. In order to remove this assumption, new boundary conditions have been defined, which include the species mass fractions of the unburned fuel that enters the exhaust manifold. The full engine simulation gives an indication of the amount of fuel but not directly the chemical composition of the fuel, which is integrated in the definition of the fuel scalars. For the definition of HC chemical composition, there are many possible assumptions that can be made.

First of all, the fuel evaporates; then it mixes with air during intake phase or the compression stroke according to the SOI. Due to the local mixing effects explored by means of the lambda-map (Figure 5.12), some of the fuel remains in very rich stoichiometric conditions.

It is possible that the fuel in rich conditions does not take part directly to the combustion. However, it undergoes the high temperature and pressure gradients of the combustion inside the cylinder. These gradients are likely to start the break-up reactions of the long-chain hydrocarbon. Therefore, it is realistic to assume that the composition is no longer the one of the initial fuel because the cracking of the long chains of hydrocarbons has already started

[29], [69], [42]. In order to gain some sensitivity of the effect of composition on post-oxidation, two different simulations have been performed with completely different assumptions about the composition of HC:

- Detailed_HC: HC are simulated using the same composition of the original gasoline (in this case a gasoline surrogate), which equals to assume that the fuel did not undergo any chemical reaction of cracking and is still composed of long chain hydrocarbons such as isooctane and n-heptane;
- Detailed_Tol: the whole fuel is assumed to be Toluene. Toluene is a typical HC product [66] and is not a long chain of hydrocarbon. In this case, the assumption is that the fuel has already completely broken into smaller and more reactive compounds, which is more likely to represent the real conditions.

While the real composition of the unburned fuel that flows to the exhaust manifold remains unknown, these two simulations can define the two limits of chemical composition of the fuel flowing to the exhaust.

Comparing the simulation Detailed_HC with Detailed, the first one has a lower heat release rate during the whole cycle (Figure 7.1) and the total heat released is definitely lower (Figure 7.2; -94 J/cyc, i.e. -13%). The lower heat release reduces the temperature in the exhaust manifold and increases the amount of CO flowing to the turbine.

Table 7.2: Sensitivity analysis of detailed reaction mechanism simulations.

	M_CO mg/cyc	M_CO_2 mg/cyc	M_H_2 mg/cyc	M_H_2O mg/cyc	M_O_2 mg/cyc	HR_{max} J/cyc	PO-rate %
Detailed	31.77	475.30	0.53	193.52	52.14	2089	34.84
Reduced	26.58	473.93	0.48	190.31	47.08	2089	35.44
Detailed_HC	39.58	464.23	0.68	192.54	55.51	2399	26.43
Detailed_Tol	33.14	473.72	0.56	193.46	54.70	2405	29.85
NOx	32.58	473.94	0.56	193.26	52.44	2089	34.76

When comparing the composition of gases flowing to the turbine (Table 7.2), in the Detailed_HC case there is less CO_2, less water and more oxygen, which indicates that post-oxidation is proceeding more slowly. Although the total amount of energy that enters the system is higher (Table 7.2), there is less post-oxidation in the same control volume.

Since it is realistic to assume that the flow fields are very similar in the two cases, the differences in the reaction rate are due to the chemical reaction path. In hydrocarbons oxidation, for temperatures above 1000 K, 60% of the total heat is released during the last step, which is common to the oxidation of all hydrocarbons [29] [62]: the oxidation of CO by means of OH radicals

$$CO + OH \rightarrow CO_2 + H \tag{7.1}$$

The radicals needed for this last step are provided by the H_2-O_2 reaction mechanism. However, until there are hydrocarbons available, most of the radicals are absorbed by reactions needed to break up the chains in smaller components and only once the hydrocarbons are consumed there are enough radicals available to start the oxidation of CO. In the Detailed_HC case, in the gasoline surrogate are present isooctane and n-heptane, i.e. two long chain hydrocarbons. The oxidation of these species has therefore the following effects:

- There is more CO in the volume of the exhaust manifold because CO is produced during the oxidation of long-chain hydrocarbons and adds up to the CO flowing into the volume as a result of the rich combustion, which is present also in the simulations with reduced reaction mechanism;
- The oxidation of CO to CO_2 slows down because the radicals needed are absorbed by the reactions of oxidation of long-chain hydrocarbons, therefore less CO can be oxidised in the same time interval and more of it flows to the turbine;
- Since the CO oxidation slows down and the oxidation of long-chain hydrocarbons releases less heat, the overall heat released is lower;
- The lower heat release cannot sustain post-oxidation that decreases more quickly, which explains the greater amount of O_2.

These effects produce a reasonable explanation of the results obtained with the simulation.

The composition chosen for the Detailed_HC case is an extreme assumption, which does not happen in real engine operating conditions. In similar cases, usually, the molecules that compose the fuel undergo a process of cracking into smaller and more reactive compounds. A more realistic composition is the one used in the simulation Detailed_Tol, where fuel is assumed to be Toluene. In this case, the heat release rate (Figure 7.2) is very close to the one of Detailed for the whole cycle. The same happens for the temperature signal before the turbine (Figure 7.3) and the molar fraction of CO flowing to the turbine (Figure 7.4). Also the composition before the turbine (Table 7.2) are very close the ones of the simulation without THC. The great difference in the post-oxidation rate (Table 7.2) is justified by the greater lower heating value (LHV) of Toluene, i.e. the amount of energy entering the model is higher than in the other cases. This does not influence other parameters such as the composition of gases flowing to turbine because of the limited time available for post-oxidation. The heat released during one cycle (Table 7.2) is 10 J/cyc lower than the Detailed case (-1.4%), which can be explained with the same effects pointed out for the Detailed_HC case: Toluene, which is more reactive than isooctane and n-heptane, absorbs at first the radicals slowing down the oxidation of CO and reducing the overall heat released. In this case, the phenomenon is less effective than the simulation with long-chain hydrocarbons because of the higher reactivity of Toluene.

The composition of HCs that enters the exhaust manifold is probably closer to Toluene than to the original composition of the gasoline because of the temperature and pressure gradients inside the combustion chamber [66], [29] that start the cracking of long chain hydrocarbons. Therefore, it is realistic to assume that the chemical reaction of post-oxidation is more similar to the case Detailed_Tol, i.e. the assumption of neglecting the THCs contribution is acceptable and the use of the reduced reaction mechanism is a good approximation. This is an expected conclusion since, as demonstrated in the previous sections, the simulations with reduced reaction mechanism match very precisely the experimental data. Probably the description of post-oxidation most realistic is like the simulation Detailed_Tol, in which post-oxidation is a bit slower and the heat release is slightly lower. The problem is that the small increase in accuracy requires a huge increase of computational time, which makes the assumption of a reduced reaction mechanism even more interesting.

There is one more case that must be analysed in order to completely justify the assumptions made: the effect of NO_X on post-oxidation. In the section §4.3 the use of a reaction mechanism that includes the NO_X reaction mechanism produced results that differ slightly from the simulations without NO_X. The deviation is evident only at low temperature, when the simulation with NO_X predicts no post-oxidation while the simulations without NO_X predict a limited heat release. For the first test a simplified model and stationary simulations have been used, which do not reflect the real engine operating condition. It is now possible to test how much this assumption affects the simulation in real engine operating conditions.

The chemical reaction mechanism Polimi_1412_ H2/CO-NOx is the only one of the selection that includes the reactions of NO_X formation and interaction with oxidation path of CO and H_2. These reaction paths are not included in the Polimi_1412_detailed reaction mechanism, therefore a further validation is needed and it offers the advantage to isolate the effect of NO_X on post-oxidation. Since the Polimi_1412_ H2/CO-NOx chemical reaction mechanism cannot simulate the oxidation of long chain hydrocarbons, for the simulation with NO_X the same boundary conditions as for the Reduced and Detailed cases have been implemented, i.e. the effect of HCs cannot be taken into account.

The effect of NO_X is to slow down CO and H_2 oxidation in rich conditions, which has already been discussed above and increases reactivity in lean conditions [62]. The simplified model used for the preliminary investigations showed a different behaviour in the heat release rate at temperatures around 1000 (Figure 4.5) in the case of a simulation with NO_X.

The heat release rate of post-oxidation for the NO_X case (Figure 7.1) is very similar to the Detailed and Reduced cases. Also the heat released during one cycle is almost the same of the Detailed case (-0.23%; Figure 7.2) and the same happens for all the other parameters reported: temperature before the turbine (Figure 7.3), CO mass fraction before the turbine (Figure 7.4) and the data reported in Table 7.2. It can be therefore inferred that the effect of NO_X on post-oxidation is in this case negligible.

The oxidation reaction starts in absence of NO_X, which is not present in the boundary conditions. The production of NO_X requires a long time, high temperatures and oxygen availability. These conditions are not typical of post-oxidation. Indeed, temperatures for NO_X formation must be above 1800 K [29], which during post-oxidation happens for very a limited time following

the exhaust of the cylinder and in a small volume at the interface between the hot rich combustion products and the fresh air. Oxygen is available but the limited time and low temperature typical of post-oxidation do not allow for NO_X formation.

It is also very unrealistic that NO_X forms inside the cylinder during the combustion and that therefore should be included in the boundary conditions because the strategy of post-oxidation requires a rich (or very rich) in-cylinder mixture, condition at which the NO_X formation is negligible [66] due to the low temperature.

The amount of NO_X that is involved in post-oxidation is very low because it is not created neither during combustion nor during the heat release in the exhaust manifold. Therefore, the inclusion in the chemical reaction mechanism of reactions of NO_X does not improve the accuracy.

This investigation shows very well the differences between a simulation with a simplified model with steady state solutions and a simulation of real engine conditions in transient time solution. In the simplified model the solution is in steady state, therefore the NO_X are created and enter the reaction path, which leads to an overestimation of their effect. In the real case, instead, the conditions for NO_X formation are too short and the effect negligible.

It has been shown that the assumption of using a reduced reaction mechanism is a very good approximation. HCs have an influence on post-oxidation slowing down the reaction; however, when considering a more realistic composition of HCs, this effect is again negligible. Also the simulation of NOx has a negligible effect on post-oxidation because there are not the conditions for NOx formation in the first place.

Finally, the limits of computing resources and time availability for the simulations represent a decisive criterion for the final choice of the reaction mechanism for the simulations. To conclude the analyse of the different simulations reported in this paragraph, it is important to give also some information about the resources required by each type of simulations.

The implementation of the detailed chemical reaction mechanism has been possible only thanks to the availability of a HPC cluster at the IFS. The HPC is composed of 108 CPU nodes, 1.5 TB of RAM and Infiniband-Interconnection.

The simulations with the detailed chemical reaction mechanism have been performed on one node characterized by 36 CPU and 400 GB of RAM, which was the very least amount of resources to perform the simulation. In these conditions the simulation of one cycle required usually more than two days of simulation (Table 7.3), i.e. more than a week for the convergence of simulation after three engine cycles. The result does not change much if different boundary conditions are considered.

The great effort required for each simulation with the detailed reaction mechanism drastically reduces the total number of engine operating points that can be analysed within the time of project. Moreover, it is demonstrated that the detailed reaction mechanism increases only partially the accuracy of the results, which are much more dependent on the assumptions done on the boundary conditions and geometrical simplifications.

Table 7.3: Computational resources and time needed for the simulation of post-oxidation using different chemical reaction mechanisms

	CPU #	Time/it s	Time/stp s	dd/cyc dd
Detailed	36	17.51	175.06	2.92
Reduced	16	5.70	57.02	0.95
Detailed_HC	36	15.95	159.51	2.66
Detailed_Tol	36	14.39	143.91	2.40
NOx	18	9.10	91.04	1.52

Simulations with the reduced chemical reaction mechanism showed a very good agreement with test-bench data, while requiring much less computational resources and time. This makes the simulations with a reduced chemical reaction mechanism extremely interesting and allows for a greater number of investigations of different operating conditions.

The simulations with the NO_X chemical reaction mechanism do not increase significantly the accuracy of the simulation in comparison to the reduced chemical reaction mechanism and require at least 60% more time, which makes this chemical reaction mechanism not interesting.

The best-suited solution for the simulation of post-oxidation for the goals of this project is the choice of the reduced chemical reaction mechanism. This is the solution adopted for all the further simulations.

8 Mapping of post-oxidation using full engine simulation

It is now possible to fully exploit the potential of 3D-CFD simulations to analyse different engine operating conditions in order to understand how post-oxidation behaves, which its limits are and which the best operating conditions are.

8.1 Investigated engine operating points

For the analysis that follows, the simulation methodology developed and validated in the previous chapters has been used for the simulation of seven further engine operating points (Table 8.1). Such engine operating points have been chosen considering the conditions that are more interesting for post-oxidation:

- Low rpm;
- Low and medium boost pressure;
- Rich in-cylinder mixture;
- Scavenging by means of great valve overlap;
- Overall stoichiometric engine operation.

The overall stoichiometric engine operation is a constraint for all engine operating points in order to reduce as much as possible the efficiency losses at the TWC, which is one of the targets of the project. The results are indeed all very close to a stoichiometric engine operation. The constraint of stoichiometric engine operation forced the reduction of the valve overlap for almost all the analysed engine operating points from 90°CA to 60°CA, which is still a long valve overlap. The valve overlap of 90°CA has two main disadvantages:

- The amount of scavenged air is usually too high, e.g. in the high load case, causing an overall lean or very lean engine operation. A reduction of the boost pressure to reduce scavenging is not always possible especially for medium loads, where the boost pressure is necessary to achieve the target imep; this increases the mass flow during the valve overlap. Another problem is that the high amount of fresh air from scavenging reduces too much the temperature of the exhaust gases. A possible solution for a stoichiometric engine operation with great amount of scavenging is to enrich the in-cylinder mixture, which in turn has an effect on imep. Moreover, to counteract the scavenging the in cylinder A/F ratio should be so rich that the combustion becomes unstable. The best solution is to reduce the amount of scavenging by reducing the valve overlap;
- The engine operation and the simulation become unstable because of the propagation of pressure waves from exhaust manifold to the intake system, as already pointed out in the analysis of the low load case. This problem affects mostly the engine operating points with low imep due to the lack of boost pressure that overtakes the pressure fluctuations. Also in this case the simplest and more effective solution is to reduce the valve overlap to 60°CA. In this way the time with both valves open is limited to when the lift of the valves is lower, which makes the interaction of intake and exhaust less problematic because the mass flow rates and pressure waves are lower.

Table 8.1: Parameters of the engine operating points used for the mapping of post-oxidation

	Rpm 1/min	imep bar	Valve overlap °CA	$\lambda_{CYLINDER}$ -	Scavenging %	λ_{ENGINE} -
1	1600	12.34	90	0.91	16.14	1.05
2	1600	14.99	60	0.93	6.16	0.99
3	1200	13.15	60	0.97	3.84	1.01
4	1200	15.06	60	0.91	9.00	0.99
5	2000	15.87	60	0.96	3.82	1.00
6	2000	14.38	60	0.98	2.24	1.00
7	1600	13.67	60	0.98	2.16	0.99

The in-cylinder A/F ratio differs among the engine operating points because it has been adapted to the different conditions in order to keep the overall engine operation very close to the stoichiometry but remains always in rich combustion conditions.

8.2 Maps of post-oxidation

Using these data, a mapping of post-oxidation has been attempted. Such mapping is not the result of an engine optimization based on extensive testing but the analysis of how post-oxidation changes in different operating conditions. Starting from this analysis it is possible to perform further refinements to exploit better the advantages of post-oxidation.

The most important variable for the quality of post-oxidation is the heat released during one cycle in the exhaust manifold by the chemical reactions (Figure 8.1). Post-oxidation heat release is higher in regions of imep ~15 bar and 1600 rpm and for the same engine speed at imep 12 bar. Elsewhere the heat release is much lower; in particular, for conditions of 13 bar imep at all engine speeds and at higher imep for engine speeds of 2000 rpm the heat release rate is particularly low. In order to understand the reasons for this result, scavenging (Figure 8.2) and in-cylinder A/F ratio (Figure 8.3) must be analysed.

Scavenging has a peak for low imep and 1600 rpm that corresponds to the engine operating point 1, which is the only one with a valve overlap of 90°CA. There is a second area with a relatively high scavenging for higher imep, i.e. higher boost pressure, and rpm up to 1600 rpm. For intermediate imep there is a very low scavenging for all engine speeds. There is a direct correlation between heat released and scavenging: the points with higher scavenging are also the ones with higher heat release. Indeed, by means of scavenging the fresh air needed for post oxidation is pushed into the exhaust. A higher scavenging means more oxygen availability and the possibility to release more heat.

The $\lambda_{CYLINDER}$ is adjusted as a function of the overall engine operation, i.e. the higher the scavenging the richer must be the mixture inside the cylinder. Consequently, there is a strong correlation between the mapping of scavenging

and the one of $\lambda_{CYLINDER}$: the areas with low scavenging are also characterized by an in-cylinder mixture close to stoichiometry and areas with greater scavenging have a lower (richer) $\lambda_{CYLINDER}$. The in-cylinder mixture is the parameter used to control the total energy entering the exhaust manifold and it must be in equilibrium with the amount of oxygen available provided by scavenging. These two parameters together determine the possible total heat release from post-oxidation and indeed the areas with higher heat release are the ones with higher scavenging and richer in-cylinder mixture.

The availability of both reactants (mostly CO and H_2) and oxygen in the exhaust manifold is not a condition sufficient for the complete post-oxidation. There are other factors, such as temperature and mixing, that influence post-oxidation and that can change among the different engine operating points. An information about how the efficiency of post-oxidation changes in different conditions is the post-oxidation rate (Figure 8.4), defined as the ratio between the actual heat release rate from post-oxidation taking place in the whole volume of the detailed model during one cycle and the maximal possible heat release rate, i.e. the total energy entering the exhaust manifold.

Post-oxidation rate is always between 40% and 65%. In these conditions, the mass-flow-rate flowing to the turbine is not completely mixed and clouds of fresh air and rich combustion products flow separated to the turbine. It is probable that a further mixing and reacting takes place inside the volute of the turbine and afterwards inside the turbine itself; however, in order to reduce efficiency losses at the TWC the post-oxidation rate before the volute should probably increase substantially. An improvement of post-oxidation rate can be obtained by means of an optimized geometry of the exhaust system and a finer tuning of the engine operation.

On the other hand, post-oxidation proved to be stable in many different engine conditions. Indeed, by controlling few parameters such as scavenging and $\lambda_{CYLINDER}$, it was always possible to achieve on average a post-oxidation rate of 56%, which means post-oxidation is a simple and flexible strategy that can be adopted in many different conditions.

The pattern of post-oxidation rate mapping is completely different from the ones analysed before, which means that the heat release is not always the result of an efficient reaction, as well as that low heat release can be the result of an effective post-oxidation.

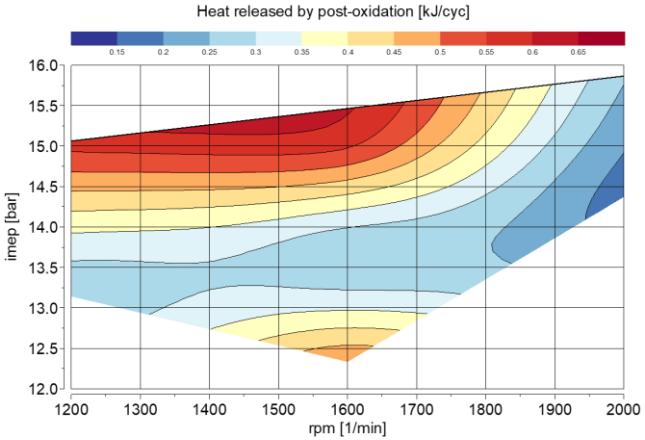

Figure 8.1: Heat release mapping from post-oxidation in the exhaust manifold

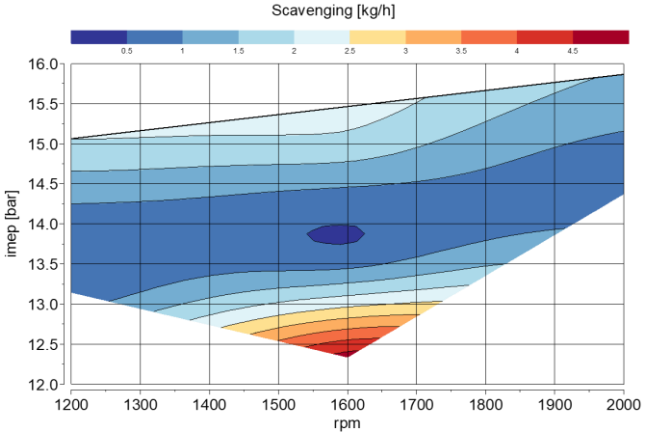

Figure 8.2: Mapping of scavenging

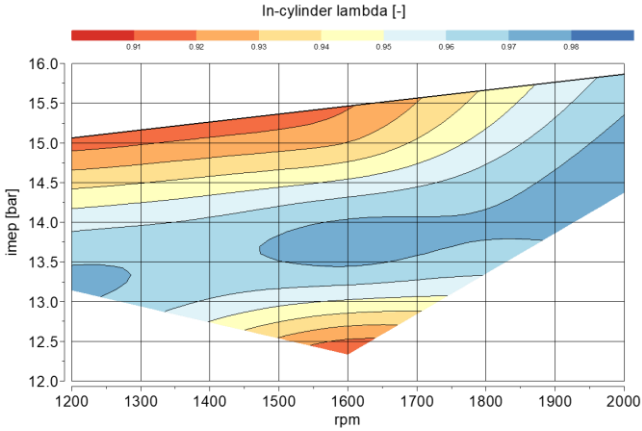

Figure 8.3: Mapping of in-cylinder A/F ratio

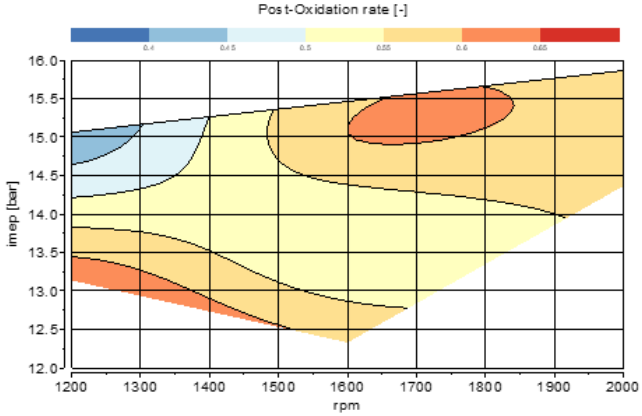

Figure 8.4: Mapping of the rate of post-oxidation, defined as the ratio of actual heat release from post-oxidation and the total energy entering the exhaust manifold

The highest points of post-oxidation rate are close to engine operating points characterized by an in-cylinder mixture closer to stoichiometry. In these cases the total energy entering the system is lower, which makes it easier to be more efficient because the mixing necessary for the complete oxidation is also lower. On the contrary, the engine operating point with the lowest value of post-oxidation rate (40%) can be explained with the great amount of energy

that enters the volume, which corresponds to a $\lambda_{CYLINDER}$ of 0.91. Therefore, the lower the entering energy, the less post-oxidation is needed and the more efficient is the mixing and reacting. This can be improved by means of the ad hoc developed geometries of the exhaust system, which allow an efficient mixing for a greater amount of gases.

Another variable that influences post-oxidation is the average value of turbulent kinetic energy (TKE) in the exhaust manifold, which in general increases as post-oxidation rate increases (Figure 8.5).

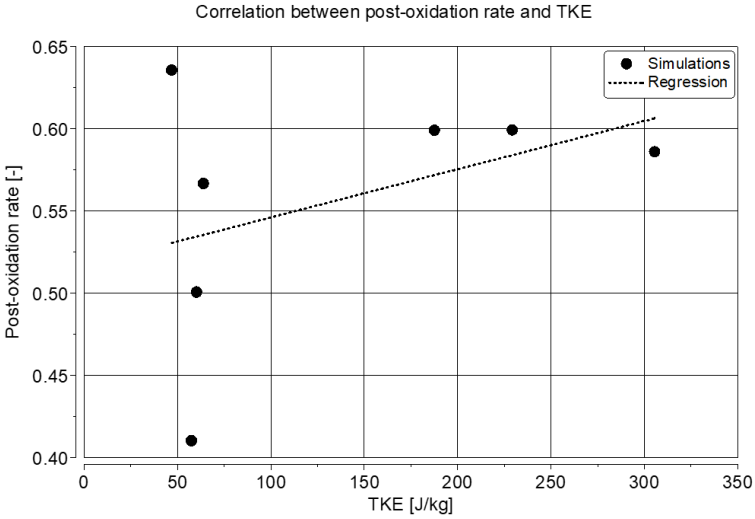

Figure 8.5: Correlation of TKE and post-oxidation rate. Dotted line is the trend line

TKE is a very general parameter, but gives some information about the mixing in the exhaust manifold: the higher the TKE, the greater the mixing. It is realistic that a better mixing enables for a more complete post-oxidation, therefore a higher post-oxidation rate, because the reactants are more quickly brought in contact during the exhaust of each cylinder. A good mixing is influenced by many parameters: geometry of the exhaust system, flow fields in the exhaust manifold, in-cylinder pressure and temperature at EVO, velocity of mass flow rates, temperature distribution in the exhaust manifold, pressure patterns, valve timing… Therefore, the generation of mixing depends on a

specific combination of factors of the engine operation and TKE can be considered an indication of the quality of mixing.

As already discussed (§6), the temperature before the turbine (Figure 8.6) increases because of post-oxidation and must be controlled for a safe engine operation. The temperature of gases flowing to the turbine must remain below the tolerance of the materials, which is usually <900°C (1200 K) [68], in order to avoid damaging the turbocharger. In post-oxidation, there are three phenomena with counteracting effects that influence the temperature of gases:

- The $\lambda_{CYLINDER}$ influences the temperature of exhaust gases at EVO; the richer the A/F ratio in the cylinder, the more fuel evaporates and reduces temperature and pressure inside the cylinder. Therefore, engine operating points with rich in-cylinder mixture start post-oxidation from a lower temperature;
- Heat release from post-oxidation raises the temperature of the exhaust gases;
- Cold air from scavenging reduces the temperature in the exhaust manifold.

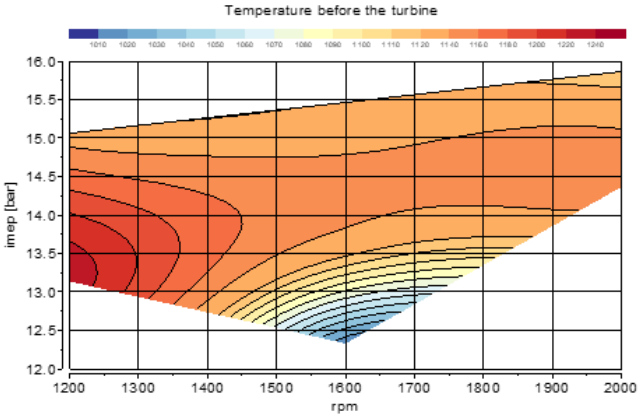

Figure 8.6: Mapping of temperature before the turbine

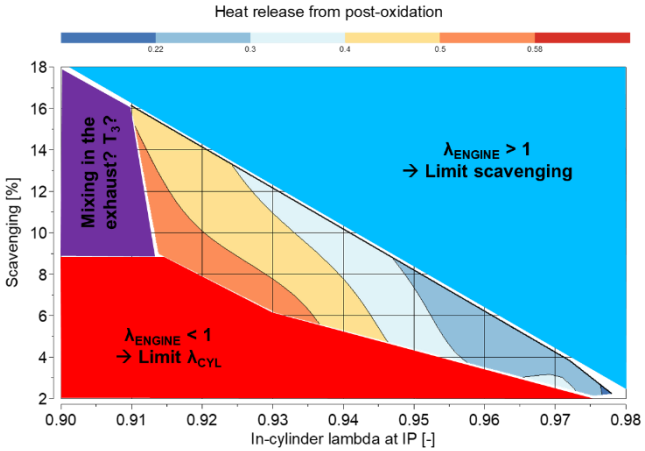

Figure 8.7: Limits of post-oxidation in stoichiometric engine operation

Other engine parameters that influence the T_3 such as the ignition point can be neglected in this analysis because are kept constant.

In Figure 8.6 is reported the temperature at the inlet of the turbine volute (T_3). In general, the T_3 remains below the limit of 1200 K ensuring a safe engine operation.

There is only one engine operating point that has a T_3 slightly above the limit (1230 K). This engine operating point is characterized by intermediate imep (13 bar), low engine speed of 1200 rpm and $\lambda_{CYLINDER}$ of 0.97, which is, in comparison to the other engine operating points, close to stoichiometry. The heat release is 0.27 kJ/cyc is low and suggests that its influence on the T_3 may be limited. The most relevant factor is in this case the amount of scavenging. Indeed, this engine operating point has the lowest scavenging (0.70 kg/h) and the lowest volumetric air consumption (17.63 kg/h) of all engine operating points due to the low boost pressure. Therefore, the amount of gases in the exhaust manifold is limited and hot because of the low scavenging. Post-oxidation in the exhaust manifold, therefore, heats up a limited amount of air and burned gases, which results in a greater temperature increase due to the lower heat capacity.

The lowest T_3 is 1000 K and happens for the engine operating point 1 (imep 12 bar; 1600 rpm; $\lambda_{CYLINDER}$ 0.91). The in-cylinder mixture is rich and the amount of scavenging is the highest of the sample both in relative terms (16%)

and in absolute terms (4.71 kg/h). The heat release from post-oxidation is 0.56 kJ/cyc, which is high and confirms that the heat release has a secondary influence on the temperature in the exhaust manifold. In this case, the temperature remains low because of the great amount of fresh air at low temperature that enters the exhaust manifold.

Between these two extremes, the T_3 of the other engine operating points are always very similar one another despite the great differences in scavenging and in-cylinder mixture. The conclusion is that in general the temperature at the exhaust is around 1100 K and scavenging is the parameter that most influences the T_3: a high value of scavenging cools the exhaust system, while a low scavenging may cause a too high T_3. This conclusion has been observed also at the test-bench [61].

In Figure 8.7 is reported the heat release rate from post-oxidation as function of in-cylinder mixture and relative scavenging. The best conditions for post-oxidation are a rich in-cylinder mixture around 0.92 and a scavenging of 8%. These conclusions are consistent with what analysed until now: the rich in-cylinder mixture provides the amount of CO and H_2 that is oxidized by the O_2 provided by the scavenging air.

The diagram in Figure 8.7 is also useful to display the limits of post-oxidation that this investigation encountered.

The first limit is the one for $\lambda_{CYLINDER}$ approaching the stoichiometric value: in these conditions CO and H_2 cannot be exhausted because the combustion is completed inside the cylinder, therefore it is impossible to carry out post-oxidation in the exhaust manifold.

The second limit is the amount of scavenging (upper region in Figure 8.7): for a fixed value of $\lambda_{CYLINDER}$ the amount of scavenging cannot be raised above a certain value at which the overall engine operation becomes lean. This is the reason for the shape of the upper limit of the heat release: the closer the in-cylinder mixture to stoichiometry, the lower that must remain the scavenging.

The third limit is represented by the $\lambda_{CYLINDER}$ (lower region in Figure 8.7): for a fixed amount of scavenging the in-cylinder mixture must remain in the range that assures an overall engine operation close to stoichiometry. Therefore, it is impossible to have a too rich $\lambda_{CYLINDER}$.

There is one region left, for which no simulations have been performed (light dark blue region on the left in Figure 8.7), which is characterized by a very rich in-cylinder mixture (<0.91) and a medium to high scavenging. It is theoretically possible to operate the engine also in these conditions with a post-oxidation strategy. However, two problems may arise:

- The amount of CO and H_2 becomes very high. In order to be oxidised, they must mix with fresh air in the correct temperature conditions. Therefore, there is a limited time during the exhaust stroke, when the whole CO and H_2 must effectively mix and react. For great amounts of CO and H_2, the mixing during the exhaust stroke might not be enough and the amount of non-oxidised CO and H_2 that flows to the TWC causing efficiency losses becomes a critical problem.

- Assuming that most of the energy entering the exhaust manifold is released during post-oxidation, this might increase the temperature of gases at the turbine inlet (T_3) above the limit of materials, damaging the turbine. As already analysed, scavenging can mitigate this effect; however, for high heat release rates it is possible that the cooling effect of scavenging is not enough.

The mapping of post-oxidation enabled for an analysis of how the phenomenon changes in different engine operating conditions. It has been demonstrated that it is possible to perform post-oxidation in many different conditions of interest, while keeping always the overall engine operation very close to stoichiometry. The most important parameters are scavenging and in-cylinder A/F ratio. Scavenging is mostly controlled by means of the boost pressure; the $\lambda_{CYLINDER}$ ratio can be regulated by means of the injection law.

Mapping of post-oxidation pointed out also the limits of these two parameters and defined the conditions in which the equilibrium of scavenging and $\lambda_{CYLINDER}$ resulted in an effective post-oxidation.

9 Sensitivity analysis

In this section is carried out a sensitivity analysis that fully exploits the possibility of the 3D-CFD simulation of testing many different configurations and of isolating the single contributions. The target is to investigate the phenomena that the mapping of post-oxidation pointed out that may have an important role in post-oxidation and whose influence must be understood:

- Exhaust gas temperature sensitivity;
- Geometry variation;

The analysis is performed using the same simulation methodology validated and adopted in the previous chapters.

9.1 Exhaust gas temperature sensitivity

For the temperature sensitivity analysis one single engine operating point have been used. The choice is due to the stability of the simulation. The engine operating point has already been analysed during the mapping of post oxidation (§8; engine operating point #2 in Table 8.1) and its most relevant parameters are reported in Table 9.1.

Table 9.1: Most relevant parameters of the engine operating point used as base case for the temperature sensitivity analysis

Rpm	Load [Nm]	Overlap [°CA]	$\lambda_{CYLINDER}$ [-]	λ_{ENGINE} [-]	Scavenging [%]
1600	180	60	0.93	0.99	6

The engine operating point is representative of the engine operation in post-oxidation conditions because of the rich in-cylinder mixture, the great amount of scavenging and the overall engine operation very close to stoichiometry. The imep is 15 bar, which means the engine is operated at high load.

The analysis focuses on a series of simulations performed using the detailed model of the exhaust manifold.

The boundary conditions from the full engine simulation remain constant for all simulations. Only temperature of gases flowing into the exhaust manifold has been numerically changed while pressure, mass flow rates and composition of the exhaust gases remain the same for all the cases. Therefore, all simulations have the same total amount of energy flowing into the system because the amount of CO and H_2 is the same in all cases. The differences in temperature of the exhaust gases change the amount of heat released by post-oxidation because the efficiency of post-oxidation changes, not because the inflowing amount of energy changes.

In order to have a realistic shift of temperature, some effect must be considered. First, the exhaust stroke is composed of two very different parts: the exhaust of combustion products and the scavenging of air. It is theoretically possible to change the temperature of both combustion products and fresh air; however, the temperature of fresh air, which is already at a temperature close to the ambient one, cannot realistically change much, i.e. cannot be further reduced. Therefore, combustion products and scavenging air have been separated and only the temperature of exhaust gases has been changed.

For each change of the temperature in the boundary conditions a simulation have been carried out of at least two engine cycles until the solution converged.

In Table 9.2 is an overview of the simulations carried out for the analysis. The definition of heat release from post-oxidation used here considers the whole volume of the detailed mesh from the exhaust valves up to the turbine volute; the reference case is indicated with BASE, ΔHR is the variation of heat release during one cycle with respect to the base case in percentage; masses of CO and H_2 are measured before the turbine; T_3 is the temperature measured before the turbine

The investigation is based on five simulations: the reference case, called BASE, plus four simulations in which the temperature of exhaust gases has been changed. These cases are indicated using as name the shifter applied to the temperature of exhaust gases. There are three simulations in which the temperature has been reduced and one simulation in which the temperature is increased of 100 K.

Table 9.2: Temperature sensitivity analysis.

Shifter [K]	HR [J/cyc]	ΔHR [%]	Post-ox rate [%]	M_{CO} [mg/cyc]	M_{H2} [mg/cyc]	T_3 [K]
+100	580.02	+14.44	62.69	16.36	0.40	1293
BASE	506.82	-	54.78	26.08	0.64	1178
-100	380.00	-25.02	41.07	36.96	0.66	1067
-200	211.31	-58.31	22.84	48.18	0.85	933
-300	76.06	-84.99	8.22	56.67	1.15	828

The results show that post-oxidation is extremely sensitive to temperature. Assuming that the mixing of exhaust gases and fresh air can be considered very similar in all cases, the contribution that is mostly influenced by the temperature variation is the chemical kinetics of post-oxidation.

For the oxidation of CO and H_2, there are two possible chemical paths: one at high temperature and one for temperatures below 1000 K [30], [29]. The low temperature chemical reaction mechanism is much slower due to the lack of highly reactive radicals. Therefore, when reducing the temperature in the exhaust manifold, a greater amount of gases will be in conditions of low temperature, therefore reacting slowly and lowering the heat release.

In Figure 9.1, the heat release rate from post-oxidation in the whole volume of the detailed model of the exhaust manifold is reported for the different simulations and in Figure 9.2 is reported the temperature before the turbine. Finally, Figure 9.3 shows the heat release of post-oxidation in the exhaust manifold during one cycle.

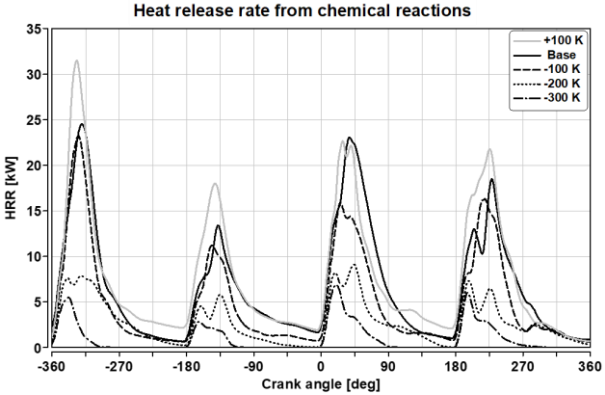

Figure 9.1: Temperature sensitivity analysis – Heat release rate

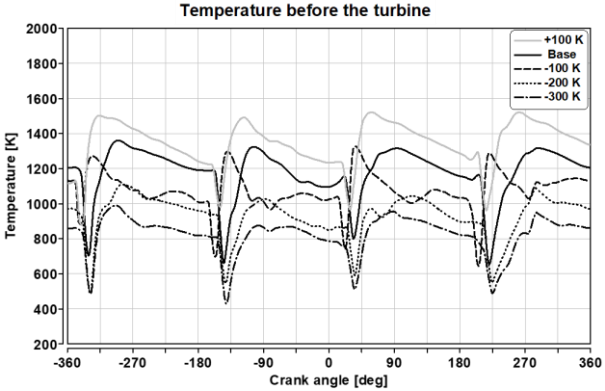

Figure 9.2: Temperature sensitivity analysis – Temperature profile before the turbine

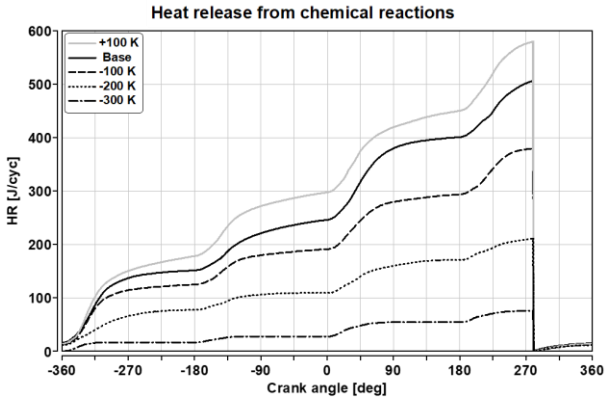

Figure 9.3: Temperature sensitivity analysis – Heat release from post-oxidation during one cycle

As temperature of the exhaust gases increases of 100 K, 14% more heat is released during one cycle and the post-oxidation rate raises to 63% (+8%). The relatively small temperature increase of the exhaust gases increases the efficiency of the post-oxidation reaction, which in these conditions exploits better the energy of rich combustion products and increases the enthalpy of gases before the turbine. Another effect of the temperature increase is that the mass of CO and H_2 flowing to the turbine during one cycle drastically reduces. This is not connected to a better mixing in the exhaust, which can be considered to be constant; it is more probable that there are volumes of already mixed CO, H_2 and air that cannot react due to the too low temperature. With an increase of temperature these volumes are in the conditions to start the reaction and release heat, increasing even more the total heat release. For all these benefits, temperature increase of the exhaust gases can be a good solution for post-oxidation.

However, the temperature increase does not have only positive effects: the T_3 increases above the limit of 1200 K that is fundamental for the safe operation of the turbine. Although in real engine conditions the temperature increase of the exhaust gases is possible by, e.g., delaying the ignition point, for this engine operating point this is not possible because of the T_3 limit. There are other conditions analysed during the mapping of post-oxidation characterized by a lower T_3 due to the greater scavenging and in which an increase of the temperature of the exhaust gases can be a good strategy.

In general, due to the great sensitivity of post-oxidation to temperature, the engine should be operated in a way to maximize the temperature of the exhaust gases, while remaining in a condition of safety for the turbine.

On the other hand, if temperature is reduced, the heat release of post-oxidation in the exhaust manifold decreases drastically and the amount of CO and H_2 flowing to the turbine increases. In the case with a shifter of -300 K, the heat release is so limited that it can be considered very close to the lowest possible temperature for post-oxidation, i.e. for even lower temperatures the heat release of post-oxidation becomes negligible.

The pattern of heat release rate remains the same for all cases: at the EVO of each cylinder there is a peak of heat release rate that afterwards decreases. As temperature decreases, the peak of heat release becomes lower and the heat release decreases more rapidly. The cases with shifters -200 K and -300 K have a heat release rate that is much lower than the other ones, which is probably due to the limited volume of gases that are in temperature conditions enough to start the reactions. Deep chemical investigation revealed that also in these cases the reaction path at low temperatures is negligible.

Due to the lower reaction rate, less heat is released by post-oxidation and the temperature increase is lower. The lower increase of temperature is not able to sustain the reaction of post-oxidation and the heat release rate decreases rapidly until it completely stops as for the case with shifter -300 K.

The average temperature before the turbine decreases. The cases -200 K and -300 K have a T_3 on average below the limit of 1000 K; this value is, however, the average temperature on the surface, i.e. there are non-mixed volumes of gases at very different temperatures that flow through the surface. The difference is that the amount of gases at high temperature is more limited.

In conclusion, post-oxidation is extremely sensitive to temperature changes. In particular, if the temperature of combustion products decreases, the heat release decreases and more CO and H_2 flow to the turbine. If T_3 is lower than 1000 K, the reaction rate drops because the chemical mechanism shifts to the low temperature reactions that are much slower than the high temperature ones. The best strategy to operate post-oxidation is to keep the T_3 as close as possible to the limit of materials in order to increase the post-oxidation rate and the enthalpy before the turbine.

9.2 Geometry variation

Post-oxidation requires a good mixing of exhaust gases and fresh air in the exhaust manifold. The mixing is strictly related to the geometry of the exhaust manifold; therefore, different shapes of the exhaust manifold may affect post-oxidation. The geometry analysed up to now is characterized by a 10 cm adaptor (Figure 9.4) between the head of the engine and the four-in-one exhaust manifold. The adaptor is necessary for the installation of the sensors at the test-bench, however, it changes the flow field in the exhaust. In particular, the adaptor creates volumes close to the exhaust valves where the mixing is very limited. In these volumes gathers the fresh air from scavenging that remains not mixed until the following exhaust stroke.

This geometry has the great disadvantage of keeping air and combustion products separated for most of the cycle. Another problem is that the gases from different cylinders remain separated in clouds inside the adaptors and mix only once they reach the four-in-one exhaust manifold. In order to overcome these problems, two further geometries have been tested in the detailed simulation.

One possibility is to use the original geometry of the engine without the 10 cm adaptor (Figure 9.5). This choice has the advantage to test how post-oxidation behaves in a general engine without any specific adaptation. The volume of the exhaust manifold reduces as well as the time needed by gases to reach the turbine, which are both factors that reduce post-oxidation. However, the mixing improves, due to absence of the 10 cm adaptor.

Another possibility, which has been proposed first at the test bench and later on implemented in the simulation, is to introduce the so-called by-pass adaptor (Figure 9.6). The by-pass adaptor is built on the 10 cm adaptor and it consists in a pipe (Ø = 2.5 cm) that connects the four different the adaptors by means of four relatively long (7 cm) vertical pipes. The target of the by-pass adaptor is to increase the mixing close to the exhaust valves and to resemble the mixing conditions of the original geometry. However, since it consists of a pipe that adds to the already existing adaptors, the volume of the exhaust runner increases and the flow patterns drastically change.

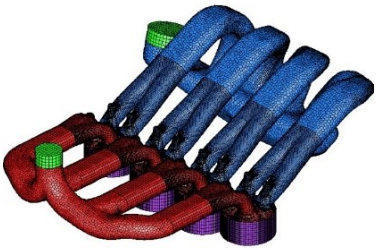

Figure 9.4: Base geometry with 10 cm adaptor

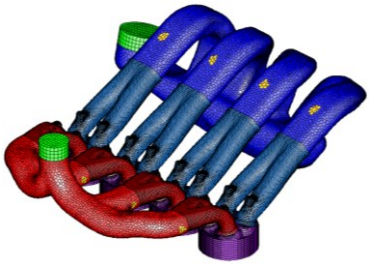

Figure 9.5: Geometry without 10 cm adaptor

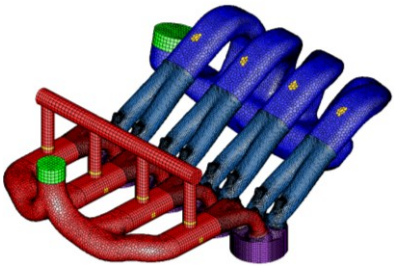

Figure 9.6: Geometry with 10 cm adaptor and by-pass adaptor

Such important changes in the geometry of the exhaust manifold influence the behaviour of the whole engine. However, the first step has been to focus on the effects of geometry changes limited to the detailed model of the exhaust manifold.

For this first analysis, the same engine operating point used as reference simulation in the temperature sensitivity analysis (§9.1) has been chosen.The only difference among the three simulations is the geometry of the exhaust manifold.

An overview of the most important variables is reported in Table 9.3, where the heat release is defined in the volume of the whole detailed model; Volume refers to the volume of the exhaust manifold from the exhaust valves to the turbine volute; BPA refers only to the volume of the by-pass adaptor.

Table 9.3: Geometry sensitivity analysis.

Geometry	HR [J/cyc]	ΔHR [%]	Post-ox rate [%]	T_3 [K]	Volume [l]	ΔVolume [%]
Adaptor	506.82	-	54.78	1178	1.393	-
No adaptor	494.71	-2.39	53.47	1222	1.094	-21
By-pass	598.93	+18.17	64.73	1117	1.602	+15
BPA	8.79	+1.73	1.47	-	0.209	-

The geometry without adaptor is characterised by less time available for post-oxidation and shorter length the gases travel before the turbine. Both conditions could reduce the overall heat released and the post-oxidation rate. However, the reduction of heat release is negligible both in absolute values and in percentage (Table 9.3), which proves three important facts:

- Even though the volume is 21% smaller, the reduction in heat release rate is only of 2%; therefore, the volume of exhaust manifold is less relevant than its geometry, i.e. it is more important to have a good mixing in the exhaust rather than a greater volume;
- The 10 cm adaptor does not improve significantly the post-oxidation rate because keeps the exhaust gases separated and reduces the cylinder-to-cylinder interaction. The shapes long and thin of the adaptor do not increase the post-oxidation rate because most of the heat release is concentrated on the thin interface between fresh air and exhaust gases, which is mostly proportional to the transversal area of the pipes and not to the length;
- Post-oxidation with high reaction rates and efficiency can be obtained also in standard engines without geometry changes.

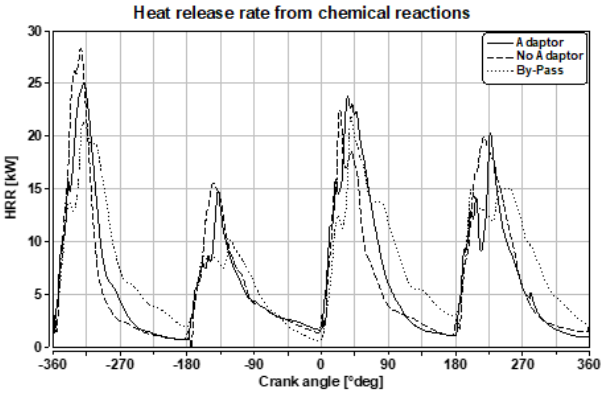

Figure 9.7: Geometry sensitivity – heat release rate of post-oxidation

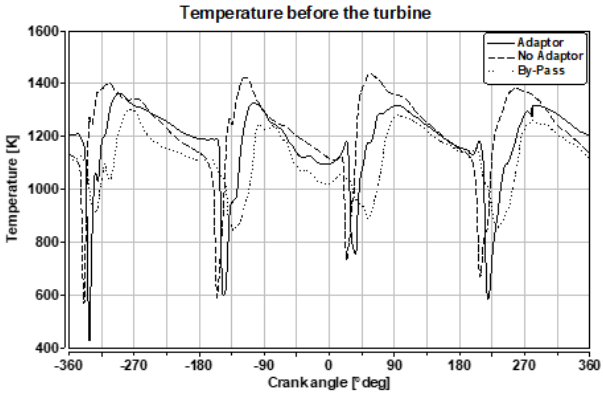

Figure 9.8: Geometry sensitivity – Temperature before the turbine (T_3)

In Figure 9.7, the heat release rate of the No Adaptor case is very similar for the case with the reference geometry. Therefore, the post-oxidation phenomenon must be like the one already described for the case with 10 cm adaptor. The T_3 profile is also similar in the cases with and without 10 cm adaptor; only the temperature peaks close to the exhaust of one cylinder are higher, due to the less time needed by the gas to reach the intake of the volute.

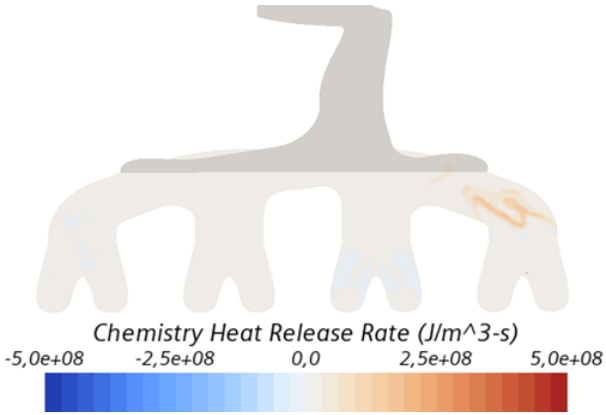

Figure 9.9: No adaptor geometry – heat release rate of post-oxidation

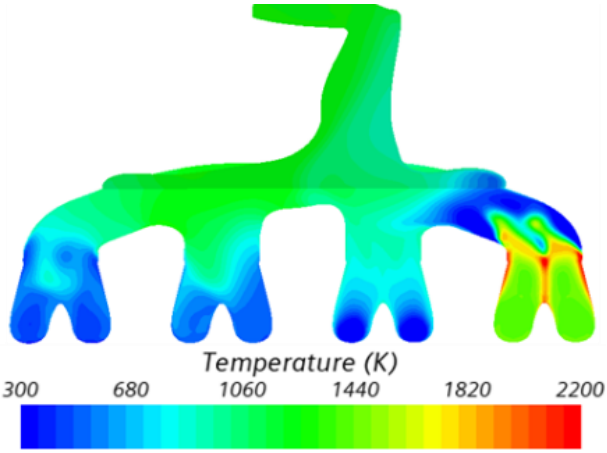

Figure 9.10: No adaptor geometry - temperature

In Figure 9.9 and Figure 9.10, it can be seen that the patterns of post-oxidation remain very similar to the case already analysed with the 10 cm adaptor. Also in the case without adaptor, there are clouds of cold air that accumulate close to the exhaust valves. When the exhaust stroke starts, the hot combustion products are pushed through the fresh air clouds and mix. Also in this case there is a thin surface characterized by the correct mixing and temperature conditions where the highest heat release rate of post-oxidation takes place. The most important differences are that in the case without 10 cm adaptor there

is greater mixing and a more relevant cylinder-to-cylinder interaction. Both effects are due to the fact that the 10 cm adaptor isolates each cylinder. On the other hand, less fresh air can be stored close to the exhaust valves due to the smaller volume, which can explain the small decrease in heat release rate during one cycle.

Another possible way to increase the cylinder-to-cylinder interaction is the installation of the by-pass adaptor. Theoretically, the by-pass exploits the high-pressure peak of the exhaust of each cylinder and redistributes the hot combustion products to the other cylinders, exactly where the cold air clouds are.

The most relevant factors to be considered are:

- The by-pass adaptor is big relative to the volume of the exhaust manifold (+15%), therefore, before the mass exhausted by one cylinder reaches the other cylinders, a great amount of gases must be pushed through the pipes of the by-pass;
- The by-pass has long (7 cm) pipes perpendicular to the flow of the gases, which limits the effective interaction with other cylinders;
- In the by-pass the gases exchange heat with the walls and cool down reducing the possibility of post-oxidation.

The simulation shows (Table 9.3) that the by-pass geometry substantially increases the heat release (+18%); however, only less than 2% of the total heat release rate takes place inside the by-pass. In Figure 9.7 can be seen that the heat release rate in the case of the geometry with by-pass adaptor has lower peaks but the curve decreases much more slowly than the other two cases. Therefore, the by-pass introduces for sure some change in the flow field that permits to increase post-oxidation but the increase of heat release does not happen inside the by-pass.

In order to understand how the by-pass influences post-oxidation we must first understand how the gases move inside the by-pass. As an example, the exhaust of cylinder 3 is analysed.

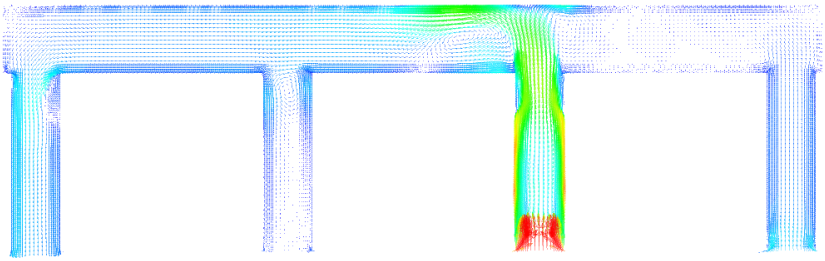

Figure 9.11: Velocity vectors on a section plane cutting through the middle of the by-pass at the beginning of the exhaust of cylinder 3

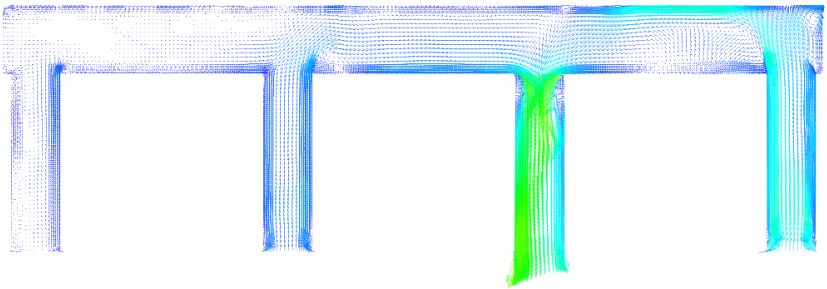

Figure 9.12: Velocity vectors on a section plane cutting through the middle of the by-pass 40°CA after the exhaust of cylinder 3

In Figure 9.11 the flow field inside the by-pass shortly after the exhaust of cylinder 3 shows that there is a mass flow rate going into the by-pass due to the high pressure generated by the exhaust event and by the mass flow rate of exhaust gases. Even though the gases flow with high velocity, the influence to the other cylinders is limited because of the great volume of the by-pass.

Few °CA later (Figure 9.12; 40°CA after the exhaust of cylinder 3) the mass flow rate inverts the direction and flows from the by-pass into the 10 cm adaptor. This event is shorter than the previous one but happens many times during the exhaust stroke of the cylinder: as soon as the pressure decreases slightly in the 10 cm adaptor, a short but fast mass flow rate from the by-pass happens. The resulting effect is to “inject” some gases into the 10 cm adaptor during the exhaust.

It must now be determined the composition of the gases that flow into the adaptor and that are later injected into the adaptor by the by-pass. At the beginning of the exhaust stroke (Figure 9.13), the fresh air clouds that gather close to the exhaust valve are pushed by the hot combustion gases into the by-pass. Because the vertical pipes of the by-pass are long, the fresh air does not reach the other cylinders but remains inside the vertical pipe, ready to flow again into the 10 cm adaptor.

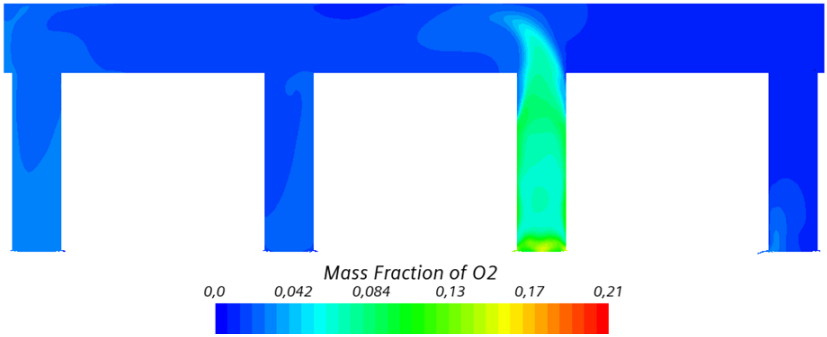

Figure 9.13: Mass fraction of O_2 on a section plane cutting through the middle of the by-pass at the beginning of the exhaust of cylinder 3

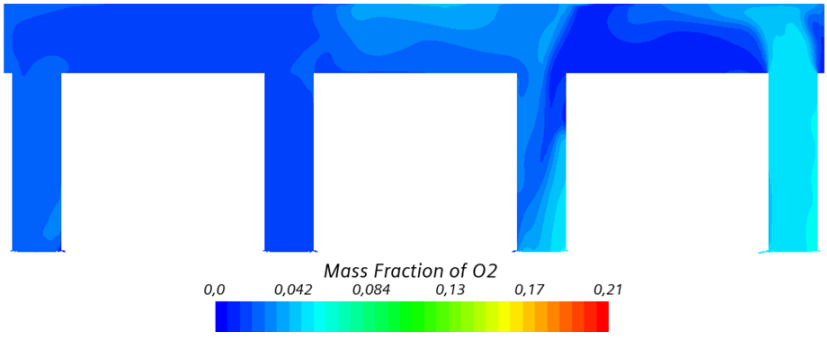

Figure 9.14: Mass fraction of O_2 on a section plane cutting through the middle of the by-pass 40°CA after the exhaust of cylinder 3

During the “injection” event that follows (Figure 9.14), the fresh air flows again into the 10 cm adaptor. In this case, the effect on the other cylinders, in

particular cylinder 4, is more evident: a small amount of air is sucked into the by-pass.

The by-pass acts in a first moment as a storage for the fresh air that gathered close to the exhaust valve. After few °CA, the pressure in the 10 cm adaptor drops and the fresh air flows back into the exhaust manifold.

The first part (Figure 9.15) of post-oxidation does not change much from what has been already described: there is high heat release rate at the interface between the hot combustion product and the fresh air. The shape of the interface changes a little, which may explain the lower peaks of heat release rate at the beginning of the exhaust stroke, but the phenomenon remains substantially the same.

In the second phase (Figure 9.16), i.e. when the mass flow rate inside the by-pass reverses towards the adaptor, a second interface creates on which another strong heat release starts. The second interface is formed on one side by fresh air coming from the by-pass and on the other side by hot rich combustion gases. The greater interface increases the total heat release rate, which therefore decreases less rapidly than in the other cases.

The by-pass changes the mixing and brings into contact the two gases that otherwise remain separated in clouds. It increases the cylinder-to-cylinder interaction only limitedly because its volume is too big; nonetheless, it has been demonstrated that the cylinder-to-cylinder interaction is not fundamental if the already existing gases can be better exploited.

The better mixing achieved with the by-pass is visible also in the temperature profile before the turbine inlet: the profile is smoother than the other cases and in general more homogeneous, which means that less clouds of separated gases flow to the turbine increasing the efficiency of the TWC and reducing the risks for the turbine.

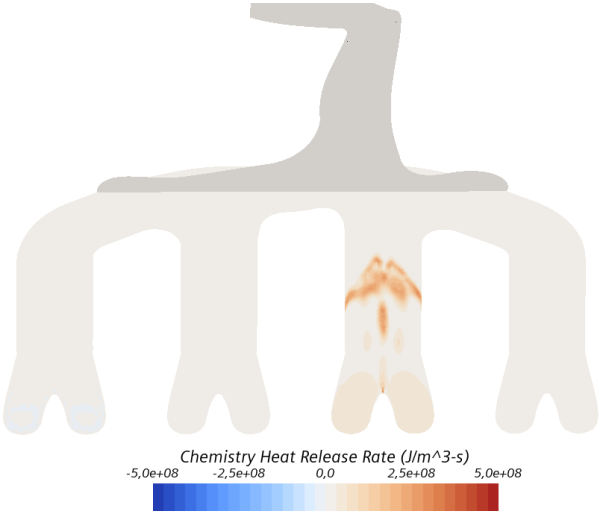

Figure 9.15: Heat release rate by post-oxidation reactions at the beginning of the exhaust of cylinder 3 – by-pass adaptor geometry

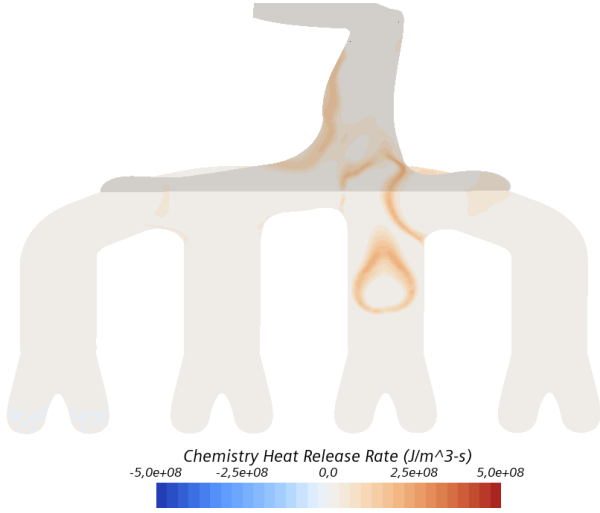

Figure 9.16: Heat release rate by post-oxidation reactions 40°CA after the exhaust of cylinder 3 – by-pass adaptor geometry

It must be now clarified why the amount of heat release happening inside the by-pass is negligible. Two factors mostly block the post-oxidation inside the by-pass:

- Temperature is low (1000 K) during the whole cycle, therefore the reactions slow down dramatically, as already stressed. Temperature remains low because the mass flow rates that enters the volume are mostly composed by fresh air and because the by-pass adaptor has a great surface to volume ratio that increases the heat exchange with the cold walls, which, as already demonstrated (§5.2.2), has a fundamental impact on post-oxidation;
- There is not the possibility to create an interface at which post-oxidation can start because the mixing is very limited.

The gases inside the by-pass remain separated and at low temperature during the whole cycle, which are the worse conditions for post-oxidation. Therefore, the positive effect of the by-pass does not consist in a greater volume and cylinder-to-cylinder interaction but in a better use of the already available gases. There could be a better design with shorter pipes and smaller volume positioned more in the direction of the flow in order to increase the positive effects.

The three geometries have been also simulated using the full-engine model and applying the boundary conditions of the engine operating point Low load already analysed. The results are reported in Table 9.4, where Air cons. is the total air consumption; Volumetric air cons. is the consumption of air without scavenging; Scav. is the scavenging.

The engine operation does not change substantially (Table 9.4). The air consumption remains very similar in all engine operating points; however, due to different pressure wave patterns in the exhaust manifold, the volumetric air consumption, i.e. the amount of air inside the cylinder, changes. This means that there is more air inside the cylinders during the combustion, therefore a $\lambda_{CYLINDER}$ closer to stoichiometry. The changes in pressure patterns do not affect only the exhaust manifold but also the intake, as the valve overlap is extremely long.

In order to keep the overall engine operation close to stoichiometry, the scavenging air must be reduced.

In conclusion, it is possible to have a very similar operation with all the investigated geometries, ensuring a safe post-oxidation operation.

Table 9.4: Full engine simulation with different geometries.

	Air cons. [kg/h]	Volumetric air cons. [kg/h]	Scav. [kg/h]	Scav. [%]	λ_{ENGINE} [-]	$\lambda_{CYLINDER}$ [-]
Adaptor	29.62	24.49	5.12	17.23	1.07	0.91
No Adaptor	29.29	25.86	3.43	11.70	1.06	0.94
By-pass	29.69	26.12	3.57	12.02	1.07	0.95

The most efficient solution from the point of view of post-oxidation is the geometry with the by-pass because it “injects” fresh air in the middle of the cloud of rich combustion products, therefore increasing the interface where post-oxidation takes place.

10 Validation of the post-oxidation model in QuickSim

The experience gathered during this project has been used for the validation of a post-oxidation model in QuickSim.

The model, although specifically designed for QuickSim, can be implemented in every 3D-CFD tool.

10.1 Model description

The application in QuickSim must take into account the targets and the characteristics of the simulation environment in order to be consequently developed.

The implementation of post-oxidation in QuickSim must rely on the description of the working fluid by means of ten scalars described above (§3.1) [28]. The scalars are able to precisely describe the most relevant phenomena as well as the chemical and thermodynamic properties of gases. The simplifications introduced with the scalars description of the fluid are that the chemical species are not directly simulated as in the detailed simulation. However, the chemical composition can be always calculated by means of the thermodynamical properties [28], which converts the information of the scalars into a chemical composition and determines for each cell the amount of energy in it as function of the chemical composition.

The implementation of the post-oxidation model in the full engine simulation environment exploits some important advantages:

- The geometry of the model includes the whole engine, therefore reducing assumptions about boundary conditions;
- The mixing process in the exhaust manifold is well simulated because the movement of exhaust valves is simulated as well as backflows from the exhaust manifold into the cylinder;

- The simulation is faster and more stable.

The more realistic simulation of mixing plays a key role for post-oxidation, as both 3D-CFD and 1D investigations demonstrated [70].

Another factor that must be implemented is the simulation of the chemical reactions without the direct use of a chemical reaction mechanism. The post-oxidation model for the 3D-CFD tool evaluates at each time-step and in each cell the chemical composition and the thermodynamic properties (pressure, temperature). Afterwards, if the conditions are correct for post-oxidation, a simplified reaction mechanism starts and follows the steps:

- Control if in the cell is present fuel; if yes, the fuel is the first to oxidize, which is what the investigations both with the detailed reaction mechanism and with Cantera confirmed. The composition of the cell changes accordingly to the oxidation and the heat release is calculated based on the characteristics of the fuel;
- If there is no fuel inside the cell, the 3D-CFD tool evaluates the chemical composition of exhaust and determines the amount of mass that is in post-oxidation conditions. The simple reaction mechanism than determines the changes in scalars and the amount of heat released.

This very simple model has the great potential of being very fast and numerically stable. Moreover, only few assumptions are introduced because it relies on 3D-CFD for the mixing and composition of the mixture.

The model can tune the temperature threshold at which the post-oxidation is activated. The threshold consists in the temperature of the cell at which the chemical reaction mechanism starts. The velocity reaction can be calibrated using a model based on an Arrenhius approach developed for the 1D model in [62]. Below is reported the resulting formula for the reaction speed, as already described in §2.1.

$$k = A \cdot T^{b} \cdot e^{\frac{-E_A}{R_u \cdot T}} \tag{2.1.3}$$

On the basis of the investigations so far, the threshold temperature should be 1000 K. The threshold uses the average temperature on the whole cell, which is of course only an approximation of the real local fluid temperature. The finer the computational grid, the closer should be the threshold to the real physical value for the start of the chemical reactions. The mesh used in the 3D-CFD

full engine simulation is coarser than the one of the detailed model of the exhaust manifold, it is therefore possible that the threshold temperature must be lower in order to match the same heat release of the validated simulations.

10.2 Model tuning and testing

To determine the value of the threshold that best fits the results, the validation has been carried out on an engine operating point that has already been simulated using the detailed model of the exhaust manifold. The simulation has the same boundary conditions in order to achieve two engine operating points that are as similar as possible, so that the results can be compared.

In Table 10.1 the most important parameters of the engine operation are reported. The results refer to exclusively to the full engine simulation carried out in QuickSim.

Table 10.1: Engine operating points for the validation of the post-oxidation model in QuickSim

		No post-ox	Post-ox	Δ_{ABS}	$\Delta_{\%}$
RPM	1/min	1200	1200	-	-
Air Consumption	kg/h	22.34	21.94	0.40	1.81
Fuel Consumption	kg/h	1.59	1.57	0.02	1.07
Air Mass @ IP	mg	563.47	552.90	10.57	1.89
Fuel Mass @ IP	mg	43.37	42.89	0.47	1.10
IMEP	bar	15.11	14.88	0.23	1.51
$\lambda_{CYLINDER}$	-	0.92	0.91	0.01	0.80
Volumetric air cons.	kg/h	20.28	19.90	0.38	1.89
Scavenging	kg/h	2.05	2.03	0.02	0.97
Scavenging rel.	%	9.19	9.27	-0.08	-0.84
λ_{ENGINE}	-	0.99	0.99	0.01	0.74

It can be seen that, although the geometry and the boundary conditions are the same, there are small differences between the two engine operating points chosen for the comparison. This is more probably due to the normal differences from cycle to cycle during engine operation than the effect of post-oxidation on the engine operation. Indeed, the application of this strategy effects mostly the behaviour of turbocharger and TWC, which are not simulated in this model and whose effects are already included in the boundary conditions, which remain the same in both cases. For a reasonable comparison the variables that most influence post-oxidation must be very similar. In this case, there is a very good agreement between the engine operating points. In particular air and fuel consumption are very similar, as well as scavenging, $\lambda_{CYLINDER}$ and λ_{ENGINE}.

The model of post-oxidation has been tested on this engine operating point using various temperature values of the threshold in order to have a sensitivity of the influence of this parameter. In Table 10.2 are the results of the simulations.

Table 10.2: Post-oxidation validation. HR is the heat released in the exhaust manifold by post-oxidation

$T_{THRESHOLD}$ [K]	HR [J/cyc]	Δ_{ABS} [J/cyc]	$\Delta_{\%}$ [%]
Detailed	575	-	-
800	679	104	18.08
900	570	-5	-0.94
1000	12	-563	-97.86

The model is very sensitive to the threshold temperature ($T_{THRESHOLD}$). For threshold values of 1000 K there is virtually no post-oxidation (-98% of heat release); for 900 K there is a very good agreement of detailed simulation and the post-oxidation model in the 3D-CFD tool; if the threshold is too low (800 K) the heat released is much higher (+18%) then the target. This is probably due to the averaging of temperature in each cell because there are probably very few cells with a temperature higher then 1000 K, while the majority are in the range of temperatures between 900 K and 1000 K.

The sensitivity of the post-oxidation model is mostly concentrated in this range of temperatures: for even higher thresholds, the heat release cannot diminish

much and for lower temperatures of threshold it does not increase remarkably because most of the energy entering the exhaust manifold has already been oxidized.

The value that best fits the heat release of the detailed chemical reaction is around 900 K. This value is not based on data fitting, but it can be physically and chemically motivated. This implies that, for the simulation of post-oxidation in the 3D-CFD tool, it is more important to have a good agreement of engine operating conditions to which the evaluation of the heat release of post-oxidation will follow.

Figure 10.1 shows the progress of post-oxidation in the exhaust manifold. The detailed curve is the heat release calculated in Star-CCM+ using the reduced reaction mechanism; the other curves are the simulations in the 3D-CFD tool using the post-oxidation model with different threshold temperatures.

The simulations both in the 3D-CFD tool and with the detailed model have a very similar shape, meaning that the implemented model in the 3D-CFD tool correctly simulates post-oxidation. The shape of the heat release has fast increases (“steps”), which correspond to the exhaust of the cylinder, during which most of post-oxidation takes place (§6). Between the two exhaust events, the heat release rate diminishes and the curve becomes more horizontal, which is also a characteristic phase of post-oxidation. Therefore, the post-oxidation simplified model is capable of simulating the different phases of post-oxidation.

Figure 10.1 shows the influence of the threshold temperature.

The detailed simulation and the simulation with threshold at 900 K show a very good agreement during the whole cycle. One difference between the two simulations is that the heat release just after the exhaust of the cylinders is in some cases faster in the simplified model. This is due to the simplicity of the model, in which the reaction rate of post-oxidation is mostly sensitive to temperature and could be better tuned. Another difference is that the simplified model uses for the calculations the assumption of chemical equilibrium, therefore is not taking into account the ignition delay.

Post-oxidation simulated with the simplified model decreases strongly between two consecutive exhaust events. As already analysed, the heat release rate of post-oxidation predicted using a chemical reaction mechanism does not

generally completely stop: there is always a small volume where temperature and composition enable the self-sustaining effect of post-oxidation. The problem is probably due to the simplified post-oxidation reaction rate used in the 3D-CFD tool model; however, since the final result has a very good agreement, such discrepancy can be considered acceptable.

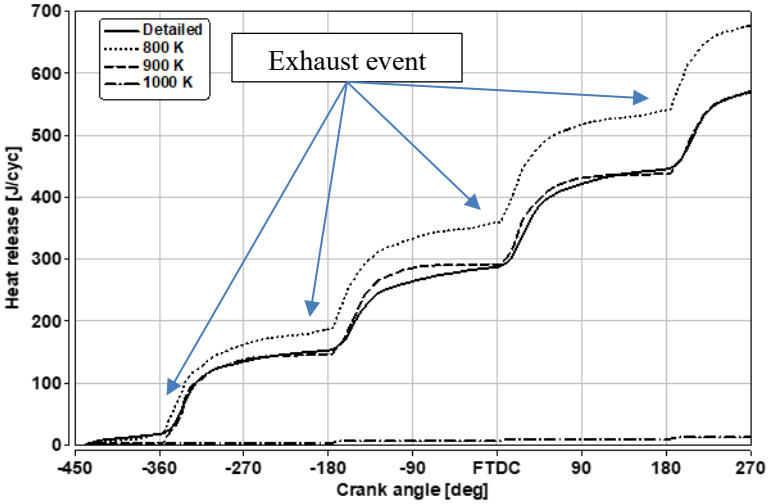

Figure 10.1: Heat release of post-oxidation in the exhaust manifold

It is possible to further improve the post-oxidation model in the 3D-CFD tool by introducing a better tuning of the reaction rate and reducing the non-realistically high heat release rate. At the same time, the computational time of the model must not increase significantly. The current model causes no appreciable increase of computational time, which is a very important feature.

The target of the simplified post-oxidation model is to be fast, reliable and well integrated in the already existing simulation environment: it serves as an estimation tool once that the most relevant data concerning full engine operation (air and fuel consumption, in-cylinder pressure…) are matched. Considering that these are the goals, the result of the implementation of the simplified post-oxidation model is satisfactory.

11 Conclusions and Outlook

A 3D-CFD simulation has been developed and validated for the simulation of post-oxidation. The methodology consisted of two simulation steps: the 3D-CFD full engine simulation and the detailed 3D-CFD simulation of the exhaust manifold.

The full engine simulation has been validated against experimental data from the test-bench and demonstrated to be able to predict the complex full engine phenomena such as scavenging, cylinder to cylinder interaction and local mixture distribution. The simulation has been used to understand the engine operation and to produce boundary conditions for the detailed 3D-CFD simulation of the exhaust manifold, which focused on the volume of the exhaust manifold up to the turbine volute. The detailed model of the exhaust manifold is characterised by a finer mesh and the implementation of a detailed chemical reaction mechanism for the simulation of the chemical reactions that take place during post-oxidation. Three different chemical reaction mechanisms have been tested, from the detailed to the reduced one. It has been demonstrated that the assumption of using a reduced reaction mechanism for the simulation is realistic for the simulation of post-oxidation. The whole methodology has been tested against experimental data and it demonstrated not only that the simulation is able to match the results of the test-bench, but also to give a detailed explanation of the results, therefore a better understanding of post-oxidation.

The 3D-CFD simulation enabled the description of post-oxidation, which takes place at the interface between fresh air clouds and rich combustion products during the exhaust of each cylinder, when the conditions of temperature and mixing are best.

The implementation of the detailed reaction mechanism enabled the sensitivity analysis of the composition of boundary conditions. The presence of long-chain hydrocarbons as boundary conditions causes a reduction of the heat release rate of post-oxidation. However, experimental evidence shows that this effect is in the case of post-oxidation negligible.

Also the effect of NOX on post-oxidation has been analysed and it has been demonstrated that its influence is negligible.

A mapping of post-oxidation in different operating conditions has been performed in order to define the limits and best applications of post-oxidation by means of scavenging. The mapping showed that post-oxidation is a stable strategy that is easily achievable; on the other side it also demonstrated that there are non-mixed clouds of fresh air and rich combustion exhaust products that flow to the turbine and to the TWC.

A sensitivity analysis demonstrated that post-oxidation is extremely sensitive to the temperature of the rich combustion exhaust gases: below 1000 K the reaction rate becomes too slow; increasing temperature, on the other hand, the efficiency of post-oxidation increases greatly. The simulation demonstrates that post-oxidation can increase the temperature of the exhaust gases by 190 K and +19%.

The simulation methodology has been applied to three different geometries in order to understand the effects of mixing in the exhaust manifold. The most interesting geometry is the one with by-pass adaptor because it is able to better exploit the amount of fresh air by “injecting” it inside the cloud of hot combustion products, therefore creating a second mixing front where the chemical reactions take place and the heat is released.

The information gathered during the investigation has been used to validate a simplified model of post-oxidation model specifically designed for the 3D-CFD tool QuickSim. The first results match well the detailed simulation of the exhaust manifold in the same engine operating point, while the model does not cause any appreciable increase of computational time.

Post-oxidation strategies have a potential application for the future engines as a simple and efficient tool to increase the temperature of the exhaust gases, especially for catalyst heating operating points. The analysis carried out in this work lays the first detailed analysis and understanding of this strategy: its basic functioning system, the most influencing factors and its limits. On these understandings the future post-oxidation strategies will be developed and finely tuned.

As the future of internal combustion engines remains uncertain, one thing is for sure: the next generation of engines will have to be cleaner and more efficient, while remaining simple and cheap. In this frame, post-oxidation fits very well.

Bibliography

[1] UNDP - United Nations Human Development Programme, Human Development Report 2020, 2020.

[2] IPCC - Intergovernamental panel on climate change, Climate Change 2007: The Physical Science Basis, 2007.

[3] W. D. Nordhaus, „A Review of the Stern Review on the Economics of Climate Change," *Journal of Economic Literatur,* pp. 686-702, 2007.

[4] N. L. Bindoff und P. A. Stott, „Detection and attribution of climate change: from global to regional," in *Climate Change 2013: The Physical Science Basis. Contribution of Working Group I to the Fifth Assessment Report of the Intergovernmental Panel on Climate Change*, Cambridge, United Kingdom and New York, NY, USA, Cambridge University Press, 2013, pp. 867-952.

[5] IEA Paris, „Global Energy Review 2021," IEA, 2021. [Online]. Available: https://www.iea.org/reports/global-energy-review-2021.

[6] ExxonMobil, 2019 Outlook for energy: a perspective to 2040, 2019.

[7] T. Jackson, Prosperity without growth, Taylor & Francis, 2011.

[8] United Nations, Paris agreement, 2015.

[9] D. Lanzarotto, M. Marchesoni, M. Passalacqua, A. Pini Prato and M. Repetto, „Overview of different hybrid vehicle architectures," *IFAC PapersOnLine,* pp. 218-222, 2018.

[10] F. Del Pero, M. Delogu and M. Pierini, „Life cycle assesment in the automotive sector: a comparative case study of internal combustion engines (ICE) and electric car," *Procedia,* pp. 521-537, 2018.

[11] P. Weber, J. Buchgeister, O. Toedter and T. Koch, „Life cycle assesment as a tool for analyzing the CO2 footprint of passanger cars with different powertrains," in *Internationaler Motorenkongress 2020*, Baden Baden, 2020.

[12] PWC, „Energiewende Outlook: Transportation sector," 2015.

[13] K. Wagemann and F. Ausfelder, „White Paper. E-Fuels - Mehr als eine Option," DECHEMA e.V., Frankfurt am Main, 2017.

[14] A. Lozanovski and C. P. Brandstetter, „Herstellung von Kraftstoffen aus CO2 und H2O unter Nutzung regenerativer Energie," 2015.

[15] A. Mokros, P. Demel, F. Knost, M. Münz and C. Beidl, „Sythetic, regenerative fuels (reFuels) as enabler for climate neutral mobility and transport," in *Internationaler Motorenkongress*, Baden Baden, 2020.

[16] J. Yadav, V. Betgeri, B. Graziano, A. Dhongde, B. Heuser, M. Schönen and N. Sittinger, „Renewable drop-in fuels as an immediate measure to reduce CO2 emissions of heavy-duty applications," in *Internationaler Motorenkongress*, Baden Baden, 2020.

[17] M. Albrecht, H. P. Deeg, D. Schwarzenthal and P. Ellts, „The influence of fuel composition and renewable fuel components of a GDI engine," *SAE Technical Paper,* 2020.

[18] K. Dums, H. P. Deeg, M. R. Marques, A. C. Kulzer and D. Schwarzenthal, „Sustained CO2 reduction in vehicle traffic with renewables fuels," in *Internationaler Motorenkongress*, Baden Baden, 2020.

[19] A. C. Kulzer, H. P. Deeg, J. Villforth, D. Schwarzenthal and M. Schilling, „Sustainable mobility using fuels with pathways to low emissions," *SAE Technical Paper,* 2020.

[20] N. Hooftman, M. Messagie, J. Van Mierlo and T. Coosemans, „A review of the European passenger car regulations - Real driving emissions vs local air quality," *Renewable and Sustainable Energy Reviews,* pp. 1-21, 2018.

[21] ADAC e.V., „ADAC," 08 04 2021. [Online]. Available: https://www.adac.de/verkehr/abgas-diesel-fahrverbote/abgasnorm/euro-7/. [Zugriff am 28 04 2021].

[22] C. Gong, K. Huang, B. Deng and X. Liu, „Catalyst light-off behavior of a spark-ignition LPG (liquefied petroleum gas) engine during cold start," *Energy,* pp. 53-59, 2011.

[23] C. Daridiotis, G. Martini, A. Marotta and U. Manfredi, „Low-temperature cold-start gaseous emissions of late technology passenger cars," *Applied Energy,* pp. 468-478, 2013.

[24] M. Weilenmann, J. Favez and R. Alvarez, „Cold-start emissions of modern passenger cars at different low ambient temperatures and their evolution over vehicle legislation categories," *Atmospheric Environment,* pp. 2419-2429, 2009.

[25] C. Koehlen, E. Holder and G. Vent, „Investigation of Post Oxidation and its Dependency on Engine Comubustion and Exhaust Manifold Design," in *SAE-Paper*, 2002.

[26] A. J. Feneley, A. Pesiridis and A. Mahmoudzadeh Andawari, „Variable geometry turbocharger technologies for exhaust energy recovery and boosting," *Renewable and Sustainable Energy Reviews,* pp. 959-975, 2017.

[27] A. Schmid, M. Grill, H.-J. Berner and M. Bargende, „Transient simulatin with scavenging in the turbo spark-ignition engine," *MTZ Worldw,* pp. 10-11, 2010.

[28] M. Chiodi, An innovative 3D-CFD-approach towards virtual development of internal combustion engines, Wiesbaden: Vieweg+Teubner, 2010.

[29] S. R. Turns, An introduction to combustion, Mc Graw Hill Education, 2011.

[30] J. Warnatz, U. Maas and R. W. Dibble, Combustion, Heidelberg: Springer, 1996.

[31] H. Versteeg and W. Malalasekra, An introduction to computational fluid dynamics, Pearson.

[32] G. Comini, G. Croce and E. Nobile, Fondamenti di termofluidodinamica computazionale, Padova: Servizi Grafici Editoriali, 2014.

[33] A. Frassoldati, T. Faravelli and E. Ranzi, „The ignition, combustion and flame structure of carbon monoxide/hydrogen mixtures. Note 1: Detailed kinetic modeling of syngas combustion also in presence of nitrogen compounds," *International Journal of Hydrogen Energy,* Bd. 32, p. 3471–3485, 2007.

[34] L. Cai and H. Pitsch, „Optimized chemical mechanism for combustion of gasoline surrogate fuels," *Combustion and Flame,* Bd. 162, p. 1623–1637, 2015.

[35] T. Lu and C. K. Law, „A directed relation graph method for mechanism reduction," *Proceedings of the Combustion Institute,* Bd. 30, p. 1333–1341, 2005.

[36] K. E. Niemeyer, C.-J. Sung and M. P. Raju, „Skeletal mechanism generation for surrogate fuels using directed relation graph with error propagation and sensitivity analysis," *Combustion and Flame,* Bd. 157, p. 1760–1770, 2010.

[37] D. C. Wilcox, Turbulence modeling for CFD, DCW Industries, Inc, 2006.

[38] T. Aizawa, „TAIZAC-TAndem Injectors Zapping ACtivation - for thermal efficiency improvement of diesel engine," in *FVV Autumn Conference*, Würzburg, 2019.

[39] A. Babajimopoulos, D. N. Assanis, D. L. Flowers, S. M. Aceves and R. P. Hessel, „A fully coupled computational fluid dynamics and multi-zone model with detailed chemical kinetics for the simulation of premixed charge compression ignition engines," *International Journal of Engine research,* pp. 497-512, 2005.

[40] S.-C. Kong and R. Reitz, „Use of detailed chemical kinetics to study HCCI engine combustion with consideration of turbulent mixig effects," *Journal of engineering for gas turbines and power,* pp. 702-706, 2002.

[41] S.-C. Kong and R. D. Reitz, „Application of detailed chemistry ond CFD for predicting direct injection HCCI engine combustion and emissions," *Proceedings of the combustion institut,* pp. 663-669, 2002.

[42] C. K. Westbrook, Y. Mizobuchi, T. J. Poinsot, P. J. Smith and J. Warnatz, „Computational combustion," *Proceedings of the Combustion Institute,* pp. 125-157, 2005.

[43] G. D. Stefanidis, B. Merci, G. J. Heynderikx and G. B. Marin, „CFD simulations of steam cracking furnaces using detailed combustion mechanisms," *Computers and chemical engineer,* pp. 635-649, 2006.

[44] Star-CCM+, User guide.

[45] T. Lu and C. K. Law, „A directed relation graph method for mechanism reduction," *Proceedings of the Combustion Institute,* pp. 1333-1341, 2005.

[46] S. B. Pope, „Computationally efficient implementation of combustion chemistry using in situ adaptive tabulation," *Combustion theory modelling,* pp. 41-63, 1997.

[47] A. Kächele, Turbocharger Integration into Multidimensional Engine Simulations to Enable Transient Load Cases, Springer, 2020.

[48] S. Schneider, M. Chiodi, H. Friedrich and M. Bargende, „Development and experimental investigation of a two-stroke opposed-piston free-piston engine," *SAE Technical Paper,* 2016.

[49] A. Heron-Himmel, S. Schneider and M. Chiodi, „Experimental study of a free piston linear alternator with an opposed piston combustion chamber," in *20. Internationales Stuttgarter symposium*, 2020.

[50] F. Cupo, Modeling of real fuels and knock occurrence for an effective 3D-CFD virtual engine development, Wiesbaden: Springer Vieweg, 2020.

[51] A. Vacca, Potential of water injection for gasoline engines by means of a 3D-CFD virtual test bench, Wiesbaden: Springer, 2020.

[52] C. Pera and V. Knop, „Methodology to define gasoline surrogates dedicated to auto-ignition in engines," *Fuel,* pp. 59-69, 2012.

[53] H. G. Weller, S. Uslu, A. D. Gosman, R. R. Maly, R. Herweg and B. Heel, „Prediction of combustion in homogeneous-charge spark-ignition engines," in *COMODIA 94*, 1994.

[54] Ö. L. Gülder, „Correlations of laminar combustion data for alternative s.i. engine fuels," in *West Coast International Meeting and Exposition*, Sae International, 1984.

[55] Y. H. Liao and W. L. Roberts, „Laminar Flame Speeds of Gasoline Surrogates Measured with the Flat Flame Method," *Energy and fuels,* 26 January 2016.

[56] Y. Ra and R. D. Reitz, „A reduced chemical kinetic model for IC engine combustion simulations with primary reference fuels," *Combustion and flame,* pp. 713-738, 2008.

[57] V. Knop and S. Jay, „Latest Developments in Gasoline Auto-Ignition Modelling Applied to an Optical CAI Engine," *Oil and Gas Science and Technology,* pp. 121-137, 2006.

[58] J. Shi, P. Lopez Aguado and N. Guerrassi, „Understanding high-pressure injection primary break-up by using large-eddy simulations and x-ray spray imaging," *MTZ - Motorentechnische Zeitschrift,* 2017.

[59] M. Wentsch, Analysis of injection processes in an innovative 3D-CFD tool for the simulation of internal combustion engines, University of Stuttgart: Springer Vieweg, 2018.

[60] R. Tromellini, J. Przewlocki, F. Cupo, M. Bargende and M. Chiodi, „Analysis of scavenging air post-oxidation by means of 3D-CFD simulation including reaction mechanism," in *Internationales Stuttgarter Syposium*, Stuttgart, 2020.

[61] M. Kumar, S. Moeeni, T. Kuboyama, T. Moriyoshi and e. al., „Investigation of H2 Formation Characterization and its Contribution to Post-Oxidation Phenomenon in a Turbocharged DISI Engine," in *Powertrains, Fuels and Lubricants Meeting*, Krakow, 2020.

[62] J. Przewlocki, Simulative investigation of post-oxidation in the exhaust Manifold of SI engines, Wiesbaden: Springer, 2021.

[63] A. Stagni, A. Frassoldati, A. Cuoci, T. Frassoldati and E. Ranzi, „Skeletal mechanism reduction through species-targeted sensitivity analysis," *Combustion and flame,* pp. 382-393, November 2016.

[64] E. Ranzi, A. Frassoldati, A. Grana, A. Cuoci, T. Faravelli, A. P. Kelley and C. K. Law, „Hierarchical and comparative kinetic modeling of laminar flame speeds of hydrocarbons and oxygenated fuels," *Progress in Energy and Combustion Science,* pp. 468-501, August 2012.

[65] A. Frassoldati, T. Faravelli and E. Ranzi, „The ignition, combustion and flame structure of carbon monoxide/hydrogen mixtures. Note 2: Detailed kinetic modeling of syngas combustion also in presence of nitrogen compounds," *International Journal of Hydrogen Energy,* pp. 3471-3485, March 2007.

[66] G. Ferrari, Motori a combustion interna, Bologna: Società editrice esculapio, 2016.

[67] F. Haußmann and B. Höpke, Optimierung des dynamischen Verhaltens hochaufgeladener Ottomotoren nach den Kriterien bester Verbrauch und bestes transientes Ansprechverhalten, Frankfurt am Main: ATL, 2015.

[68] L. Hentschel and P. Scheller, „The new 1,5l TGI evo for the "Golf Family"," in *Gasfahrzeugetagung*, Stuttgart, 2019.

[69] C. K. Westbrook, „Chemical kinetics of hydrocarbons ignition in practical combustion systems," *Proceedings of the Combustion Institute,* pp. 1563-1577, 2000.

[70] J. Przewlocki, R. Tromellini, M. Grill, M. Chiodi and M. Bargende, „Investigation and 1D modelling approach on scavenging air post-oxidation inside the exhaust manifold of a DISI engine," in *SAE WCX Digital Summit*, Detroit, 2021.

[71] Deutsches Institut für Normung e.V., „Kraftstoffe für Kraftfahrzeuge – Erdgas – Anforderungen und Prüfverfahren," *DIN 51624,* 2008.

[72] K. Altfeld and P. Schley, „Entwicklung der Erdgasbeschaffenheit in Europa," *Gaswärme International,* pp. 58-63, Februar 2012.

[73] DVGW, „Gasbeschaffenheit," *Technische Regel - Arbeitsblatt DVGW G 260 (A),* März 2013.

[74] Deutsche Energie-Agentur GmbH (dena), „Erdgas und Biomethan im künftigen Kraftstoffmix," Studie, Berlin, 2011.

[75] W. Cartellieri, G. Taucar and U. Pfeifer, „Erweiterung der Energieerzeugung durch Kraftgase," *FVV-Forschungsberichte 2-235/1/2/3, Frankfurt/M.,* 1968-1970.

[76] R. J. Kee, F. M. Rupley and J. A. Miller, *The Chemkin Thermodynamic Data Base,* 1990.